Journal of Chemistry

Environmental Biogeochemistry of Elements and Emerging Contaminants

Lead Guest Editor: Xiao-San Luo
Guest Editor: Peng Wang

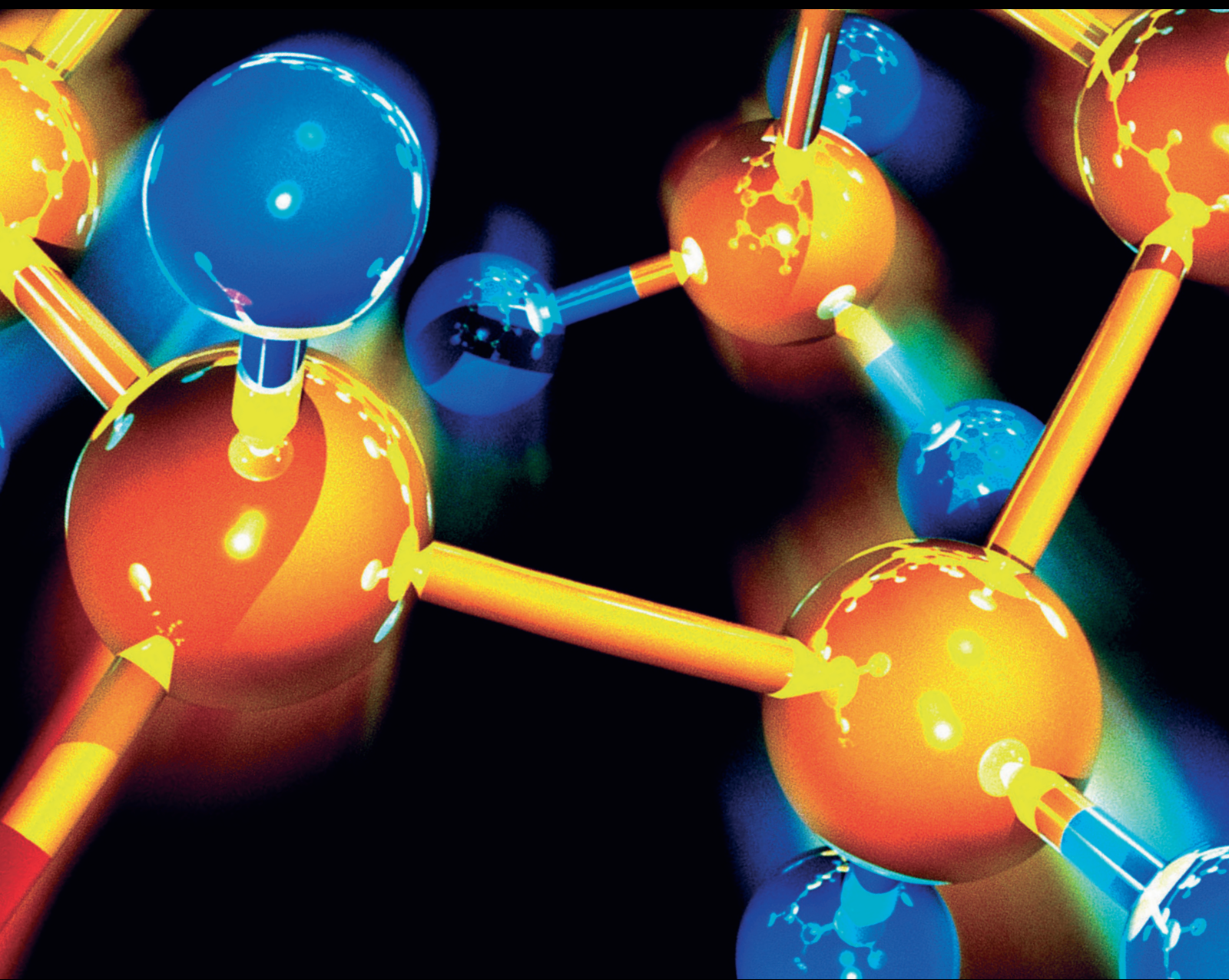

Environmental Biogeochemistry of Elements and Emerging Contaminants

Journal of Chemistry

Environmental Biogeochemistry of Elements and Emerging Contaminants

Lead Guest Editor: Xiao-San Luo
Guest Editors: Peng Wang

Contents

Hindawi
Journal of Chemistry
Volume 2018, Article ID 2763620, 2 pages
https://doi.org/10.1155/2018/2763620

Editorial

Environmental Biogeochemistry of Elements and Emerging Contaminants

Xiao-San Luo[1] **and Peng Wang**[2]

[1]*International Center for Ecology, Meteorology, and Environment, School of Applied Meteorology, Nanjing University of Information Science & Technology, Nanjing 210044, China*
[2]*College of Resources and Environmental Sciences, Nanjing Agricultural University, Nanjing 210095, China*

Correspondence should be addressed to Xiao-San Luo; xsluo@nuist.edu.cn

Received 16 May 2018; Accepted 17 May 2018; Published 5 July 2018

As the hot issues of environment and geochemistry sciences, environmental biogeochemistry investigating both elements and pollutants in soil, water, air, and organism links their behavior and effects in pedosphere, hydrosphere, atmosphere, and biosphere systematically. Typically, biogeochemical cycles of some biogenic elements, such as carbon and nitrogen, are closely related to the global climate change through greenhouse gases, while some trace elements, usually known as toxic heavy metals in the environment, pose significant risks to both ecosystem and humans. Besides the traditional chemical pollutants, recently, the emerging contaminants, such as persistent organic pollutants (POPs), nanoparticles, microplastics, antibiotics, and antibiotic resistance genes (ARG), have been attracting extensive concerns, due to their potential environmental risks. Therefore, faced with these challenges, investigations of the environmental biogeochemistry of elements and emerging contaminants are of great significance for the environmental protection and human health.

This special issue aims to provide the environmental research community with a forum to share various innovative ideas and to present up-to-date advancements in these fields. The selected seven research papers might not fully cover the topics mentioned above, since six of them are mainly related to heavy metals, and the other paper introduces the risks threatened by acid rain with atmospheric pollutants. However, they represent how current research studies still focus on the long-term practical issue of environmental biogeochemistry of this traditional nondegradable pollutant, through illustrating the pollution sources, distribution, behavior, fate, ecological effects and risks, and management, control, and remediation of heavy metals in soil and water environments.

Knowing pollution sources and risk implications is the primary step in environmental biogeochemistry of pollutants. Mining activities can cause significant soil and water pollution through solid wastes and metal-rich effluents. The mobility, chemical speciation, and ecological risks of heavy metals (Cu, Pb, and Zn) and the acid mine drainage (AMD) production in tailings of a copper mine in northern China were investigated by Chen et al. using column leaching studies. Besides the high metal concentrations in both tailings and leachates, the sequential extraction results and risk assessment code (RAC) evaluation based on the percentage of mobile fractions also revealed that heavy metals in tailings pose medium to high migration risks, which were influenced by specific hydrogeological and climate conditions. Rainfall is an important sink of scavenging atmospheric pollutants (SO_2, NO_x, and particulate matters), and it is also a significant pollutant source to soil and water ecosystems, inducing negative environmental effects such as soil acidification and eutrophication. Chemical compositions of precipitation in the typical urban site of hinterland were reported by Zhang et al. through analyzing the water-soluble ions for two-year daily samples in the Three Gorges Reservoir, China. Results showed still serious air pollution (SO_4^{2-}, NO_3^-, and NH_4^+) by local anthropogenic activities such as coal burning and traffic-related sources together with agricultural activities, although the air quality has been improved in the recent decade. Excessive sulfur emission

was the main precipitation acidity (average pH 5.0) factor, but the contribution of nitric acid was strengthening.

Key environmental biogeochemical processes include the distribution, transport, and fate of contaminants in the soil and aquatic systems, which are the main pollutant sinks and pose directly negative biological effects. The distribution and sources of heavy metals in both the waters and sediments of the Voghji River Basin (Armenia) were extensively investigated by Gabrielyan et al. to assess the environmental pollution (Mn, Co, Cu, Zn, Mo, Cd, and Pb) dramatically aggravated by drainage water and wastewater of mining regions, which disturbed the local geochemical balance. The coastal zone is also frequently disturbed by human activities such as land reclamation engineering which influences aquatic environment significantly. The spatial distributions of heavy metals in surface sediments after the land reclamation in Bohai Bay, China, were studied by Zhu et al. through grain size and speciation analysis and ecological risk assessments, demonstrating the contamination of Cd and Cr and the significant role of hydrodynamic condition change on pollutant distribution. With regard to the biological effects of heavy metals, the root responses and the corresponding intracellular mechanisms (elongation, antioxidative enzyme activities, and lipid peroxidation) of duckweed to Cd stress were investigated by Xue et al. based on Cd speciation accumulated in roots, which could be a predictor of Cd toxicity to aquatic plants.

Finally, control and remediation of soil and water pollution is the problem-solving step. As typical ways of pollution control, source elimination, environmental remediation, and land safe use are feasible choices. For pollutant removal, Fe-loaded corn straw biochar was successfully synthesized by Fan et al. and used as adsorbent for enhanced arsenate removal from aqueous solution, suggesting that it can be an efficient green method for the remediation of As-contaminated water or soil. The As speciation analysis indicated three mechanisms were involved in As (V) removal: sorption, strong inner-sphere surface complexes, and partial occlusion into the crystalline Fe oxides or carbonized phase. For safe use of heavy metal-contaminated agricultural soil, intercropping of gramineous pasture ryegrass and leguminous pasture alfalfa was proposed by Cui et al. to increase the plant resistance to heavy metals, which reduces plant oxidative damage and increases antioxidant activity. As an alternative to phytostabilization, it provides a strategy to raise biomass and reduce the Pb accumulation by forage plants in contaminated environments.

Compiling these papers, we hope to enrich readers the most recent progresses on different aspects of environmental biogeochemistry. Of course, it is worth pointing out that the investigated objects should not be limited by technology; besides heavy metals, the environmental biogeochemistry of biogenic element cycles and emerging contaminants and their interactions among various environmental systems are also significant and are developing rapidly.

Acknowledgments

The Guest Editors would like to thank all the authors for their contributions to this special issue and appreciate all the reviewers and related editorial board members for critical assessments and valuable comments to improve the quality of these papers.

Xiao-San Luo
Peng Wang

Hindawi
Journal of Chemistry
Volume 2018, Article ID 7803408, 11 pages
https://doi.org/10.1155/2018/7803408

Research Article

Intercropping of Gramineous Pasture Ryegrass (*Lolium perenne* L.) and Leguminous Forage Alfalfa (*Medicago sativa* L.) Increases the Resistance of Plants to Heavy Metals

Tuantuan Cui,[1] Linchuan Fang,[1,2] Mengke Wang,[1] Mao Jiang,[1] and Guoting Shen[1]

[1]*College of Natural Resources and Environment, Northwest A&F University, Yangling 712100, China*
[2]*State Key Laboratory of Soil Erosion and Dryland Farming on the Loess Plateau, Northwest A&F University, Yangling 712100, China*

Correspondence should be addressed to Linchuan Fang; flinc629@hotmail.com

Received 5 January 2018; Revised 29 March 2018; Accepted 15 April 2018; Published 5 July 2018

Academic Editor: Xiao-San Luo

Intercropping can increase the biomass of plants and reduce the accumulation of heavy metals in plants. However, the mechanisms of intercropping increasing plant biomass and resistance to heavy metals are still unclear. Therefore, the pot experiment had been conducted to investigate the effect of intercropping treatment on the growth of gramineous pasture ryegrass (*Lolium perenne* L.) and leguminous forage alfalfa (*Medicago sativa* L.) in metal-contaminated soil. Our results showed that intercropping alleviated inhibition of heavy metals to plant growth and increased nitrogen and chlorophyll contents in the shoots and roots. Moreover, the Pb concentrations in the shoots and roots of ryegrass and alfalfa in the intercropping were significantly lower than those in the monoculture. And, the contents of saccharase and alkaline phosphatase were significantly increased in the intercropping treatment. Additionally, the intercropping treatment could reduce the oxidative damage and increase enzymatic antioxidant activities to improve the resistance of plants in contaminated soil. The intercropping treatment can increase the resistance of plants to heavy metals through reduction of plant oxidative damage and increase of antioxidant activity. It could provide us with a strategy that intercropping of ryegrass and alfalfa can increase biomass and reduce the absorption of Pb on forage plants.

1. Introduction

Heavy metals pollution has become a serious environmental problem, posing significant risk to human health as well as to ecosystems [1, 2]. Therefore, remediating heavy metal-contaminated soil has received a worldwide concern. Phytoremediation has several advantages such as ease of operation in the field, relatively low cost, and soil improvement without secondary pollution; therefore, it has become one of the major methods for the remediation of heavy metal-polluted soils [3]. Techniques of phytoremediation include phytoextraction, phytofiltration, phytostabilization, phytovolatilization, and phytodegradation [4]. Phytostabilization is the use of certain plants and strategies for stabilization of contaminants in contaminated soils [5].

Intercropping is one of the traditional agricultural managements, which has shown the improvement of land use efficiency [6]. Intercropping had been used to remediate heavy metal-polluted soils and was found to have many advantages [7]. It has been reported that intercropping can not only increase plant biomass but also change the accumulation of heavy metals in plants [8]. Intercropping can also produce agricultural products while cleaning the heavy metal-contaminated soil [9]. Intercropping has been proposed as an alternative to phytostabilization for heavy metal-contaminated soil [10]. However, the mechanisms of intercropping influencing heavy metal accumulation and biomass in plants remain unclear.

Over 100 intercropping combinations currently have been applied in China, 70% of the combined groups are including leguminous crops [11]. It has been found that the intercropping of gramineous and leguminous could enhance plant nutrients availability and uptake which supply substances to promote plant growth [12, 13]. Leguminous and gramineous intercropping systems are widely used, due to

the ability of nitrogen fixation by leguminous crops. Under leguminous and gramineous intercropping systems, the part of N fixed by leguminous plant can be transferred through various channels and then be used by the gramineous crops, so as to improve N utilization efficiency [14, 15]. For example, the intercropping system of gramineous wheat and leguminous soybean can substantially increase wheat yield and promote nutrient utilization [6].

Ryegrass (*Lolium perenne* L.) is widely reported as a kind of pasture which is suitable for planting in heavy metal-contaminated soil [16–19]. Previous studies have demonstrated that ryegrass could potentially rehabilitate Cd- and Pb-contaminated soils [20, 21]. Alfalfa (*Medicago sativa* L.) is the important perennial forage and has a wide distribution in the world [22]. Some studies showed that alfalfa has a potential capability to restore heavy metal-contaminated soil [23]. Ryegrass and alfalfa are two important forages in northern China [22, 24]. Planting these two forages in the heavy metal-contaminated soil would be harmful to the livestock industry. Previous studies showed that intercropping can reduce heavy metals uptake by plants [8]. However, it is still unclear about the uptake characteristics of heavy metals by plant under the intercropping patterns of ryegrass and alfalfa. Furthermore, the mechanisms of intercropping influencing the resistance of plants to heavy metals are also investigated in this study.

We hypothesized that the intercropping of ryegrass and alfalfa could influence the plant growth and the heavy metals resistance. The absorption characteristics of plants were indicated by means of determination of heavy metals content and biomass. The nutritional status of plants was measured by chlorophyll and N contents. The oxidative damage and enzymatic antioxidants activities were utilized to evaluate the resistance of plant to heavy metals. The objectives of this study were to investigate (1) the effects of intercropping of ryegrass and alfalfa on the uptake characteristics of heavy metals in plants, and (2) the mechanisms of intercropping influencing the resistance of plants to heavy metals. The investigation may provide a better understanding of the mechanism of detoxification of heavy metals by intercropping.

2. Materials and Methods

2.1. Sample Preparation. The topsoil (0–20 cm) was collected from the Pb-Zn mine located in Feng County, Shaanxi Province, China (106°36′15″E, 33°52′35″N). The soil samples were stored in clean Ziploc plastic bags and transferred to the laboratory immediately. The basic physicochemical properties of the soils were determined and are presented in Table 1. Ryegrass and alfalfa seeds were sown in the pots after sterilization with 30% sodium hypochlorite solution for 2 min, washed three times with tap water, and rinsed with deionized water (DIW).

2.2. Pot Experiment. After the soil was air-dried, it was passed through a 2 mm sieve. The air-dried soils (8 kg per pot) were placed in plastic pots (height: 25 cm; diameter: 25 cm). The moisture was maintained at ~60% of the maximum water-holding capacity to balance one week. And then the moisture was maintained at ~80% of the maximum water-holding capacity. No fertilizers were added throughout the experiment. In the control treatment, there was no plant in the pot. In the monoculture treatment, alfalfa and ryegrass were grown separately. In the intercropping treatment, the equidistance between alfalfa and ryegrass was separated. The experiment design is shown in Figure 1, which four different treatments were carried out as follows: (1) control: unplanted soil; (2) MA: monoculture of alfalfa; (3) MR: monoculture of ryegrass; and (4) IAR: intercropping of alfalfa and ryegrass.

Table 1: Soil physical-chemical properties and heavy metals concentration.

Physical-chemical properties	
pH (soil : water, 1 : 2.5)	8.08
SOM ($g \cdot kg^{-1}$)	25.8
TN ($g \cdot kg^{-1}$)	1.59
TP ($g \cdot kg^{-1}$)	0.31
The total concentration of heavy metals ($mg \cdot kg^{-1}$)	
Pb	652
Cd	4.95
Zn	160
Cu	30.1

Note. SOM: soil organic matter; TN: total N; TP: total P.

Before the seed germination, 100 seeds of the same size were guaranteed in each pot. After 10 days, the seedlings were planted to ensure that 60 germination seeds were planted in each basin, and 30 of each plant were in the intercropping treatment. The pot experiment was performed in a greenhouse under natural light at 22~28°C.

2.3. Sampling and Analysis. Soil moisture was determined gravimetrically in fresh soils at 105°C to constant weight. Soil pH of air-dried samples (sieved to 1 mm) was determined using the glass electrode (Startorius PB10) with a soil to water (non-CO_2 deionized water) ratio of 1 : 2.5. Soil organic matter (SOM) was analyzed using the standard procedure of dichromate [25]. Total nitrogen (TN) was measured by titration. Inorganic N of NH_4^+ and NO_3^- was extracted by 2 M KCl, and the extractant was subsequently analyzed using a Seal autoanalyzer. Available phosphorus (AP) was measured using the 0.5 mol/L $NaHCO_3$ extraction-ammonium molybdate-antimony potassium tartrate and ascorbic acid spectrophotometric method. Soil heavy metals contents were determined by using three acid digestion (HNO_3, HCl, and $HClO_4$), and the digested samples were analyzed by ICP-AES technique (inductively coupled plasmaoptical emission spectrometer, PerkinElmer-Optima 7300 DV, USA).

The plants were harvested after 75 days, and the fresh shoots and roots were harvested separately. The fresh shoots were used to measure chlorophyll content using the acetone method immediately. The fresh shoots and roots from each treatment were immediately stored at −80°C for measuring the oxidative damage system and enzyme activity later. The content of malondialdehyde (MDA) was used to evaluate the lipid peroxidation [26]. Briefly, grounded shoot and root samples were extracted by 10% trichloroacetic acid (2 mL).

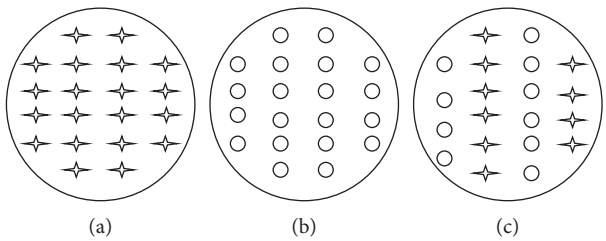

Figure 1: Pot experiment design drawing. (a) Monoculture of ryegrass; (b) Monoculture of alfalfa; (c) Intercropping of alfalfa and ryegrass. ✧ represents ryegrass; ○ represents alfalfa.

After centrifugation at 8000g for 10 min, the MDA in the supernatant was measured using an MDA reagent kit (Suzhou Comin Biotechnology Co., Ltd. Suzhou, China) based on the absorbance at 532 and 600 nm. The activity of total peroxidase (POD, EC 1.11.1.7), catalase (CAT, EC 1.11.1.6), and ascorbate peroxidase (APX, EC 1.11.1.11) in the shoot and root were correspondingly assessed using the enzyme-specific commercial reagent kit (Suzhou Comin Biotechnology Co., Ltd. Suzhou, China). These activity indicators were determined by the absorbance of the supernatant after reactions at different wavelengths (i.e., 470, 240, and 290 nm for POD, CAT and APX, resp.) (Epoch, US), following the manufacturer's instructions. The enzyme activities of POD, CAT, and APX were calculated from the initial rate of the reaction using the extinction coefficient of tetraguaiacol, H_2O_2, and ascorbate, respectively.

The shoots and roots were thoroughly washed with distilled water before heavy metals analysis. Fresh samples were dried at 105°C for 30 mins, and then dried to constant weight at 75°C. The oven-dried plant samples were digested using $HNO_3/HClO_4$ (4 : 1, v/v) to analyze the concentrations of metals. The nitrogen (N) concentration in plant tissues were determined after concentrated H_2SO_4 and H_2O_2 digestion by the high resolution automatic chemical analyzer.

After plants were harvested, the soil (through a 2 mm sieve) was immediately stored in the 4°C to measure enzyme activity. Catalase (EC 1.11.1.6) used H_2O_2 as the substrate and was quantified with a spectrophotometer (UV3200, Shimadu Corporation, Japan) at 240 nm. Saccharase (EC 3.2.1.26) enzyme activity was analyzed according to the method described by Guan [27]. Alkaline phosphatase assays, following the methods of Eivazi and Tabatabai [28, 29], were quantified on the release of p-nitrophenol at 400 nm. Urease was measured following the method of Guan [27], using urea as the substrate and was quantified at 578 nm.

2.4. Data Analysis. All statistical analysis was carried out in SPSS 21.0 (SPSS Inc, Chicago, USA). The differences of parameters among different treatments (heavy metal concentrations, soil properties, enzyme activities, etc.) were analyzed using one-way ANOVA with LSD test at a 0.05 significance level. Pearson correlation analysis was performed to measure the relationships between enzyme activities and heavy metals, soil properties. All bar graphs were drawn using Origin Pro 9.0 (Origin Lab, Hampton, USA).

Table 2: The biomass of ryegrass and alfalfa with different treatments.

Treatments	Ryegrass		Alfalfa	
	Shoot ($g \cdot plant^{-1}$)	Root ($g \cdot plant^{-1}$)	Shoot ($g \cdot plant^{-1}$)	Root ($g \cdot plant^{-1}$)
Monoculture	0.52 ± 0.09^a	0.14 ± 0.01^b	0.34 ± 0.05^b	0.24 ± 0.02^b
Intercropping	0.57 ± 0.07^a	0.18 ± 0.03^a	0.47 ± 0.04^a	0.37 ± 0.05^a

Note. Values are the means ± standard error ($n = 4$). Means followed by the same letter are not significantly different at $p < 0.05$.

3. Results

3.1. Plant Biomass, Chlorophyll, and N Content. Table 2 shows the biomass of plants roots and shoots. For ryegrass, no significant differences were found on the biomass of the shoots between those grown in different planting patterns; the biomass of roots grown in the intercropping treatment was significantly higher than those grown in the monoculture treatment. For alfalfa, compared with the monoculture treatment, the intercropping treatment significantly increased the biomass of shoots and roots.

Nitrogen concentrations in the shoots of ryegrass were substantially improved by the intercropping treatment (Figure 2(a)). The intercropping treatment was significantly increased the nitrogen concentrations in both shoots and roots of alfalfa (Figures 2(a) and 2(b)). In the monoculture treatment of ryegrass, the chlorophyll concentration was 1.7 mg/g, whereas in the intercropping treatment, the chlorophyll concentration was significantly increased to 2.5 mg/g (Figure 3). The chlorophyll concentrations in alfalfa were 3.2 and 2.6 mg/g in the monoculture and intercropping treatments, respectively. The chlorophyll concentrations in the intercropping treatment of alfalfa were apparently higher than those in the intercropping treatment.

3.2. Concentrations and Total Uptakes of Metals in Plants. The concentrations and total uptakes of metals in ryegrass and alfalfa were presented in Table 3. The Pb concentration and total uptake in ryegrass shoots were significantly decreased by 60% and 56%, respectively, in the intercropping treatment, compared to those in the monoculture treatment. And the Pb concentration and total uptake in roots were significantly decreased by 50% and 32%, respectively. The total uptake of Zn both in shoots and roots of alfalfa was significantly decreased in the intercropping treatment. Compared with the monoculture treatment, there were no significant differences with the concentrations of Cd and Zn in the shoots and roots of ryegrass in the intercropping treatment. The intercropping treatment resulted in a significant decrease in the concentrations of Pb in the shoots and roots of alfalfa by 23% and 60%, respectively. The concentrations of Cd were significantly decreased in the shoots of alfalfa by 22% in the intercropping treatment. Intercropping treatment significantly increased the Zn total uptake of alfalfa tissues, and no remarkable variations were observed in the Zn content of the alfalfa.

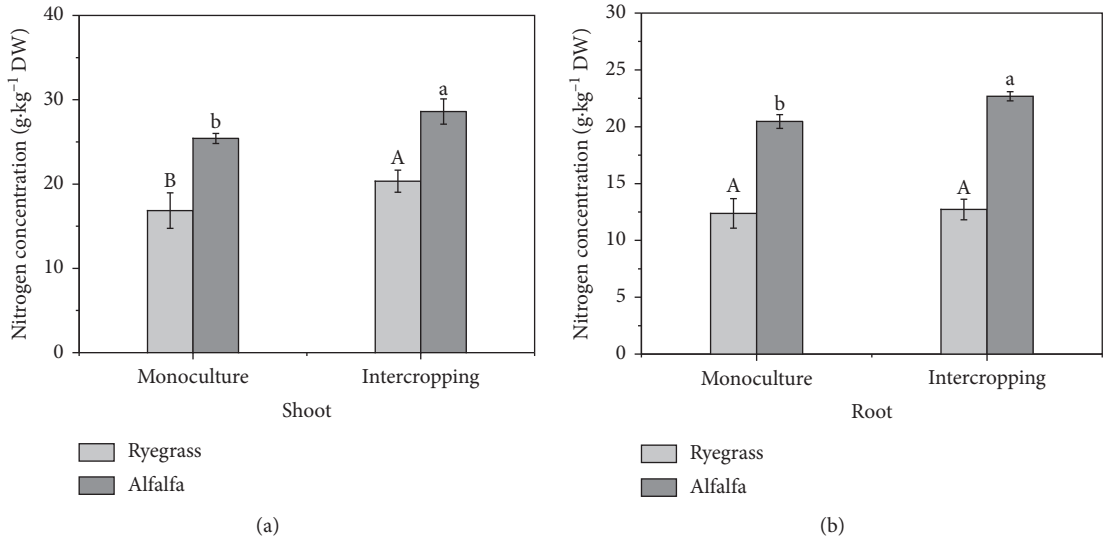

Figure 2: The nitrogen content in shoots (a) and roots (b) of ryegrass and alfalfa under monoculture and intercropping treatments. Bars are the standard error ($n = 3$). Means followed by the same letter are not significantly different at ($p < 0.05$).

3.3. Soil Enzymatic Activities and Physicochemical Properties. The changes of soil enzymes (urease activity, saccharase activity, alkaline phosphatase activity, catalase activity, and polyphenol oxidase activity) are shown in Table 4. The impacts of the planting pattern on soil enzymes were inconsistent and enzyme-specific. Compared with the alfalfa monoculture treatment, the intercropping treatment significantly increased the urease activity but less than the ryegrass monoculture treatment. The saccharase activity in the intercropping treatment was significantly higher than other treatments. The alkaline phosphatase activity showed a similar pattern to the saccharase activity change. After planting the plant, the catalase activity of the soil was increased but showed no remarkable variations among the planning pattern. Compared with the ryegrass monoculture treatment, the polyphenol oxidase activity was significantly increased in the intercropping treatment but showed no differences with other treatments.

The soil physicochemical properties are presented in Table 5. The soil pH with planted treatment was significantly higher than those with unplanted treatment. The contents of SOM showed no significant changes among different planning patterns. Compared with the unplanted soil, the TN and AK in soil were significantly decreased by the planting pattern of all treatments. There were no significant differences with the concentrations of TN in the soil among different planting patterns. Among all the treatments, the intercropping treatments had the highest soil NH_4^+-N and NO_3^--N. The AP had no change among different treatments.

3.4. Correlation Analysis. The correlations among soil physicochemical properties and soil enzyme activities are presented in Table 6. The soil urease, saccharase, and catalase were significantly positive correlated with soil pH and were significantly negative correlated with soil TN. Saccharase was significantly positive correlated with soil NH_4^+-N and

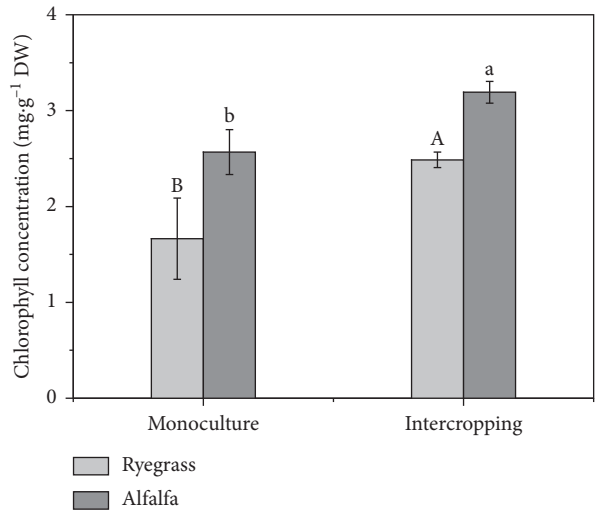

Figure 3: The chlorophyll content in shoots of ryegrass and alfalfa under monoculture and intercropping treatments. Bars are the standard error ($n = 3$). Means followed by the same letter are not significantly different at $p < 0.05$.

NO_3^--N. Alkaline phosphatase was significantly positive correlated with soil NO_3^--N. There was a significant positive correlation between alkaline phosphatase and NO_3^--N. The soil saccharase was significantly positive correlated with soil phosphatase and catalase.

Table 7 shows the correlations among heavy metal concentrations, oxidative damages and enzymatic activities in plants. The Pb concentrations of plants were strongly positive correlated with MDA, H_2O_2, and $O_2^{\cdot-}$ contents in plants but were significantly negative correlated with the APX activities. The Cd concentrations of plants were significantly positive correlated with MDA contents in plants. The Zn concentrations of plants were significantly positive correlated with H_2O_2 contents in plants but were strongly

Table 3: Concentration and total uptake of metals in ryegrass and alfalfa tissues.

Plant	Metal	Treatment	Concentration ($mg \cdot kg^{-1}$)		Total uptake ($\mu g \cdot plant^{-1}$)	
			Shoot	Root	Shoot	Root
Ryegrass	Pb	Monoculture	75.2 ± 9.8^{a}	394 ± 5.2^{a}	39.0 ± 5.1^{a}	52.3 ± 0.7^{a}
		Intercropping	30.3 ± 0.5^{b}	198 ± 7.6^{b}	17.2 ± 0.3^{b}	35.5 ± 1.4^{b}
	Cd	Monoculture	1.14 ± 0.1^{a}	46.9 ± 0.3^{a}	0.59 ± 0.07^{b}	6.39 ± 0.1^{a}
		Intercropping	1.29 ± 0.1^{a}	36.5 ± 8.9^{a}	0.73 ± 0.06^{a}	6.57 ± 1.6^{a}
	Zn	Monoculture	87.2 ± 10.9^{a}	168 ± 7.5^{a}	45.4 ± 5.7^{b}	45.4 ± 5.7^{b}
		Intercropping	94.3 ± 4.6^{a}	193 ± 24.0^{a}	53.6 ± 2.6^{a}	53.6 ± 2.6^{a}
Alfalfa	Pb	Monoculture	69.7 ± 2.2^{a}	66.7 ± 1.0^{a}	23.5 ± 0.8^{a}	15.8 ± 0.2^{a}
		Intercropping	53.8 ± 2.4^{b}	26.6 ± 6.1^{b}	25.4 ± 1.1^{a}	9.91 ± 2.3^{a}
	Cd	Monoculture	2.71 ± 0.4^{a}	3.84 ± 1.3^{a}	0.91 ± 0.30^{a}	1.16 ± 0.01^{a}
		Intercropping	2.11 ± 0.1^{b}	2.55 ± 1.3^{a}	0.95 ± 0.04^{a}	0.55 ± 0.14^{b}
	Zn	Monoculture	62.3 ± 8.9^{a}	33.6 ± 5.4^{a}	21.0 ± 3.0^{b}	7.95 ± 1.3^{b}
		Intercropping	57.9 ± 6.2^{a}	30.0 ± 2.0^{a}	27.4 ± 3.0^{a}	11.2 ± 0.7^{a}

Note. Values are the means ± standard error ($n = 4$. Means followed by the same letter are not significantly different at $p < 0.05$.

Table 4: Soil enzyme activities after plant harvest under the different treatments.

Treatment	Urease (NH_3^+-N $mL^{-1}g^{-1}24\,h^{-1}$)	Saccharase ($C_6H_{12}O_6$ $mg^{-1}g^{-1}24\,h^{-1}$)	Alkaline phosphatase (μg PNP $g^{-1}h^{-1}$)	Catalase 1.1 mol L^{-1} $KMnO_4$ $mL^{-1}g^{-1}$ 20 min^{-1})	Polyphenol oxidase (Purpurogallin $mg^{-1}g^{-1}$ 2 h^{-1})
Control	2.61 ± 0.1^{ab}	7.28 ± 1.1^{d}	1.45 ± 0.06^{bc}	1.56 ± 0.1^{b}	3.40 ± 0.1^{a}
MR	2.79 ± 0.07^{a}	15.3 ± 0.2^{b}	1.50 ± 0.1^{b}	2.11 ± 0.2^{a}	3.04 ± 0.2^{b}
MA	2.60 ± 0.1^{b}	11.2 ± 2.4^{c}	1.29 ± 0.1^{c}	1.98 ± 0.1^{a}	3.47 ± 0.2^{a}
IRA	2.70 ± 0.01^{a}	20.5 ± 0.1^{a}	1.70 ± 0.09^{a}	2.18 ± 0.1^{a}	3.37 ± 0.3^{a}

Note. Values are the means ± standard error ($n = 4$). Means followed by the same letter in the same column are not significantly different at $p < 0.05$. MR: monoculture ryegrass; MA: monoculture alfalfa; IRA: intercropping of ryegrass and alfalfa.

Table 5: The soil physical-chemical properties under different treatments.

Treatment	pH	SOM ($g \cdot kg^{-1}$)	TN ($g \cdot kg^{-1}$)	NO_3^--N ($mg \cdot kg^{-1}$)	NH_4^+-N ($mg \cdot kg^{-1}$)	Available P ($mg \cdot kg^{-1}$)	Available K ($mg \cdot kg^{-1}$)
Control	8.2 ± 0.01^{b}	24.6 ± 0.8^{b}	1.49 ± 0.01^{a}	12.0 ± 1.60^{a}	2.66 ± 0.24^{b}	0.61 ± 0.15^{a}	29.5 ± 0.1^{a}
MR	8.7 ± 0.10^{a}	25.8 ± 1.8^{ab}	1.09 ± 0.10^{b}	11.7 ± 2.23^{ab}	2.65 ± 0.16^{bc}	0.58 ± 0.05^{a}	22.9 ± 0.6^{b}
MA	8.6 ± 0.10^{a}	26.4 ± 0.7^{a}	1.14 ± 0.01^{b}	9.0 ± 2.15^{b}	2.94 ± 0.07^{ab}	0.36 ± 0.10^{b}	22.4 ± 0.2^{b}
IRA	8.5 ± 0.07^{a}	27.1 ± 0.9^{a}	1.16 ± 0.01^{b}	13.5 ± 2.06^{a}	3.20 ± 0.34^{a}	0.49 ± 0.09^{ab}	23.8 ± 0.8^{b}

Note. Values are the means ± standard error ($n = 4$). Means followed by the same letter in the same column are not significantly different at $p < 0.05$. MR: monoculture ryegrass; MA: monoculture alfalfa; IRA: intercropping of ryegrass and alfalfa.

negative correlated with the POD activities. The CAT activities were significantly negative correlated with the MDA and $O_2^{\cdot-}$ contents in plants. The APX activities were significantly negative correlated with the MDA, H_2O_2, and $O_2^{\cdot-}$ contents in plants.

3.5. Oxidative Damage and Quantification of Enzymatic Antioxidants of Plant. To investigate the oxidative damage induced by heavy metals, lipid peroxidation was estimated by measuring MDA content (Figures 4(a) and 4(b)). Compared with the ryegrass monoculture treatment, the MDA content in the shoots was significantly decreased by 28%. For alfalfa, the intercropping treatment significantly decreased the MDA content of shoots and roots by 28% and 30%, respectively. The $O_2^{\cdot-}$ content of ryegrass and alfalfa tissues is shown in Figures 4(c) and 4(d). The contents of $O_2^{\cdot-}$ in the roots of alfalfa had no significant differences among different planning patterns. In the shoots of the alfalfa, the $O_2^{\cdot-}$ contents of the intercropping treatment were significantly lower than those in the monoculture treatment by 32%. For alfalfa, the intercropping treatment significantly decreased the H_2O_2 content of shoots and roots by 15% and 24%, respectively (Figures 4(e) and 4(f)).

Compared with the ryegrass monoculture treatment, the POD activity of roots was significantly increased by the intercropping treatment (Figure 5(b)). The roots POD activity of alfalfa in the monoculture and intercropping treatments showed no significant differences; however, POD activity in the shoots of alfalfa was substantially improved by the intercropping treatment (Figures 5(a) and 5(b)). Compared with the ryegrass monoculture treatment for the roots part, the CAT activity was significantly increased by the intercropping treatment (Figure 5(d)). For the shoots of alfalfa, the CAT activity was significantly increased by the intercropping treatment (Figure 5(c)). The APX activity in ryegrass shoots and roots in the monoculture and intercropping treatments showed no significant differences

Table 6: Pearson correlation matrix among soil physicochemical properties and soil enzyme activities.

	pH	SOM	TN	AP	AK	NO_3^--N	NH_4^+-N	Urease	Saccharase	Alkaline phosphatase	Catalase	Polyphenel oxidase
pH	1											
SOM	0.426	1										
TN	**−0.957****	−0.481	1									
AP	−0.387	−0.221	0.399	1								
AK	**−0.745****	**−0.629****	**0.757****	0.239	1							
NO_3^--N	−0.231	0.106	0.160	0.402	0.105	1						
NH_4^+-N	0.238	0.425	−0.338	−0.485	−0.098	0.161	1					
Urease	**0.580***	0.386	**−0.635****	0.009	−0.370	0.320	0.020	1				
Saccharase	**0.616***	**0.505***	**−0.662****	−0.209	−0.437	**0.525***	**0.607***	**0.594***	1			
Alkaline phosphatase	0.021	0.278	−0.057	0.362	0.001	**0.664****	0.255	0.293	**0.581***	1		
Catalase	**0.789****	0.413	**−0.787****	−0.162	**−0.621***	0.073	0.401	0.383	**0.719****	0.229	1	
Polyphenel oxidase	−0.315	0.121	0.246	−0.210	0.194	−0.087	0.218	−0.213	−0.154	−0.192	−0.288	1

Note. SOM: soil organic matter; TN: total N; AP: available P; AK: available K; *correlation is significant at $p < 0.05$ (two-tailed); **correlation is significant at $p < 0.01$ (two-tailed).

Table 7: Pearson correlation matrix among heavy metal concentrations, oxidative damages, and enzymatic activities in plants.

	Pb	Cd	Zn	MDA	$O_2^{\cdot-}$	H_2O_2	POD	CAT	APX
Pb	1								
Cd	0.281	1							
Zn	**0.501***	−0.197	1						
MDA	**0.588***	**0.768****	−0.082	1					
$O_2^{\cdot-}$	**0.694****	0.166	0.209	**0.637****	1				
H_2O_2	**0.894****	0.104	**0.520***	0.472	**0.753****	1			
POD	−0.271	**0.500***	**−0.843****	0.336	0.183	−0.326	1		
CAT	−0.263	−0.218	−0.175	**−0.539***	**−0.535***	−0.321	0.070	1	
APX	**−0.552***	−0.491	0.042	**−0.836****	**−0.775****	**−0.671***	−0.136	**0.591***	1

Note. *Correlation is significant at $p < 0.05$ (two-tailed); **correlation is significant at $p < 0.01$ (two-tailed).

(Figures 5(e) and 5(f)). For the shoots of alfalfa, the APX activity was significantly increased by the intercropping treatment.

4. Discussion

4.1. Effect of the Intercropping Treatment on Heavy Metal Uptake in Plants. It has been reported that the intercropping could enhance the availability and uptake of plant nutrients and produce substances promoting plant growth [12, 13]. Our result indicated that the intercropping can increase the biomass of both ryegrass and alfalfa. This means that the intercropping can increase the yield of both ryegrass and alfalfa in the process of phytostabilization. Intercropping can increase the biomass of two pastures on the one hand due to the physiological characteristics of alfalfa. Alfalfa is an important leguminous forage, which can effectively fix and absorb nitrogen in the soil and air, respectively [14]. When it was intercropped with gramineous crops, the part of the fixed and absorbed nitrogen can transfer through various channels and was used by the gramineous crops, so as to improve the utilization efficiency of nitrogen [14, 15]. On the other hand, intercropping of the leguminous and gramineous crop can separate the usage space and time from the aboveground and underground, making it efficient to use of light, heat, water, and other resources in nature, which could significantly improve the yield [6]. Chen et al. [30] reported that the intercropping of wheat and faba bean can significantly improve wheat yield, promote nutrient utilization, and effectively control disease. Furthermore, the N and chlorophyll concentration of plant was significantly increased under the intercropping treatment compared with the monoculture treatments. The results also verify the above two hypotheses. This means that intercropping could promote the growth of two pastures by increasing levels of plant nitrogen and chlorophyll.

Intercropping of different plants can regulate the accumulation of heavy metals in plants [31, 32]. In the present study, our result showed that intercropping can significantly decrease Pb concentration in ryegrass and alfalfa tissues (Table 3). It means that the intercropping patterns of ryegrass and alfalfa can significantly reduce the Pb uptake from soil to achieve the purpose of phytostabilization. It can provide us with a strategy that intercropping of ryegrass and alfalfa can be used on the Pb-contaminated soil. It has been reported that ryegrass has a strong ability to absorb cadmium; thus, intercropping could not reduce the accumulation of cadmium in plants [33]. Similar studies showed that the Pb concentrations in maize grain and cabbage were significantly lower when they were intercropped with

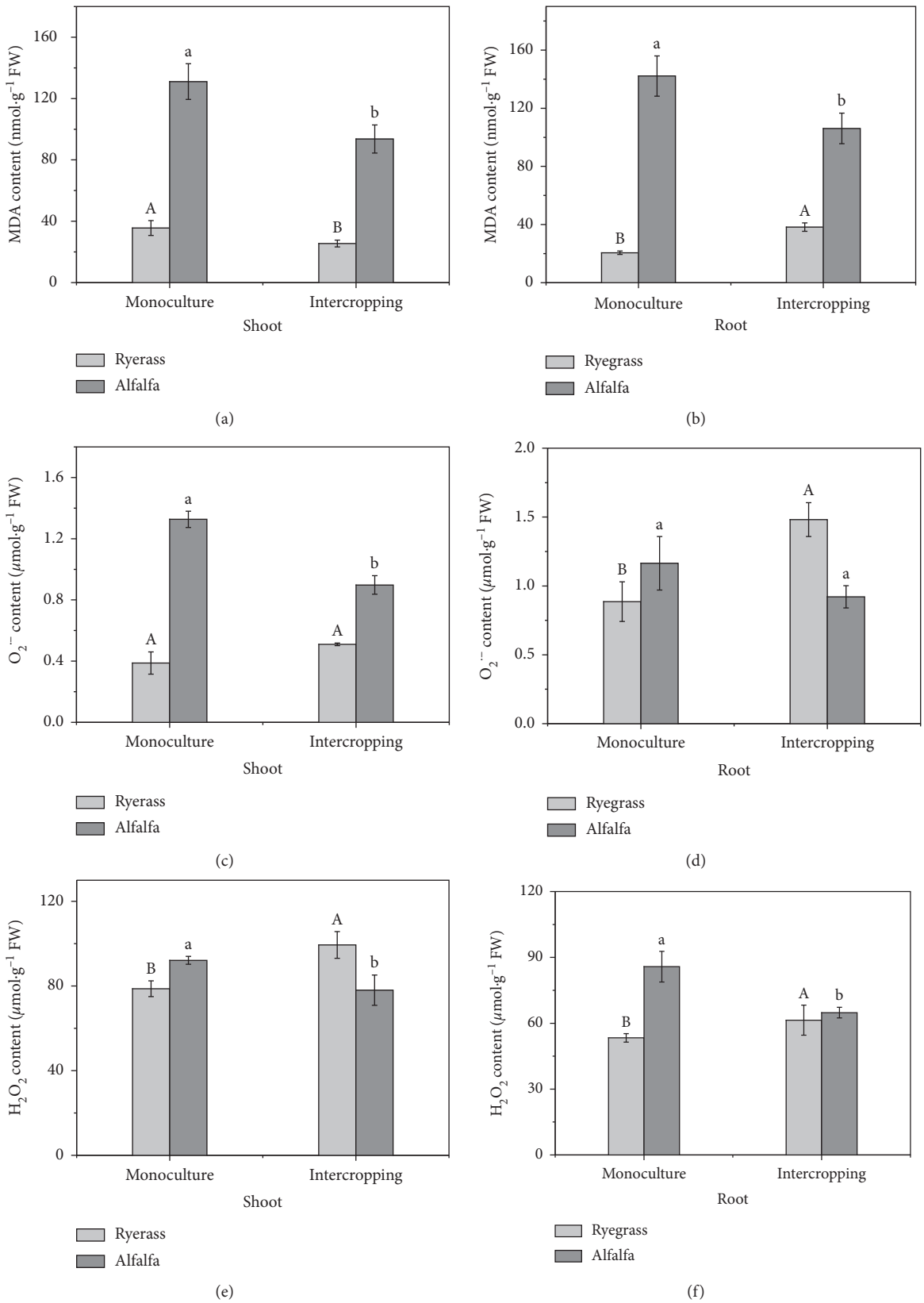

Figure 4: The MDA, $O_2^{\cdot-}$ and H_2O_2 content in shoots and roots of ryegrass and alfalfa under the monoculture and intercropping treatments. MDA content in shoots (a), MDA content in roots (b), $O_2^{\cdot-}$ content in shoots (c), $O_2^{\cdot-}$ content in roots (d), H_2O_2 content in shoots (e), and H_2O_2 content in roots (f). Bars are the standard error ($n = 3$). Means followed by the same letter are not significantly different at $p < 0.05$ of ryegrass and alfalfa with different treatments.

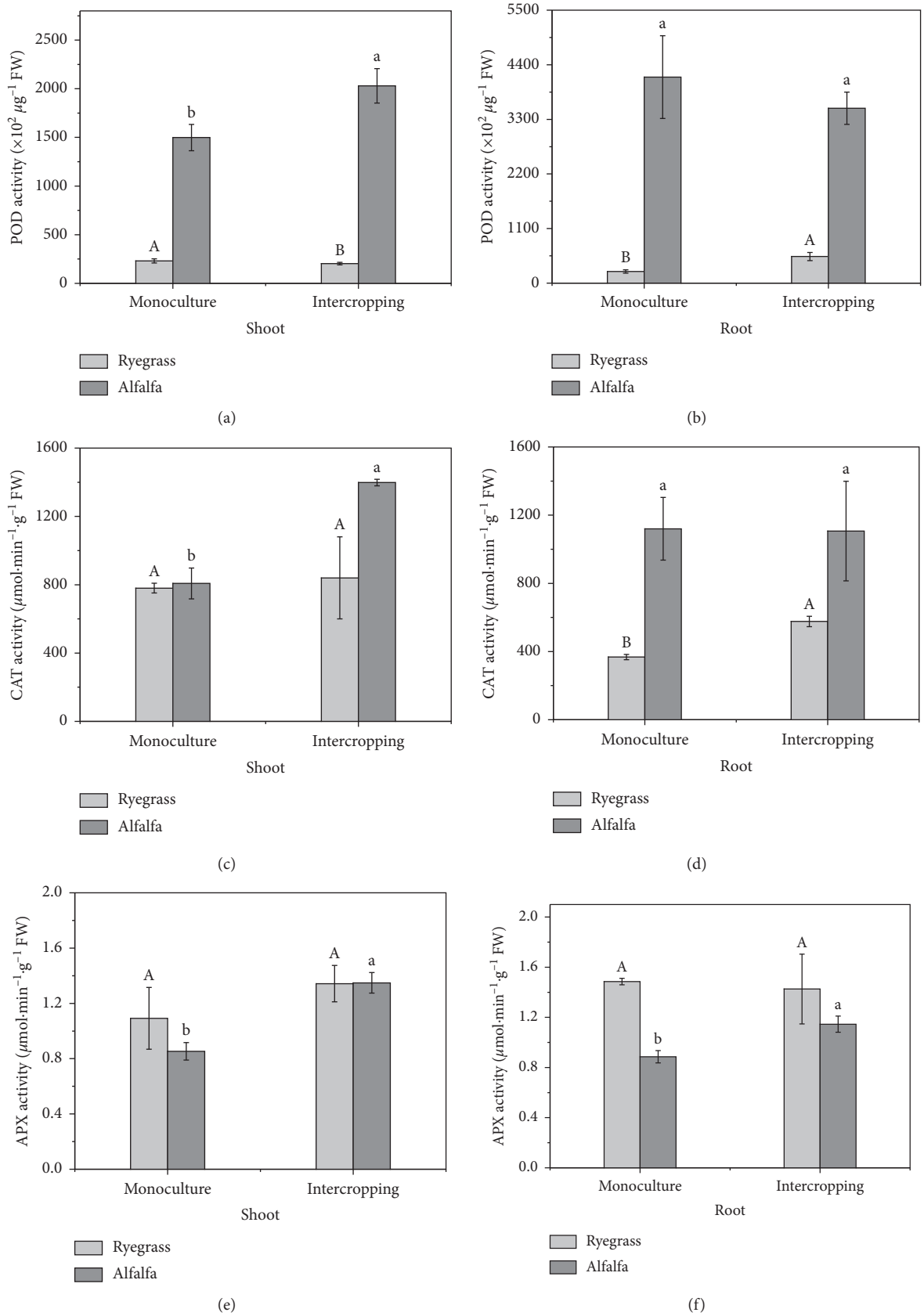

Figure 5: The antioxidant enzyme system contents in shoots and roots of ryegrass and alfalfa under the monoculture and intercropping treatments. POD activity in shoots (a), POD activity in roots (b), CAT activity in shoots (c), CAT activity in roots (d), APX activity in shoots (e), and APX activity in roots (f). Bars are standard error ($n = 3$). Means followed by the same letter are not significantly different at $p < 0.05$ of ryegrass and alfalfa with different treatments.

Japanese clover than when the respective crops were grown in monoculture [9, 34]. In this study, the ability of heavy metal uptake of ryegrass roots was much higher than that of alfalfa. Ryegrass can absorb heavy metals around the roots so as to provide a relatively safe environment for roots. Ryegrass and alfalfa intercropping may form roots interlaced each other to provide a safe living environment for alfalfa to reduce the concentrations of heavy metals in alfalfa. Wang et al. [9] found that the intercropping of *Pteris vittata* L. and faba bean can not only reduce the As content in the soil around the roots of *Pteris vittata*. L but also reduce the As content in the soil around the roots of faba bean. The intercropping could reduce the heavy metals in the bean. Correspondingly, the nitrogen fixation at the root of alfalfa can provide nutrients to ryegrass to enhance the resistance of ryegrass to heavy metals. It has been reported that nitrogen was an important detoxification factor for cadmium stress in plants [35]. Phytostabilization could eliminate the availability of toxic metals in soil through complexing with metals by certain plants root exudates [4]. Intercropping may increase the amount of root secretions by promoting the growth and development of plant roots. Zhan et al. [7] found that the intercropping of *Sonchus asper* L. and *Vicia faba* L. could decrease the effectiveness of heavy metals in soil by changing the low molecular weight organic acids secreted by the root system. Intercropping may increase the amount of root secretions by promoting the growth and development of plant roots. Previous studies working on intercropping treatment reported that it could reduce heavy metals contents in the plants [8]. The effects of the planting pattern on metal accumulation in plants may also depend on types of the metal and interactions between two coexisting plant species. In this study, intercropping not only reduced the Pb accumulation in plants but also increased plants biomass.

4.2. Effect of the Intercropping Treatment on the Resistance of Plants to Heavy Metals. Although the physical and chemical properties of the soil has no significant changes under different treatments, the intercropping treatment has the highest values of soil SOM, TN, NH_4^+-N, NO_3^--N, and AP. This means that intercropping may promote the growth and development of plant roots by improving the physical and chemical properties of soil. Moreover, soil enzyme activity plays an important role and is usually recommended as standard biological indicators of soil health [36, 37]. Soil enzyme activity is critically important for soil quality and can provide indications of changes in metabolic capacity and nutrient cycling due to management practices [38, 39]. In turn, soil mineral nutritional factors may support the growth and metabolic activity of plants. In this study, soil saccharase and alkaline phosphatase enzyme activities were affected by the intercropping treatment. Urease, catalase, and polyphenol oxidase had no significant change among different planted patterns. This means that intercropping can improve soil nutrient metabolism by improving soil saccharase and alkaline phosphatase enzyme activities. The increase in alkaline phosphatase may be due to intercropping which increases the P cycle in the soil [40]. Li et al. [41] founded that chickpea can improve the alkaline phosphatase in both hydroponic and soil cultures, leading to an interspecific facilitation in utilization of organic P in maize/chickpea intercropping.

In this study, Pearson correlation clarified that the dominant urease, saccharase, and catalase were significantly positive correlated with soil pH but were significantly negative correlated with soil TN (Table 6). Saccharase was significantly positive correlated with soil NH^+_4-N and NO^-_3-N. It means that pH and TN were the main factors affecting the activity of soil enzyme. Alkaline phosphatase was significantly positive correlated with soil NO_3^--N. It has been reported that the content of phosphatase and soil P in intercropping treatment is positively correlated [41]. Our result showed that soil urease was significantly negative correlated with soil TN.

The superfluous accumulation of ROS (reactive oxygen species) caused oxidative stress in plants, especially for sensitive cellular membranes. MDA is the ultimate decomposition product of membrane lipid peroxidation, which is the expression of the degree of peroxidation of plant cell membrane, and its content can reflect the degree of damage of the plant [42]. The higher the content of MDA indicated that the higher the degree of peroxidation of the plant cell membrane, the more serious damage to the cell membrane. MDA can be typically used as the indicator of lipid peroxidation in plants, which has been certified by previous studies [43]. $O_2^{\cdot-}$ is the free radical which is first formed in the oxygen metabolism of the organism, and it is the precursor of all the oxygen radicals. H_2O_2 is an important component of ROS. Excessive heavy metals can cause oxidative stress in the plant body and increase the H_2O_2 level and lipid peroxidation in plants [43, 44]. Similarly in *Arabidopsis*, oxidative stress after exposure to Cd is due to H_2O_2 accumulation [45]. A decrease of MDA content indicates that the oxidation degree of plant cell membrane is decreased, and the destruction of cell membrane is decreased. A decrease of $O_2^{\cdot-}$ content can reduce cell structure damage and prevent plant physiological disorders. The decreased H_2O_2 of ROS content can alleviate oxidative damage. In present study, compared with the alfalfa monoculture treatment, intercropping significantly decreased MDA, H_2O_2, and $O_2^{\cdot-}$ contents in plant shoots and roots, except for the $O_2^{\cdot-}$ content of alfalfa roots (Figure 4). The Pb concentrations of plants were significantly correlated with MDA, H_2O_2, and $O_2^{\cdot-}$ contents in plants (Table 7), which indicated that intercropping treatment can decrease the harmful substance and alleviate oxidative damage under heavy metal stress. The results indicated that intercropping treatment can mitigate the toxic effects of heavy metals by decreasing the harmful substance and alleviating oxidative damage. At the cellular level, excessive heavy metals can cause the physiological imbalance between oxygen-free radicals and plant antioxidant enzymes in plants [43, 44]. The enzymatic antioxidant system, including CAT, APX, and POD, is capable of scavenging excess ROS and prevent plants from lipid peroxidation. For instance, plants can protect cells from the damage of excessive ROS caused by

environmental stress through a strong antioxidant enzyme activity [46, 47].

In plant cells, the POD, CAT, and APX play vital roles in regulating the H_2O_2 level for signaling during metabolic changes, but the POD and APX are proposed to be predominantly responsible for modulating the H_2O_2 level, especially under the heavy metals stress environments [45]. In present study, compared with the monoculture treatment, intercropping significantly increased POD and CAT activities in the shoots of alfalfa (Figure 5). The APX activity in alfalfa shoots and roots was significantly increased by the intercropping treatment. And the CAT and APX activities were significantly negative correlated with the MDA and $O_2^{\cdot-}$ contents in plants; this means the intercropping treatment can decrease the harmful substance and alleviate oxidative damage under heavy metal stress by increasing the antioxidant enzyme system. Under the heavy metals stress, plants usually clear reactive oxygen radicals by strengthening protection on enzyme activity to maintain stability and integrity of cell membrane. Many results indicated that the increase of enzymatic antioxidant enzymes in plants would lead to decrease in the concentration of Pb in plants [48]. Overall, the response of alfalfa to heavy metals with decreasing the oxidative damage and increasing the antioxidant enzyme system could alleviate heavy metals toxicity in plants.

5. Conclusions

The present study demonstrated that intercropping of ryegrass and alfalfa treatment can promote plant growth and increase plant biomass in the heavy metal-contaminated soil. The plants grown in the intercropping treatment had a significantly low Pb concentration in plant shoots and roots than those in the monoculture treatments, which could be contributed to the reduction of oxidative damage and increase of enzymatic antioxidant activities in plants under intercropping. Hence, the intercropping of these two forage species could be a potentially safe phytoremediation pattern to reduce heavy-metal risks and increase yield in a large scale under heavy metal-contaminated soils. Further research is required to completely understand the mechanism of the interaction between the roots of two plants in intercropping conditions.

Data Availability

The data used to support the findings of this study are available from the corresponding author upon request.

Conflicts of Interest

The authors declare that there are no conflicts of interest regarding the publication of this paper.

Acknowledgments

This work was financially supported by the National Natural Science Foundation of China (41571314 and 41201226) and CAS "Light of West China" Program (XAB2016A03).

References

[1] L. Chen, S. Luo, X. J. Li, Y. Wan, J. B. Chen, and C. B Liu, "Interaction of Cd-hyperaccumulator *Solanum nigrum*, L. and functional endophyte *Pseudomonas*, sp. Lk9 on soil heavy metals uptake," *Soil Biology and Biochemistry*, vol. 68, no. 1, pp. 300–308, 2014.

[2] X. S. Luo, Y. Xue, Y. L. Wang, L. Cang, B. Xu, and J. Ding, "Source identification and apportionment of heavy metals in urban soil profiles," *Chemosphere*, vol. 127, pp. 152–157, 2015.

[3] H. Ali, E. Khan, and M. A. Sajad, "Phytoremediation of heavy metals–concepts and applications," *Chemosphere*, vol. 91, no. 7, pp. 869–881, 2013.

[4] E. A. Gwozdz and M. Kopyra, "Plant cell responses to heavy metals—biotechnological aspects," *Biotechnologia*, vol. 3, pp. 107–123, 2003.

[5] A. A. Erakhrumen, "Phytoremediation: an environmentally sound technology for pollution prevention, control and remediation in developing countries," *Educational Research Review*, vol. 2, no. 7, pp. 151–156, 2007.

[6] F. S. Zhan and L. Li, "Using competitive and facilitative interactions in intercropping systems enhances crop productivity and nutrient-use efficiency," *Plant and Soil*, vol. 248, no. 1-2, pp. 305–312, 2003.

[7] F. D. Zhan, L. Qin, X. H. Guo et al., "Cadmium and lead accumulation and low-molecular-weight organic acids secreted by roots in an intercropping of a cadmium accumulator *Sonchus asper* L. with *Vicia faba* L," *RSC Advances*, vol. 6, no. 40, pp. 33240–33248, 2016.

[8] L. Y. Lin, X. L. Yan, X. Y. Liao, Y. X. Zhang, and X. Ma, "Arsenic accumulation in *Panax notoginseng* monoculture and intercropping with *Pteris vittata*," *Water, Air, and Soil Pollution*, vol. 226, no. 4, p. 113, 2015.

[9] S. Q. Wang, S. H. Wei, D. D. Ji, and J. Y. Bai, "Co-planting Cd-contaminated field using hyperaccumulator *Solanum nigrum* L. through interplant with low accumulation welsh onion," *International Journal of Phytoremediation*, vol. 17, no. 9, pp. 879–884, 2015.

[10] X. M. Wan, M. Lei, T. B. Chen, and J. X. Yang, "Intercropped *Pteris vittata* L. and *Morus alba* L. presents a safe utilization mode for arsenic-contaminated soil," *Science of the Total Environment*, vol. 579, pp. 1467–1475, 2016.

[11] C. Li, Y. Dong, H. Li, J. Shen, and F. Zhang, "The dynamic process of interspecific interactions of competitive nitrogen capture between intercropped wheat (*Triticum aestivum* L) and faba bean (*Vicia faba* L.)," *PLoS One*, vol. 9, no. 12, Article ID e115804, 2014.

[12] Y. M. Zuo, X. L. Li, Y. P. Cao, and F. S. Zhang, "Effect of maize/peanut intercropping on iron nutrition of peanut," *Plant Nutrition and Fertilizer Science*, vol. 3, no. 2, pp. 153–159, 1997.

[13] H. E. Dessougi, A. Z. Dreele, and N. Claassen, "Growth and phosphorus uptake of maize cultivated alone in mixed culture with other crops or after incorporation of their residues," *Journal of Plant Nutrition and Soil Science*, vol. 166, no. 2, pp. 254–261, 2003.

[14] H. Hauggaard-Nielsen, M. Gooding, P. Ambus et al., "Pea-barley intercropping for efficient symbiotic N_2-fixation, soil N acquisition and use of other nutrients in European organic cropping systems," *Field Crops Research*, vol. 113, no. 1, pp. 64–71, 2009.

[15] C. J. Li, Y. Y. Li, C. B. Yu et al., "Crop nitrogen use and soil mineral nitrogen accumulation under different crop combination and patterns of strip intercropping in northwest China," *Plant and Soil*, vol. 342, no. 1-2, pp. 221–231, 2011.

[16] T. Gunther, U. Dornberger, and W. Fritsche, "Effects of ryegrass on biodegradation of hydrocarbons in soil," *Chemosphere*, vol. 33, no. 2, pp. 203–215, 1996.

[17] S. A. Cheema, M. I. Khan, C. F. Shen et al., "Degradation of phenanthrene and pyrene in spiked soils by single and combined plants cultivation," *Journal of Hazardous Materials*, vol. 177, no. 1–3, pp. 384–389, 2010.

[18] L. Meng, M. Qiao, and H. P. H. Arp, "Phytoremediation efficiency of a PAH-contaminated industrial soil using ryegrass, white clover, and celery as mono- and mixed cultures," *Journal of Soils and Sediments*, vol. 11, no. 3, pp. 482–490, 2011.

[19] K. Wang, H. G. Huang, Z. Q. Zhu et al., "Phytoextraction of metals and rhizoremediation of PAHs in co-contaminated soil by co-planting of *Sedum alfredii* with ryegrass (*Lolium perenne*) or castor (*Ricinus communis*)," *International Journal of Phytoremediation*, vol. 15, no. 3, pp. 283–298, 2012.

[20] M. Arienzo, P. Adamo, and V. Cozzolino, "The potential of *Lolium perenne* for revegetation of contaminated soil from a metallurgical site," *Science of the Total Environment*, vol. 319, no. 1–3, pp. 13–25, 2004.

[21] J. T. Si, B. G. Tian, H. T. Wang, B. Nicholas, S. Jackie, and C. Mark, "Assessing availability, phytotoxicity and bioaccumulation of lead to ryegrass and millet based on 0.1 mol/L $Ca(NO_3)_2$ extraction," *Journal of Environmental Sciences*, vol. 18, pp. 958–963, 2006.

[22] H. Dai and G. Jia, "Effects of Se on the growth, tolerance, and antioxidative systems of three alfalfa cultivars," *Environmental Science and Pollution Research*, vol. 24, no. 6, pp. 1–6, 2017.

[23] T. Thayalkumaran, B. H. Robinson, I. Vogeler, D. R. Scotter, B. E. Clothier, and H. J. Percival, "Plant uptake and leaching of copper during EDTA-enhanced phytoremadiation of repacked and undisturbed soil," *Plant and Soil*, vol. 254, no. 2, pp. 415–423, 2003.

[24] S. K. Dong, M. Y. Kang, and X. J. Yun, "Economic comparison of forage production from annual crops, perennial pasture and native grassland in the alpine region of the Qinghai-Tibetan Plateau, China," *Grass and Forage Science*, vol. 62, no. 4, pp. 405–415, 2007.

[25] S. Buckingham, E. Tipping, and J. Hamilton-Taylor, "Dissolved organic carbon in soil solutions: a comparison of collection methods," *Soil Use and Management*, vol. 24, no. 1, pp. 29–36, 2008.

[26] K. Yan, W. Chen, G. Y. Zhang et al., "Elevated CO_2 ameliorated oxidative stress induced by elevated O_3 in *Quercus mongolica*," *Acta Physiologiae Plantarum*, vol. 32, no. 2, pp. 375–385, 2010.

[27] S. Y. Guan, *Soil Enzyme and its Research Approaches*, China Agriculture Press, Beijing, China, 1986, in Chinese.

[28] F. Eivazi and M. A. Tabatabai, "Phosphatases in soils," *Soil Biology and Biochemistry*, vol. 9, no. 3, pp. 167–172, 1977.

[29] F. Eivazi and M. A. Tabatabai, "Glucosidases and galactosidases in soils," *Soil Biology and Biochemistry*, vol. 20, no. 5, pp. 601–606, 1988.

[30] Y. X. Chen, F. S. Zhang, and L. Tang, "Wheat powdery mildew and foliar N concentration as influenced by N fertilization and belowground interactions with intercropped with faba bean," *Plant and Soil*, vol. 291, no. 1-2, pp. 1–13, 2007.

[31] J. W. Huang, J. J. Chen, W. R. Berti, and S. D. Cunningham, "Phytoremediation of lead-contaminated soils: role of synthetic chelates in lead phytoextraction," *Environmental Science and Technology*, vol. 31, no. 3, pp. 800–805, 1997.

[32] Y. H. Chen, Z. G. Shen, and X. D. Li, "The use of vetiver grass (*Vetiveria zizanioides*) in the phytoremediation of soils contaminated with heavy metals," *Applied Geochemistry*, vol. 19, no. 10, pp. 1553–1565, 2004.

[33] T. Li, W. H. Xu, Y. R. Chai, Z. Y. Wang, and D. T. Xie, "Differences of Cd uptake and expression of Cd-tolerance related genes in two varieties of ryegrasses," *Bulgarian Chemical Communications*, vol. 49, no. 9, pp. 697–705, 2017.

[34] L. Liu, L. L. Hu, J. J. Tang, Y. F. Li, Q. Zhang, and X. Chen, "Food safety assessment of planting patterns of four vegetable-type crops grown in soil contaminated by electronic waste activities," *Journal of Environmental Management*, vol. 93, no. 1, pp. 22–30, 2012.

[35] F. Zhang, X. Wan, and Y/ Zhong, "Nitrogen as an important detoxification factor to cadmium stress in poplar plants," *Journal of Plant Interactions*, vol. 9, no. 1, pp. 249–258, 2013.

[36] J. H. Xue and Y. X. Fei, "Effects of intercropping *Cunninghamia lanceolata* in tea garden on contents and distribution of heavy metals in soil and tea leaves," *Journal of Ecology and Rural Environment*, vol. 22, no. 4, pp. 71–74, 2006.

[37] M. B. Hinojosa, J. A. Carreira, J. M. Rodríguez-Maroto, and R. García-Ruíz, "Effects of pyrite sludge pollution on soil enzyme activities: ecological dose–response model," *Science of the Total Environment*, vol. 369, no. 2-3, pp. 89–99, 2008.

[38] Y. Gao, P. Zhou, L. Mao, Y. E. Zhi, C. H. Zhang, and W. J. Shi, "Effects of plant species coexistence on soil enzyme activities and soil microbial community structure under Cd and Pb combined pollution," *Journal of Environmental Sciences*, vol. 22, no. 7, pp. 1040–1048, 2010.

[39] L. C. Fang, Y. Q. Liu, H. X. Tian, H. S. Chen, and Y. Q. Wang, "Proper land use for heavy metal-polluted soil based on enzyme activity analysis around a Pb-Zn mine in Feng County, China," *Environmental Science and Pollution Research*, vol. 24, no. 36, pp. 28152–28164, 2017.

[40] S. Saha, V. Prakash, S. Kundu, N. Kumar, and B. L. Mina, "Soil enzymatic activity as affected by long term application of farm yard manure and mineral fertilizer under a rainfed soybean wheat system in N-W Himalaya," *European Journal of Soil Biology*, vol. 44, no. 3, pp. 309–315, 2008.

[41] S. M. Li, L. Li, F. S. Zhang, and C. Tang, "Acid phosphatase role in chickpea/maize intercropping," *Annals of Botany*, vol. 94, no. 2, pp. 297–303, 2004.

[42] C. J. Duan, L. C. Fang, C. L. Yang, W. B. Chen, Y. X. Cui, and S. Q. Li, "Reveal the response of enzyme activities to heavy metals through in situ zymography," *Ecotoxicology and Environmental Safety*, vol. 156, pp. 106–115, 2018.

[43] J. Chen, W. H. Wang, T. W. Liu, F. H. Wu, and H. L. Zheng, "Photosynthetic and antioxidant responses of *Liquidambar formosana* and *Schima superba* seedlings to sulfuric-rich and nitric-rich simulated acid rain," *Plant Physiology and Biochemistry*, vol. 64, no. 5, pp. 41–51, 2013.

[44] R. Mittler, "Oxidative stress, antioxidants and stress tolerance," *Trends in Plant Science*, vol. 7, no. 9, pp. 405–410, 2002.

[45] U. H. Cho and N. H. Seo, "Oxidative stress in Arabidopsis thaliana exposed to cadmium is due to hydrogen peroxide accumulation," *Plant Science*, vol. 168, no. 1, pp. 113–120, 2005.

[46] M. Hojati, S. A. Modarressanavy, S. T. Enferadi et al., "Cadmium and copper induced changes in growth, oxidative metabolism and terpenoids of *Tanacetum parthenium*," *Environmental Science and Pollution Research*, vol. 24, no. 13, pp. 1–12, 2017.

[47] F. Morina, L. Jovanović, L. Prokić, and S. Veljovićjovanović, "Physiological basis of differential zinc and copper tolerance of *Verbascum* populations from metal-contaminated and uncontaminated areas," *Environmental Science and Pollution Research*, vol. 23, no. 10, pp. 10005–10020, 2016.

[48] S. Verma and R. S. Dubey, "Lead toxicity induces lipid peroxidation and alters the activities of antioxidant enzymes in growing rice plants," *Plant Science*, vol. 164, no. 4, pp. 645–655, 2003.

Hindawi
Journal of Chemistry
Volume 2018, Article ID 2049353, 13 pages
https://doi.org/10.1155/2018/2049353

Research Article

Spatial Distribution and Contamination Assessment of Heavy Metals in Surface Sediments of the Caofeidian Adjacent Sea after the Land Reclamation, Bohai Bay

He Zhu,[1,2,3] Haijian Bing,[1] Huapeng Yi,[2] Yanhong Wu,[1] and Zhigao Sun[4]

[1]*Key Laboratory of Mountain Surface Processes and Ecological Regulation, Institute of Mountain Hazards and Environment, Chinese Academy of Sciences, Chengdu 610041, China*
[2]*School of Resources and Environmental Engineering, Ludong University, Yantai 264025, China*
[3]*University of Chinese Academy of Sciences, Beijing 100049, China*
[4]*Key Laboratory of Humid Subtropical Eco-Geographical Process (Fujian Normal University), Ministry of Education, Fuzhou 350007, China*

Correspondence should be addressed to Yanhong Wu; yanhong_wu@yeah.net and Zhigao Sun; zhigaosun@163.com

Received 5 January 2018; Accepted 12 March 2018; Published 22 April 2018

Academic Editor: Ana Moldes

Land reclamation can significantly influence spatial distribution of heavy metals in inshore sediments. In this study, the distribution and contamination of heavy metals (Cd, Cr, Cu, Ni, Pb, and Zn) in inshore sediments of Bohai Bay were investigated after the land reclamation of Caofeidian. The results showed that the concentrations of Cd, Cr, Cu, Ni, Pb, and Zn in the sediments were 0.20–0.65, 27.16–115.70, 11.14–39.00, 17.37–65.90, 15.08–24.06, and 41.64–139.56 mg/kg, respectively. These metal concentrations were generally higher in the area of Caofeidian than in other Chinese bays and estuaries. Spatially, the concentrations of Cd, Cr, Cu, Ni, and Zn were markedly lower in the sediments close to Caofeidian compared with other regions, whereas the concentrations of Pb showed an opposite case. Hydrodynamic conditions after the land reclamation were the major factor influencing the distribution of heavy metals in the sediments. Grain sizes dominated the distribution of Cu and Zn, and organic matters and Fe/Mn oxides/hydroxides also determined the distribution of the heavy metals. Multiple contamination indices showed that the inshore sediments were moderately to highly contaminated by Cd and slightly contaminated by other heavy metals. Similarly, Cd showed a high potential ecorisk in the sediments, and other metals were in the low level. Chromium contributed to higher exposure toxicity than other metals by the toxicity unit and toxic risk index. The results of this study indicate that after the land reclamation of Caofeidian the contamination and ecorisk of heavy metals in the sediments markedly decreased in the stronger hydrodynamic areas.

1. Introduction

Heavy metal contamination is a major issue in marine environment due to the toxicity, persistence, nonbiodegradability, and bioaccumulation [1–3]. After entering food chain, they can cause potential threat to human beings and other organisms [4]. In aquatic systems, sediments are the main sink of various contaminants discharged from industrial and agricultural processes [5–7], and they are regarded as an effective archive recording heavy metal contamination [2, 8, 9]. To date, a large number of studies have reported the accumulation of heavy metals in the sediments of aquatic ecosystems [3, 10–13]. The main reason is that once the conditions of sedimentary environment change, heavy metals are apt to release into water from the sediments [14–16]. Therefore, it is necessary to understand the characteristics of heavy metals in aquatic sediments and assess their contamination states.

The coastal zone is one of the most frequent areas disturbed by human activities through plant and port construction, land reclamation, and tourism [1, 17–19]. Human activities, on the one hand, will increase the loadings of heavy metals in the aquatic system through direct industrial discharge, city sewage, domestic runoff, and so forth [20–22];

on the other hand, they can change pristine sedimentary environment which may contribute to the release of heavy metals from sediments. Among these human activities, land reclamation engineering is significant to influence aquatic environment [23–25]. It not only alters the hydrodynamic conditions surrounding the land but also may increase inputs of heavy metals through sewage discharge and shipping after the engineering. The distribution of heavy metals and their controlling factors in sediments of coastal zone still need to be explored under the land reclamation.

The toxicity of heavy metals is the priority in aquatic ecosystems [26–28]. In order to control the contamination of marine sediments and protect marine biological resources, China, USA, Canada, and other countries have established the standard of marine sediment quality for heavy metals [29, 30]. Meanwhile, various methods have been applied to assess the contamination and ecorisk of heavy metals in sediments, including enrichment factor [31, 32], index of geoaccumulation [33, 34], toxic units and toxic risk index [35], and potential ecorisk index [22, 36]. However, each method has its limitation or specialization, and thus it is necessary to use multiple methods in order to accurately obtain the contamination and ecorisk states of heavy metals in sediments [11, 15].

Bohai Bay is located in the western Bohai Sea. Due to the weak exchange capacity of the water in Bohai Bay, the contaminants from surrounding industrial cities are not easy to spread. Recently, the Bohai Bay has been regarded as a main region of contaminant accumulation, especially in the sediments [37–39]. These studies investigated the distribution of heavy metals and assessed their contamination, and the results showed that human activates increased the accumulation of heavy metals in the sediments of Bohai Bay [25, 40]. However, most of the studies were conducted in the areas of Tianjin Port [41, 42], whereas there are very few reports about the distribution and contamination states of heavy metals in the sediments of northern Bohai Bay. This limits our understanding of heavy metal distribution in the entire area of Bohai Bay. More importantly, the large-scale reclamation project has been finished in Caofeidian for few years. This engineering certainly influences the environment conditions of inshore and adjacent marine area. Whether the land reclamation causes significant difference of the distribution and contamination of heavy metals in the sediments around Caofeidian deserves to be explored.

In this study, the surface sediments in the coastal areas of Caofeidian were collected to analyze the concentrations of heavy metals (Cd, Cr, Cu, Ni, Pb, and Zn). The main objectives are (1) to investigate distribution characteristics of these heavy metals in the sediments, (2) to explore the possible controlling factors for their spatial distributions, and (3) to assess the contamination and potential ecological risk of the heavy metals. This is the first time to reveal the distribution of heavy metal contamination in the surface sediments of Caofeidian after the land reclamation project.

2. Materials and Methods

2.1. Study Area. Caofeidian is located in the northern Bohai Bay (38°58′52″–38°54′42″N, 118°33′36″–118°30′03″E, Figure 1). It is surrounded by Hebei province and Tianjin City on the north and west, respectively. Hai River, Luan River, Yongding River, and other small rivers discharge water into the inshore and adjacent areas of Caofeidian. Laolonggou, located in the eastern Caofeidian, is the ancient Luanhe River with previous tidal channel [43]. The study area has complex geomorphic types with a large number of sandbanks distributed in this area. The average water depth around the Caofeidian is approximately 30 m (Figure 1), and the deepest site (B20) reaches approximately 36 m due to the strong hydrodynamic conditions. Due to the presence of sandbanks and deep water depth, a large-scale reclamation project has been implemented in Caofeidian in 2003, and the project is basically finished in 2011. Now it becomes one of the busiest ports in the Bohai Sea with a cargo throughput of >5 billion tons in 2014 [28].

2.2. Sample Collection. The sampling was carried out in August 2014. Twenty-two sampling sites in the inshore and adjacent areas of Caofeidian were selected to collect the surface sediments (Figure 1). At each site, the sediment samples were collected using a gravity sampler, and then the surface sediments (0–5 cm) were sliced by a plastic spatula in the field. The samples were put in polyethylene bags and stored at −20°C for further analysis. In laboratory, the sediment samples were freeze-dried. The samples for the grain size analysis passed through 2 mm sieves, and those for the analysis of total organic carbon (TOC) and elements passed through 100-mesh Nylon screen.

2.3. Chemical Analysis. The grain sizes of the surface sediments were measured by a Mastersizer-2000 laser particle size analyzer (Malvern, UK) after removal of organic matters with 30% H_2O_2 with the dispersion of sodium hexametaphosphate. Three classes of grain sizes were divided into clay (<4 μm), silt (4–63 μm), and sand (>63 μm). The concentrations of TOC in the sediments were measured by subtracting the inorganic carbon from the total carbon, which was determined by a Shimadzu TOC-VCPH/SSM-5000A and Elementar vario MACRO cube CHNS analyzer, respectively.

The concentrations of metals in the sediments were measured according to the method of Gao and Chen [23]. Briefly, approximately 0.1 g samples were digested in Teflon Vessel with the mixed concentrated acids of HF-HNO_3-$HClO_4$ (5 : 2 : 1) and then heated (140–150°C) to dryness. The residue was digested with HNO_3 again. At the end, the extraction was diluted to 50 mL volume. The concentrations of Fe and Mn were measured by an inductively coupled plasma atomic emission spectrometer (ICP-AES), and those of Cd, Cr, Cu, Ni, Pb, and Zn were detected by an inductively coupled plasma mass spectroscopy (ICP-MS). Quality assurance and control were evaluated using duplicates, blanks, and standard reference materials (GBW 07401) from the National Research Center for Standards in China. According to the measurement of the repeated samples and reference materials, the relative standard deviation was below 3% for ICP-AES and below 5% for ICP-MS, respectively. The recovery of the reference materials was 95.3%–107.3%.

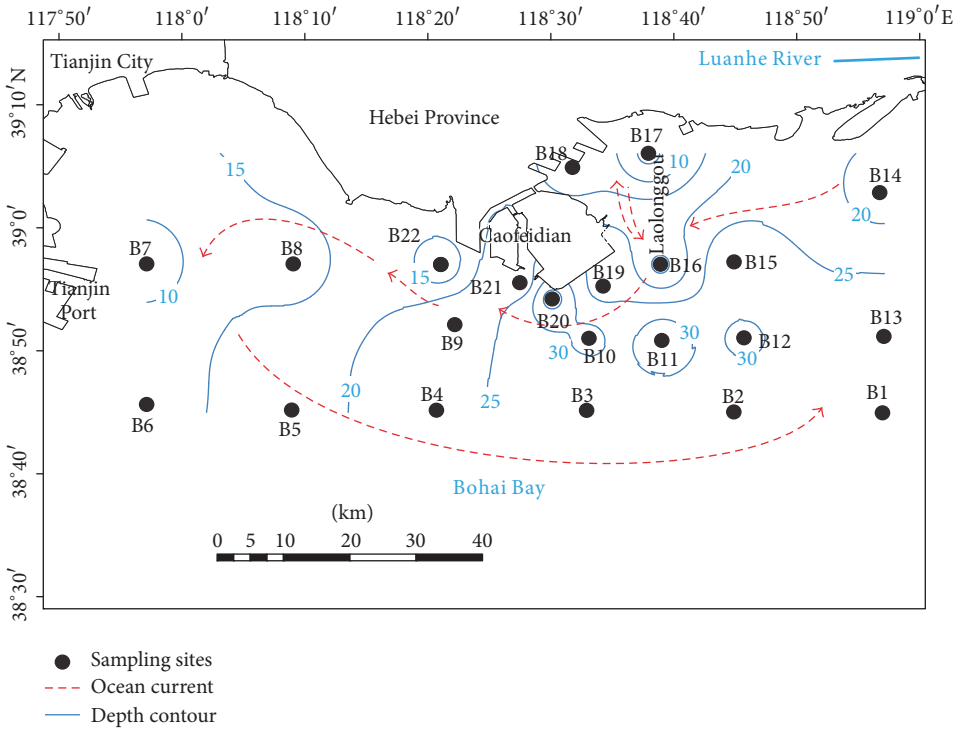

FIGURE 1: The location of the study area and the sampling sites in the Bohai Bay.

2.4. Calculation of Contamination and Ecorisk Indices

2.4.1. Enrichment Factors (EFs). The EFs of heavy metals in the sediments are calculated as follows [11]:

$$\mathrm{EF} = \frac{(\mathrm{Me/Fe})_{\mathrm{sample}}}{(\mathrm{Me/Fe})_{\mathrm{background}}}, \tag{1}$$

where $(\mathrm{Me/Fe})_{\mathrm{sample}}$ is the concentration ratio of a metal to Fe in a sample and $(\mathrm{Me/Fe})_{\mathrm{background}}$ is the corresponding ratio in the background.

2.4.2. Geoaccumulation Index. The geoaccumulation index (I_{geo}) is another indicator used to assess the contamination of heavy metals in sediments [33]:

$$I_{\mathrm{geo}} = \log_2\left(\frac{C_n}{k \times B_n}\right), \tag{2}$$

where C_n is the concentration of a metal measured in a sample, B_n is the geochemical background of the metal, and k is a background matrix correction factor (1.5) due to lithogenic effects [31]. The contamination classes of I_{geo} are classified as $I_{\mathrm{geo}} \leq 0$, uncontaminated; $0 < I_{\mathrm{geo}} \leq 1$, uncontaminated to moderately contaminated; $1 < I_{\mathrm{geo}} \leq 2$, moderately contaminated; $2 < I_{\mathrm{geo}} \leq 3$, moderately to heavily contaminated; $3 < I_{\mathrm{geo}} \leq 4$, heavily contaminated; $4 < I_{\mathrm{geo}} \leq 5$, heavily to extremely contaminated; $I_{\mathrm{geo}} > 5$, extremely contaminated [33].

2.4.3. Potential Ecorisk Index (E_r^i). The potential ecorisk index is commonly used to assess the ecorisk of heavy metals in sediments [36]:

$$E_r^i = T_r^i * \frac{C_o^i}{C_n^i},$$
$$\mathrm{RI} = \sum_{i=1}^{n} E_r^i, \tag{3}$$

where E_r^i is the potential ecorisk index, T_r^i is the toxic response coefficient of a given metal, C_o^i is the concentration of a metal measured in a sample, and C_n^i is its geochemical background. The toxic response coefficient of Cd, Cr, Cu, Ni, Pb, and Zn is 30, 2, 5, 2, 5, and 1, respectively. The potential ecorisk level of heavy metals in sediments is classified as $E_r^i \leq 40$, low; $40 < E_r^i \leq 80$, moderate; $80 < E_r^i \leq 160$, high; $160 < E_r^i \leq 320$, very high; $E_r^i > 320$, extremely high. The risk classes of RI are classified as <150, low risk; 150–300, moderate risk; 300–600, considerable risk; ≥600, disastrous risk [39].

2.4.4. The Toxic Units (TUs) and Toxic Risk Index (TRI). The TU defined by Pedersen et al. [48] is the ratio of a metal concentration to the probable effects level (PEL). ∑TUs is the sum of the ratio of six heavy metals to PEL. These indices can assess heavy metal toxicity relative to the standard. ∑TUs < 4 represents nontoxicity and ∑TUs > 6 represents acute toxicity:

Table 1: The concentrations of heavy metals and physiochemical properties in the sediments.

	Unit	Max	Min	Average
Cd	mg/kg	0.65	0.20	0.34
Cr	mg/kg	115.70	27.16	85.59
Cu	mg/kg	39.00	11.14	28.82
Ni	mg/kg	65.90	17.37	41.35
Pb	mg/kg	24.06	15.08	21.02
Zn	mg/kg	139.56	41.64	88.64
Fe	mg/g	50.02	20.72	37.09
Mn	mg/kg	868.15	302.49	571.33
Clay	%	17.91	7.67	13.05
Slit	%	80.52	37.71	63.42
Sand	%	54.62	3.29	23.53
TOC	%	0.95	0.26	0.72

$$\sum \mathrm{TUs} = \sum_{i=1}^{n} \frac{C_s^i}{C_{\mathrm{PEL}}^i}. \quad (4)$$

The TRI is used to assess the integrated toxic risk based on the threshold effect level (TEL) and PEL of heavy metals [26]:

$$\mathrm{TRI} = \sqrt{\frac{\left(C_s^i/C_{\mathrm{TEL}}^i\right)^2 + \left(C_s^i/C_{\mathrm{PEL}}^i\right)^2}{2}}, \quad (5)$$

where C_s^i is the concentration of a metal measured in the sample, and C_{TEL}^i and C_{PEL}^i are the TEL and PEL of the metal, respectively. The TRI can be classified as no toxic risk (TRI < 5), low toxic risk (5 ≤ TRI < 10), moderate toxic risk (10 ≤ TRI < 15), considerable toxic risk (15 ≤ TRI < 20), and very high toxic risk (TRI ≥ 20).

2.5. Statistical Analysis. Pearson correlation analysis was applied to establish the relationships between heavy metals and sediment physiochemical properties by the software package SPSS 16.0 for Windows. The spatial distribution characteristics of heavy metals and physiochemical properties in the sediments were performed by the software ArcGIS 10.2 with the method of inverse distance weighted (IDW).

3. Results and Discussion

3.1. Sediment Physiochemical Properties. The composition of grain sizes showed the order of silt (37.71–80.41%, average: 63.42%) > sand (3.29–54.62%, 23.53%) > clay (7.39–17.91%, 13.05%) (Table 1). Spatially, clay and silt presented a similar distribution pattern (Figure 2). The lower contents of silt and clay were observed in the Laolonggou, compared with other regions, whereas the higher contents occurred in the western Caofeidian and the central Bohai Bay. The spatial distribution of sand generally showed the opposite case to that of clay and silt.

The concentrations of TOC varied between 0.26% and 0.95% with the average of 0.72% (Table 1). The concentrations of TOC were relatively lower in the eastern Caofeidian than in other areas, and the highest was observed in the central Bohai Bay (Figure 2). The concentrations of Fe and Mn varied between 50.02 and 20.72 (average: 37.09, g/kg) and between 302.49 and 868.15 (average: 571.33, mg/kg), respectively (Table 1). The concentrations of Fe and Mn were lower in the eastern and western Caofeidian than in the central Bohai Bay (Figure 2).

3.2. The Concentrations of Heavy Metals in the Sediments. The concentrations of heavy metals in the sediments are presented in Table 1. Specifically, the concentrations (mg/kg) varied between 0.20 and 0.65 (average: 0.36) for Cd, between 27.16 and 115.70 (78.64) for Cr, between 11.14 and 39.00 (29.07) for Cu, between 17.37 and 65.90 (41.35) for Ni, between 15.08 and 24.06 (21.11) for Pb, and between 41.64 and 139.56 (89.60) for Zn. The concentrations of all the heavy metals in the sediments exceeded their background standards in the upper continental crust (Table 2). Compared with some bays and estuaries in China, the Cd concentrations in the inshore sediments of Caofeidian were higher except for the Liaodong Bay (Table 2). For other heavy metals, their concentrations in our study area were generally higher than those in other estuaries.

The distribution of heavy metals in the sediments displayed significantly different spatial patterns (Figure 3). The concentrations of Cd in the sediments were generally lower in the surrounding areas of Caofeidian relative to the southeastern and southwestern area. The similar distribution of Cr, Cu, Ni, and Zn was observed spatially, and their lower concentrations occurred in the eastern and western Caofeidian compared with other areas. The distribution of Pb in the sediments showed that its concentrations were markedly higher in the inshore areas of Caofeidian and the central Bohai Bay compared with the western study area.

3.3. Factors Controlling the Distribution of Heavy Metals. Hydrodynamic conditions are a main factor influencing the distribution of heavy metals in the sediments. The concentrations of heavy metals except for Pb were higher in the central Baohai Bay compared with those in the western and eastern Caofeidian (Figure 3). The oceanic current in the northern

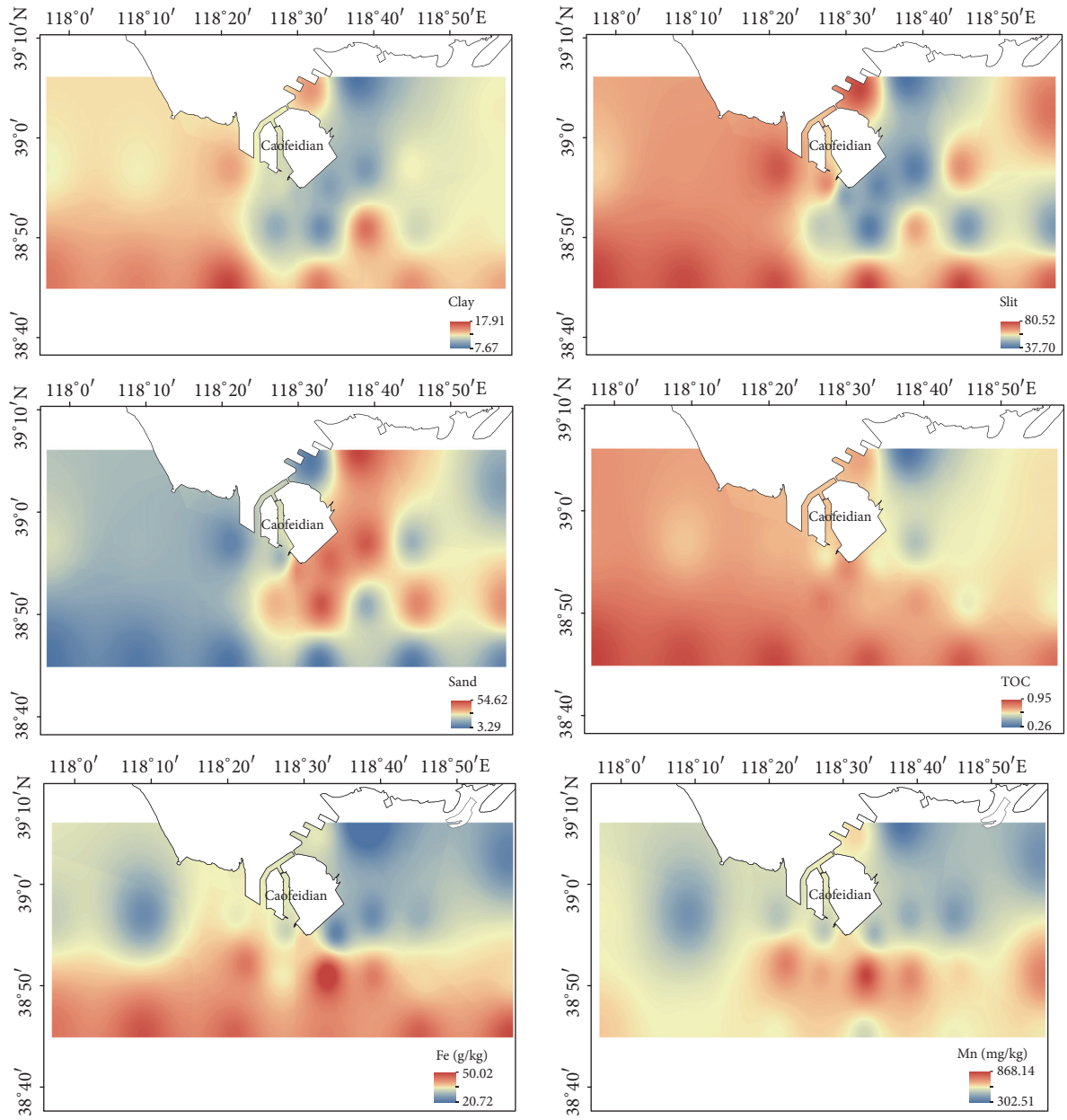

Figure 2: The spatial distribution of grain sizes, TOC, Fe, and Mn in the sediments.

Bohai Bay has been observed flowing from east to west [49]. The land reclamation of Caofeidian blocks the oceanic current which should have passed through the Caofeidian area before the reclamation project. The channel of the oceanic current becomes narrow in the northern Bohai Bay, resulting in much erosion in the Laolonggou area (Figure 1), and then the current enters the cape of Caofeidian [24, 49]. The variation of the hydrodynamic conditions around the Caofeidian cape led to the fine particles washed out and hard to deposit in the eastern area and the cape of Caofeidian [43]. This was a major reason for the low distribution of heavy metals in the eastern area and the cape of Caofeidian. With the flow of the oceanic current forward, the hydrodynamic conditions became weakened which favored the sediment deposition and then the heavy metal accumulation in the western Caofeidian.

The results of Pearson correlation analysis showed that Cu and Zn correlated significantly with clay and silt ($p < 0.05$, Table 3). The concentrations of heavy metals in sediments increase with decreasing particle because the fine-grained sediments tend to adsorb much more heavy metals due to their high specific surface area [50, 51]. The fine particles were markedly observed in the western Caofeidian and the central Bohai Bay compared with the Laolongou and the cape of Caofeidian (Figure 2). Lu et al. (2009) also reported that the grain sizes of the sediments in the study area decreased from the eastern to western Caofeidian [24]. The tidal current induced the runoff and sorting of the sediments

Table 2: The concentrations of heavy metals in the sediments of Caofeidian adjacent sea and other reports (Unit: mg/kg). The concentrations using to assess the contamination of heavy metals are also shown.

	Cd	Cr	Cu	Ni	Pb	Zn	
Caofeidian inshore	0.19–0.65 0.36	27.16–115.70 78.64	11.14–39.01 29.07	17.37–65.90 41.35	15.08–24.06 21.11	41.64–139.56 89.60	This study
Intertidal Bohai Bay	0.12	68.6	24	28	25.1	73	[10]
Laizhou Bay	0.12	60	22	-	21.9	60.4	[44]
Coastal Bohai bay	0.22	101.4	38.5	40.7	34.7	131.1	[22]
Liaodong Bay	1.2	46.4	19.4	22.5	31.8	71.7	[7]
Luan River Estuary	0.09	41.14	17.17	15.6	30.98	44.63	[28]
Yangtze River Estuary	0.19	79.1	24.7	31.9	23.8	82.9	[15]
Yangtze River Estuary	0.15	34.64	17.46	-	30.47	66.91	[45]
Background (UCC)	0.10	35	25	20	20	71	[46]
Class-1	0.50	80	35	-	60	150	[30]
Class-2	1.5	150	100	-	130	350	
Class-3	5.00	280	200	-	250	600	
TEL	0.68	52.3	18.7	15.9	30.2	124	[47]
PEL	4.21	160	108	42.8	112	271	

UCC: upper continental crust; TEL (threshold effect level): guideline values indicate the metal concentrations below which adverse effects on biota are rarely observed; PEL (probable effects level): guideline values indicate the metal concentrations above which adverse effects on biota are probably observed.

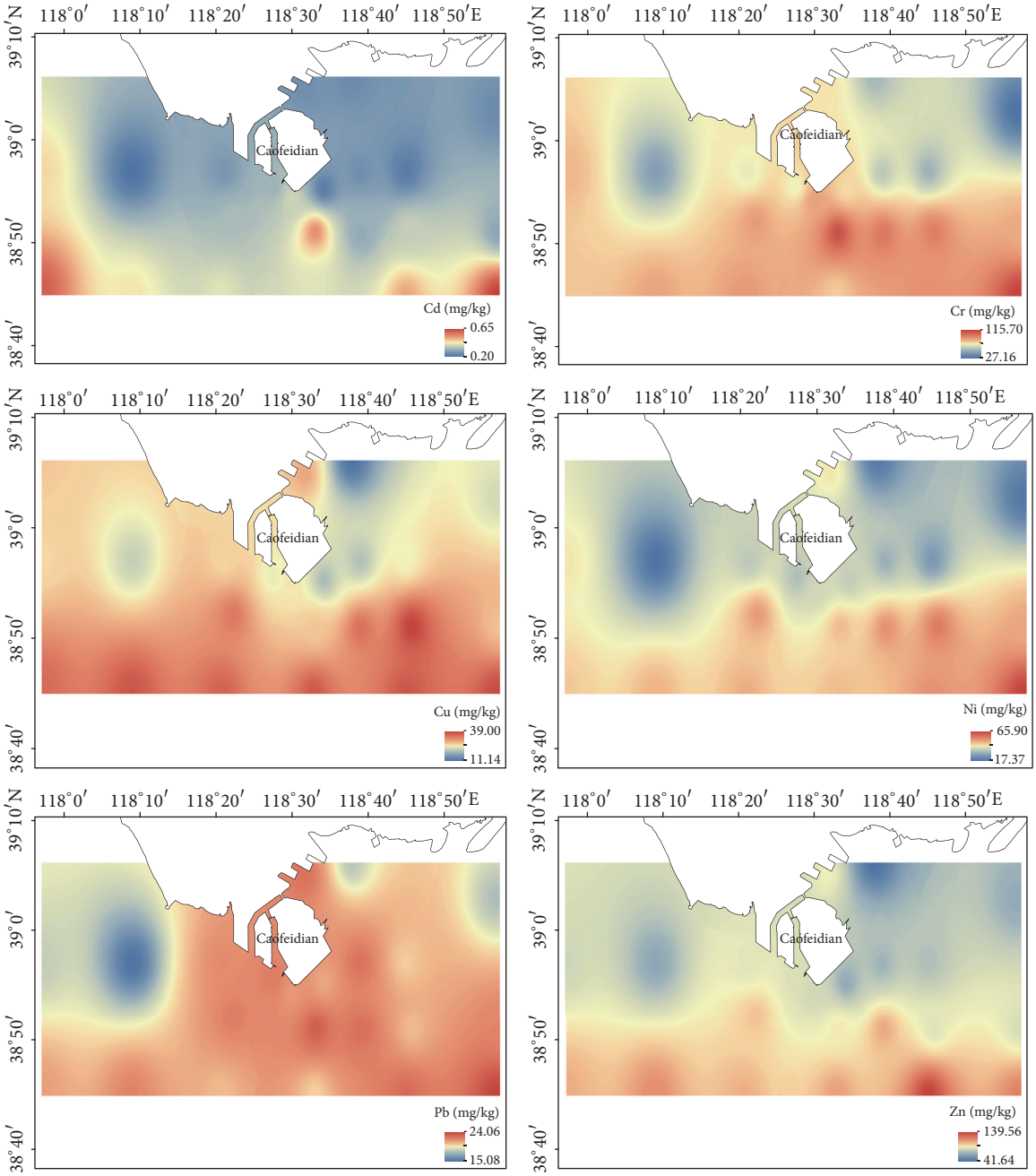

Figure 3: The spatial distribution of heavy metals in the sediments.

[52, 53]. As a result, the concentrations of Cu and Zn in the sediment showed the higher values in the western Caofeidian and the central Bohai Bay than in the Laolonggou and the cape of Caofeidian. However, other heavy metals did not show significant relationships with the fine particles, which indicated that other factors determined their distribution in the sediments.

Organic matters and Fe/Mn oxides/hydroxides were considered as the controlling factors in the spatial distribution of heavy metals in the sediments. Organic matters can regulate the geochemical behavior of heavy metals via adsorption, desorption, and complexation [54]. In our study, Cd, Cr, Cu, Ni, and Zn in the sediments showed a significant positive correlation with TOC ($p < 0.05$, Table 3), which indicated that the adsorption and/or complexation of the organic matters might control the distribution of these metals in the sediments. However, there was a clear spatial difference of the distribution between TOC and heavy metals in the western Caofeidian. This indicated that organic matters were not the major controlling factor in the distribution of the heavy metals in this area. The Fe/Mn oxides/hydroxides coated on clay minerals or in individual minerals are important carriers of heavy metals. In this study, the heavy metals in the sediments correlated significantly with Fe and Mn ($p < 0.01$,

Table 3: Pearson correlation of heavy metals with physicochemical properties in the sediments.

	Mn	Fe	Cd	Cr	Cu	Ni	Pb	Zn	Clay	Slit	Sand	TOC
Mn	1											
Fe	0.80**	1										
Cd	0.52*	0.77**	1									
Cr	0.81**	0.82**	0.71**	1								
Cu	0.60**	0.86**	0.64**	0.68**	1							
Ni	0.77**	0.84**	0.71**	0.92**	0.86**	1						
Pb	0.61**	0.63**	0.45*	0.69**	0.47*	0.69**	1					
Zn	0.57**	0.89**	0.71**	0.68**	0.90**	0.81**	0.60**	1				
Clay	0.16	0.51*	0.32	0.21	0.70**	0.42	0.14	0.68**	1			
Slit	−0.09	0.35	0.27	−0.04	0.53*	0.17	0.02	0.58**	0.88**	1		
Sand	0.06	−0.38	−0.28	0.01	−0.56**	−0.21	−0.04	−0.61**	−0.91**	−1.00**	1	*
TOC	0.47*	0.80**	0.64**	0.50*	0.81**	0.61**	0.30	0.85**	0.76**	0.68**	−0.70**	1

**Correlation is significant at the 0.01 level (two-tailed); *Correlation is significant at the 0.05 level (two-tailed).

Table 3), and spatially the distribution of heavy metals was in agreement with that of Fe and Mn. This indicated that the Fe/Mn oxides/hydroxides played an important role in the distribution of heavy metals, especially in the western Caofeidian.

As shown in Figure 3, the distribution of Pb in the sediments was different from that of other heavy metals. Besides the factors of hydrodynamic conditions and Fe/Mn oxides/hydroxides, the accumulation of Pb in the sediments could be attributed to its sources. In the coastal area of Caofeidian, the ancient Luanhe River alluvium contains a high geological background of Pb [55]. Thus, the erosion of land materials may be a reason for the different distribution of Pb from other metals in the sediments. Moreover, the Luanhe River is the main input river to the Caofeidian areas, and the concentration of Pb in the sediments of Luanhe River was higher than that in other rivers surrounding Bohai Bay (Table 2). This is why the concentration of Pb was markedly higher in the sediments of eastern Caofeidian (Figure 3). In addition, a large number of steel and chemical plants and the Caofeidian Port were established after the land reclamation of Caofeidian. The industrial emissions from electroplating materials and paint coatings for corrosion protection as well as shipping contaminants further induced the complex distribution of Pb in the sediments [56].

3.4. Contamination and Risk Assessment of Heavy Metals in the Sediments

3.4.1. Contamination Assessment of Heavy Metals. Sediment quality guidelines (SQGs) have been widely applied to assess the metal contamination levels in sediments. The contamination states of heavy metals in the study area were determined by comparing the metal levels in the sediments of the Chinese Marine Sediment Quality (GB 18668-2002) [30] and the TEL/PEL SQGs [53, 54] (Table 2). The results showed that the concentrations of Cd, Pb, and Zn in the sediments were blew Class 1 accounted for 100% of the total sampling sites. There were 54.5% and 31.8% sampling sites with the concentrations of Cr and Cu varying Class 1 and Class 2. According to the TEL and PEL, the adverse biological effect cannot occur when the concentrations of heavy metals are below the TEL, but it may emerge if the values reach the PEL [28, 57]. Our results showed that the concentrations of Cd, Cr, Cu, Ni, Pb, and Zn in the sediments below the TEL accounted for 100%, 18.2%, 4.6%, 0%, 100%, and 9.1% of the total sampling sites, respectively. There were 81.8%, 95.5% 40.9%, and 90.9% of the sampling sites with the concentrations of Cr, Cu, Ni, and Zn varying between the TEL and PEL, suggesting occasional toxic to the ecosystem by these metals. In addition, 59.1% of the sampling sites showed the Ni concentrations exceeding the TEL (Table 4).

The EF > 1.5 commonly indicates a marked enrichment of heavy metals in the sediments [1, 28]. As shown in Table 4, the EF of Cd were higher than 2.5 with the average of 3.44 suggesting a clear contamination in the sediments, whereas the sediments were not contaminated by Cu with its EF of 0.75–1.46. The EF values of Cr and Ni were higher than 1.5 but lower than 3.0, which generally showed a low contamination level. The EF values of Pb and Zn indicated that the sediments were slightly contaminated by Pb and Zn. Similar to the results of EF (Table 4), the I_{geo} values also showed that the Cd in the sediments of most of the study areas was in the moderate to heavy contamination level, Cr and Ni generally showed the uncontaminated to moderately contaminated level, and Cu, Pb, and Zn were in the uncontaminated level. Spatially, the distribution of heavy metal contamination in the sediments was in agreement with the distribution of their concentrations (Figure 3).

3.4.2. Risk Assessment of Heavy Metals. According to the Hakanson potential ecorisk index (Table 4), the potential ecorisk of Cd in the sediments was in a high level (65.45–212.75, average: 118.80). Other heavy metals in the sediments showed a very low ecorisk level (less than 10), suggesting their low potential ecorisk to marine biome. Moreover, the RI varied between 77.93 and 236.83 with the average of 137.29, and Cd accounted for 86.5% of the RI, suggesting Cd as the main metal for the sediment safety due to its high toxicity. Based on the RI, 36.4% of the sampling sites presented the moderate ecorisk level.

The index of $\sum$TUs is used to assess the toxic effect of heavy metals in sediments, since it enables the comparison of the potential toxicity among various sediments based on chemical models [58]. In our study, $\sum$TUs of heavy metals in the sediments were below 4.0 indicating no toxicity to the marine organisms. Spatially, $\sum$TUs of the heavy metals in the sediments were higher in the central Bohai Bay than in the Caofeidian areas (Figure 4). The TU of an individual metal decreased in the order of Ni (0.97) > Cr (0.49) > Zn (0.33) > Cu (0.27) > Pb (0.19) > Cd (0.09), and the average contribution of each metal to the $\sum$TUs was 41.4% for Ni, 21.1% for Cr, 14.2% for Zn, 11.5% for Cu, 8.1% for Pb, and 3.7% for Cd. Although the EF and I_{geo} of Cd in the sediments were the highest among the heavy metals, its contribution to the $\sum$TUs was the least. This suggested that the high contamination of Cd must not induce toxicity to the marine biome, and the volumes or contents of Cd have to be considered, especially its bioavailable forms.

The TRI considering the TEL and PEL was applied to assess the toxic risk of heavy metals in the sediments to marine organisms (Figure 4). The results showed that the TRI of heavy metals in the sediments varied between 3.08 and 8.25 with the average of 5.6, and 31.8% of the sites in the Caofeidian area were in the nontoxic level and 68.2% of the sites in the central Bohai Bay were in the low toxic level. The average contribution of each metal to the TRI was 34.7% for Ni, 19.8% for Cr, 19.7% for Cu, 9.9% for Zn, 9.1% for Pb, and 6.7% for Cd, which revealed Ni as the main metal contributing to the sediment toxicity.

3.5. Implication of the Land Reclamation of Caofeidian for the Heavy Metal Contamination. Land reclamation for agriculture or harbor can cause a series of environmental issues. For example, Bai et al. found that the concentrations of heavy metals in the sediments of Pearl River Estuary increased with the reclamation time [59]. Rahman and Ishiga reported that marine sediments became significantly contaminated by

Table 4: Contamination and ecorisk indices of heavy metals in the sediments.

	Cd	Cr	Cu	Ni	Pb	Zn
<Class 1 (%)	100	45.5	68.2	-	100	100
Class 1 - Class 2 (%)	0	54.5	31.8	-	0	0
<TEL (%)	100	18.2	4.6	0	100	9.1
TEL - PEL (%)	0	81.8	95.5	40.9	0	90.9
>PEL (%)	0	0	0	59.1	0	0
EF	2.50–5.00	1.00–2.82	0.75–1.46	1.08–2.64	0.81–1.54	0.91–1.52
	3.44	2.11	1.09	1.92	1.03	1.19
I_{geo}	0.54–2.24	−0.95–1.14	−1.75–0.06	−0.79–1.14	−0.99–−0.32	−1.35–0.39
	1.32	0.52	−0.42	0.38	−0.51	−0.30
Hakanson	65.45–212.75	1.55–6.61	2.23–7.80	1.73–6.59	3.77–6.01	0.57–1.97
	118.80	4.49	5.81	4.13	5.28	1.26

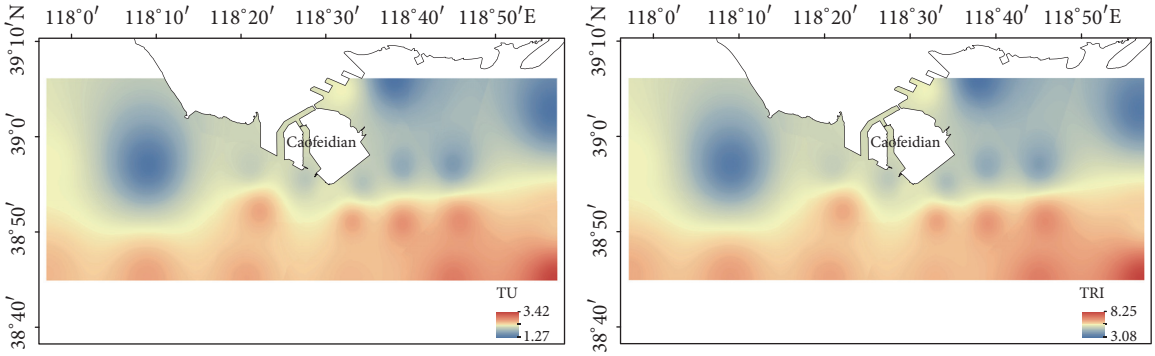

Figure 4: The spatial distribution of the TUs and TRI of heavy metals in the sediments.

heavy metals in the coastal region near the urban areas and harbors of Japan [60]. The study of Xiao et al. revealed the wetland reclamation elevated the accumulation of heavy metals in the soils of Cixi [61]. Zhang et al. found that the reclamation processes in coastal areas resulted in serious contamination of heavy metals to the aquatic ecosystem of Pearl River Estuary [62]. All the studies above showed the land reclamation had negative effects on the aquatic ecosystems. However, according to the spatial distribution of the concentrations, contamination, and ecorisk indices of heavy metals in the sediments of our study area (Figures 3 and 4), the reclamation project of Caofeidian did not induce the markedly high contamination and ecorisk of heavy metals in the sediments. In contrast, the low contamination level of heavy metals in the sediments of Laolonggou and the cape of Caofeidian was clearly observed. This was mainly related to the way of the project and its effect on the hydrodynamic conditions [24]. Whether the accumulation of heavy metals in the sediments increases after the land reclamation project of Caofeidian still needs to be explored in future.

4. Conclusions

The concentrations of heavy metals were generally higher in the sediments of Caofeidian area than of other Chinese bays and estuaries. The markedly lower concentrations of Cd, Cr, Cu, Ni, and Zn in the sediments existed surrounding the land of Caofeidian compared with other regions, whereas those of Pb was markedly higher in the inshore areas of Caofeidian and the central Bohai Bay. Hydrodynamic conditions were the major factors affecting the distribution of heavy metals. The composition of grain sizes determined the distribution of Cu and Zn in the sediments, and organic matters and Fe/Mn oxides/hydroxides also controlled the distribution of heavy metals. The inshore sediments were moderately contaminated by Cd, whereas they were uncontaminated or uncontaminated to moderately contaminated by other metals. Similarly, Cd showed a high potential risk in the sediments, and other metals were in the low risk level. Chromium was a main metal that contributed to the exposure toxicity.

Data Availability

The data used to support the findings of this study are available from the corresponding author upon request.

Conflicts of Interest

The authors declare that they have no conflicts of interest.

Acknowledgments

This study was financially supported by the National Nature Science Foundation of China (no. 41371104) and the Youth Innovation Promotion Association Fund, Chinese Academy of Science.

References

[1] A. Armid, R. Shinjo, A. Zaeni, A. Sani, and R. Ruslan, "The distribution of heavy metals including Pb, Cd and Cr in Kendari Bay surficial sediments," *Marine Pollution Bulletin*, vol. 84, no. 1-2, pp. 373–378, 2014.

[2] C. Christophoridis, D. Dedepsidis, and K. Fytianos, "Occurrence and distribution of selected heavy metals in the surface sediments of Thermaikos Gulf, N. Greece. Assessment using pollution indicators," *Journal of Hazardous Materials*, vol. 168, no. 2-3, pp. 1082–1091, 2009.

[3] F. Kucuksezgin, E. Uluturhan, and H. Batki, "Distribution of heavy metals in water, particulate matter and sediments of Gediz River (Eastern Aegean)," *Environmental Modeling & Assessment*, vol. 141, no. 1-3, pp. 213–225, 2008.

[4] Y. Kara and A. Zeytunluoglu, "Bioaccumulation of toxic metals (Cd and Cu) by Groenlandia densa (L.) Fourr.," *Bulletin of Environmental Contamination and Toxicology*, vol. 79, no. 6, pp. 609–612, 2007.

[5] H. Gan, J. Lin, K. Liang, and Z. Xia, "Selected trace metals (As, Cd and Hg) distribution and contamination in the coastal wetland sediment of the northern Beibu Gulf, South China Sea," *Marine Pollution Bulletin*, vol. 66, no. 1-2, pp. 252–258, 2013.

[6] B. Hu, R. Cui, J. Li et al., "Occurrence and distribution of heavy metals in surface sediments of the Changhua River Estuary and adjacent shelf (Hainan Island)," *Marine Pollution Bulletin*, vol. 76, no. 1-2, pp. 400–405, 2013.

[7] B. Hu, J. Li, J. Zhao, J. Yang, F. Bai, and Y. Dou, "Heavy metal in surface sediments of the Liaodong Bay, Bohai Sea: distribution, contamination, and sources," *Environmental Monitoring & Assessment*, vol. 185, no. 6, pp. 5071–5083, 2013.

[8] M. Baborowski, O. Büttner, P. Morgenstern, T. Jancke, and B. Westrich, "Spatial variability of metal pollution in groyne fields

of the Middle Elbe - Implications for sediment monitoring," *Environmental Pollution*, vol. 167, pp. 115–123, 2012.

[9] G. W. Bryan and W. J. Langston, "Bioavailability, accumulation and effects of heavy metals in sediments with special reference to United Kingdom estuaries," *Environmental Pollution*, vol. 76, no. 2, pp. 89–131, 1992.

[10] H. Bing, J. Zhou, Y. Wu, X. Wang, H. Sun, and R. Li, "Current state, sources, and potential risk of heavy metals in sediments of Three Gorges Reservoir, China," *Environmental Pollution*, vol. 214, pp. 485–496, 2016.

[11] F. Li, X.-Y. Zeng, C.-H. Wu et al., "Ecological risks assessment and pollution source identification of trace elements in contaminated sediments from the Pearl River Delta, China," *Biological Trace Element Research*, vol. 155, no. 2, pp. 301–313, 2013.

[12] A. Zahra, M. Z. Hashmi, R. N. Malik, and Z. Ahmed, "Enrichment and geo-accumulation of heavy metals and risk assessment of sediments of the Kurang Nallah—feeding tributary of the Rawal Lake Reservoir, Pakistan," *Science of the Total Environment*, vol. 470-471, pp. 925–933, 2014.

[13] J. Viers, B. Dupré, and J. Gaillardet, "Chemical composition of suspended sediments in World Rivers: New insights from a new database," *Science of the Total Environment*, vol. 407, no. 2, pp. 853–868, 2009.

[14] N. A. Hill, S. L. Simpson, and E. L. Johnston, "Beyond the bed: effects of metal contamination on recruitment to bedded sediments and overlying substrata," *Environmental Pollution*, vol. 173, pp. 182–191, 2013.

[15] H. Wang, J. Wang, R. Liu, W. Yu, and Z. Shen, "Spatial variation, environmental risk and biological hazard assessment of heavy metals in surface sediments of the Yangtze River estuary," *Marine Pollution Bulletin*, vol. 93, no. 1-2, pp. 250–258, 2015.

[16] J. Bai, Q. Zhao, Q. Lu, J. Wang, and K. R. Reddy, "Effects of freshwater input on trace element pollution in salt marsh soils of a typical coastal estuary, China," *Journal of Hydrology*, vol. 520, pp. 186–192, 2015.

[17] S. Rahmanpour, N. F. Ghorghani, and S. M. Lotfi Ashtiyani, "Heavy metal in water and aquatic organisms from different intertidal ecosystems, Persian Gulf," *Environmental Modeling & Assessment*, vol. 186, no. 9, pp. 5401–5409, 2014.

[18] L. Wang, N. A. Coles, C. Wu, and J. Wu, "Spatial variability of heavy metals in the coastal soils under long-term reclamation," *Estuarine, Coastal and Shelf Science*, vol. 151, pp. 310–317, 2014.

[19] J. Bai, J. Jia, G. Zhang et al., "Spatial and temporal dynamics of heavy metal pollution and source identification in sediment cores from the short-term flooding riparian wetlands in a Chinese delta," *Environmental Pollution*, vol. 219, pp. 379–388, 2016.

[20] H. Bing, Y. Wu, E. Liu, and X. Yang, "Assessment of heavy metal enrichment and its human impact in lacustrine sediments from four lakes in the mid-low reaches of the Yangtze River, China," *Journal of Environmental Sciences*, vol. 25, no. 7, pp. 1300–1309, 2013.

[21] I. D. L. Foster and S. M. Charlesworth, "Heavy metals in the hydrological cycle: Trends and explanation," *Hydrological Processes*, vol. 10, no. 2, pp. 227–261, 1996.

[22] X. Wang, H. Bing, Y. Wu, J. Zhou, and H. Sun, "Distribution and potential eco-risk of chromium and nickel in sediments after impoundment of Three Gorges Reservoir, China," *Human and Ecological Risk Assessment*, vol. 23, no. 1, pp. 172–185, 2017.

[23] X. Gao and C.-T. A. Chen, "Heavy metal pollution status in surface sediments of the coastal Bohai Bay," *Water Research*, vol. 46, no. 6, pp. 1901–1911, 2012.

[24] Y. Lu, R. Ji, and L. Zuo, "Morphodynamic responses to the deep water harbor development in the Caofeidian sea area, China's Bohai Bay," *Coastal Engineering Journal*, vol. 56, no. 8, pp. 831–843, 2009.

[25] Y. Zhang and X. Gao, "Rare earth elements in surface sediments of a marine coast under heavy anthropogenic influence: The Bohai Bay, China," *Estuarine, Coastal and Shelf Science*, vol. 164, pp. 86–93, 2015.

[26] L. Gao, Z. Wang, S. Li, and J. Chen, "Bioavailability and toxicity of trace metals (Cd, Cr, Cu, Ni, and Zn) in sediment cores from the Shima River, South China," *Chemosphere*, vol. 192, pp. 31–42, 2018.

[27] Q. An, Y. Wu, J. Wang, and Z. Li, "Assessment of dissolved heavy metal in the Yangtze River estuary and its adjacent sea, China," *Environmental Modeling & Assessment*, vol. 164, no. 1-4, pp. 173–187, 2010.

[28] J. Liu, P. Yin, B. Chen, F. Gao, H. Song, and M. Li, "Distribution and contamination assessment of heavy metals in surface sediments of the Luanhe River Estuary, northwest of the Bohai Sea," *Marine Pollution Bulletin*, vol. 109, no. 1, pp. 633–639, 2016.

[29] CCME, *Canadian sediments quality guidelines for the protection of aquatic life: summary tables. Canadian Environmental Quality Guidelines*, Canadian Council of Ministers of the Environment Winnipeg, 1999.

[30] AQSIQ, "Administration of quality supervision, inspection and quarantine of the People's Republic of China," in *Marine Sediment Quality of China (GB 18668-2002)*, p. 2, Standards Press of China, Beijing, China, 2002.

[31] C. C. M. Ip, X.-D. Li, G. Zhang, O. W. H. Wai, and Y.-S. Li, "Trace metal distribution in sediments of the Pearl River Estuary and the surrounding coastal area, South China," *Environmental Pollution*, vol. 147, no. 2, pp. 311–323, 2007.

[32] X. Li, O. W. H. Wai, Y. S. Li, B. J. Coles, M. H. Ramsey, and I. Thornton, "Heavy metal distribution in sediment profiles of the Pearl River estuary, South China," *Applied Geochemistry*, vol. 15, no. 5, pp. 567–581, 2000.

[33] G. Muller, "Index of geoaccumulation in sediments of the Rhine River," *Geojournal*, vol. 2, no. 108, pp. 108–118, 1969.

[34] F.-L. Li, C.-Q. Liu, Y.-G. Yang, X.-Y. Bi, T.-Z. Liu, and Z.-Q. Zhao, "Natural and anthropogenic lead in soils and vegetables around Guiyang city, southwest China: A Pb isotopic approach," *Science of the Total Environment*, vol. 431, pp. 339–347, 2012.

[35] F. Xu, B. Hu, S. Yuan et al., "Heavy metals in surface sediments of the continental shelf of the South Yellow Sea and East China Sea: Sources, distribution and contamination," *Catena*, vol. 160, pp. 194–200, 2018.

[36] L. Hakanson, "An ecological risk index for aquatic pollution control. A sedimentological approach," *Water Research*, vol. 14, no. 8, pp. 975–1001, 1980.

[37] M. Liu, A. Zhang, Y. Liao, B. Chen, and D. Fan, "The environment quality of heavy metals in sediments from the central Bohai Sea," *Marine Pollution Bulletin*, vol. 100, no. 1, pp. 534–543, 2015.

[38] Z. Xie, H. Zhang, X. Zhao, Z. Du, L. Xiang, and W. Wang, "Assessment of Heavy Metal Contamination and Wetland Management in a Newly Created Coastal Natural Reserve, China," *Journal of Coastal Research*, vol. 32, no. 2, pp. 374–386, 2016.

[39] Z. Sun, X. Mou, C. Tong et al., "Spatial variations and bioaccumulation of heavy metals in intertidal zone of the Yellow River estuary, China," *Catena*, vol. 126, pp. 43–52, 2015.

[40] G. Wu, J. Shang, L. Pan, and Z. Wang, "Heavy metals in surface sediments from nine estuaries along the coast of Bohai Bay, Northern China," *Marine Pollution Bulletin*, vol. 82, no. 1-2, pp. 194–200, 2014.

[41] X. Gao and P. Li, "Concentration and fractionation of trace metals in surface sediments of intertidal Bohai Bay, China," *Marine Pollution Bulletin*, vol. 64, no. 8, pp. 1529–1536, 2012.

[42] X. Gao, Y. Yang, and C. Wang, "Geochemistry of organic carbon and nitrogen in surface sediments of coastal Bohai Bay inferred from their ratios and stable isotopic signatures," *Marine Pollution Bulletin*, vol. 64, no. 6, pp. 1148–1155, 2012.

[43] C.-P. Kuang, S.-Y. Chen, Y. Zhang et al., "A two-dimensional morphological model based on next generation circulation solver II: Application to Caofeidian, Bohai Bay, China," *Coastal Engineering Journal*, vol. 59, no. 1, pp. 14–27, 2012.

[44] G. Xu, J. Liu, S. Pei, M. Gao, G. Hu, and X. Kong, "Sediment properties and trace metal pollution assessment in surface sediments of the Laizhou Bay, China," *Environmental Science and Pollution Research*, vol. 22, no. 15, pp. 11634–11647, 2015.

[45] D. Han, J. Cheng, X. Hu et al., "Spatial distribution, risk assessment and source identification of heavy metals in sediments of the Yangtze River Estuary, China," *Marine Pollution Bulletin*, vol. 115, no. 1-2, pp. 141–148, 2017.

[46] S. R. Taylor and S. M. McLennan, "The chemical composition evolution of the continental crust," *Reviews of Geophysics*, vol. 33, no. 2, pp. 241–265, 1995.

[47] D. D. Macdonald, R. S. Carr, F. D. Calder, E. R. Long, and C. G. Ingersoll, "Development and evaluation of sediment quality guidelines for Florida coastal waters," *Ecotoxicology*, vol. 5, no. 4, pp. 253–278, 1996.

[48] F. Pedersen, E. Bjørnestad, H. V. Andersen, J. Kjølholt, and C. Poll, "Characterization of sediments from Copenhagen Harbour by use of biotests," *Water Science and Technology*, vol. 37, no. 6-7, pp. 233–240, 1998.

[49] Y.-J. Lu, L.-Q. Zuo, R.-Y. Ji, X. Xu, and J.-W. Huang, "Effect of development of Caofeidian harbor area in Bohai bay on hydrodynamic sediment environment," *China Ocean Engineering*, vol. 22, no. 1, pp. 97–112, 2008.

[50] Y. Dou, J. Li, J. Zhao, B. Hu, and S. Yang, "Distribution, enrichment and source of heavy metals in surface sediments of the eastern Beibu Bay, South China Sea," *Marine Pollution Bulletin*, vol. 67, no. 1-2, pp. 137–145, 2013.

[51] R. Xiao, M. Zhang, X. Yao, Z. Ma, F. Yu, and J. Bai, "Heavy metal distribution in different soil aggregate size classes from restored brackish marsh, oil exploitation zone, and tidal mud flat of the Yellow River Delta," *Journal of Soils and Sediments*, vol. 16, no. 3, pp. 821–830, 2016.

[52] S. L. Yang and H. F. Yang, "Temporal Variations in Water and Sediment Discharge from the Changjiang (Yangtze River) and Downstream Sedimentary Responses," in *Ecological Continuum from the Changjiang (Yangtze River) Watersheds to the East China Sea Continental Margin*, Estuaries of the World, pp. 71–91, Springer International Publishing, 2015.

[53] J. Bai, R. Xiao, K. Zhang, and H. Gao, "Arsenic and heavy metal pollution in wetland soils from tidal freshwater and salt marshes before and after the flow-sediment regulation regime in the Yellow River Delta, China," *Journal of Hydrology*, vol. 450-451, pp. 244–253, 2012.

[54] J. C. Santos Bermejo, R. Beltrán, and J. L. Gömez Ariza, "Spatial variations of heavy metals contamination in sediments from Odiel river (Southwest Spain)," *Environment International*, vol. 29, no. 1, pp. 69–77, 2003.

[55] J. Zhang, "Biogeochemistry of Chinese estuarine and coastal waters: Nutrients, Trace metals and biomarkers," *Journal of Material Cycles and Waste Management*, vol. 3, no. 1-3, pp. 65–76, 2002.

[56] R. A. Sutherland, "Bed sediment-associated trace metals in an urban stream, Oahu, Hawaii," *Environmental Geology*, vol. 39, no. 6, pp. 611–627, 2000.

[57] E. R. Long, L. J. Field, and D. D. Macdonald, "Predicting toxicity in marine sediments with numerical sediment quality guidelines," *Environmental Toxicology & Chemistry*, vol. 17, no. 4, pp. 714–727, 2010.

[58] G. Zhang, J. Bai, Q. Zhao, Q. Lu, J. Jia, and X. Wen, "Heavy metals in wetland soils along a wetland-forming chronosequence in the Yellow River Delta of China: Levels, sources and toxic risks," *Ecological Indicators*, vol. 69, pp. 331–339, 2016.

[59] J. Bai, R. Xiao, B. Cui et al., "Assessment of heavy metal pollution in wetland soils from the young and old reclaimed regions in the Pearl River Estuary, South China," *Environmental Pollution*, vol. 159, no. 3, pp. 817–824, 2011.

[60] M. A. Rahman and H. Ishiga, "Trace metal concentrations in tidal flat coastal sediments, Yamaguchi Prefecture, southwest Japan," *Environmental Modeling & Assessment*, vol. 184, no. 9, pp. 5755–5771, 2012.

[61] R. Xiao, J. Bai, Q. Lu et al., "Fractionation, transfer, and ecological risks of heavy metals in riparian and ditch wetlands across a 100-year chronosequence of reclamation in an estuary of China," *Science of the Total Environment*, vol. 517, pp. 66–75, 2015.

[62] G. Zhang, J. Bai, R. Xiao et al., "Heavy metal fractions and ecological risk assessment in sediments from urban, rural and reclamation-affected rivers of the Pearl River Estuary, China," *Chemosphere*, vol. 184, pp. 278–288, 2017.

Hindawi
Journal of Chemistry
Volume 2018, Article ID 5137694, 8 pages
https://doi.org/10.1155/2018/5137694

Research Article

Enhanced As (V) Removal from Aqueous Solution by Biochar Prepared from Iron-Impregnated Corn Straw

Jiaming Fan,[1] Xin Xu,[1] Qunli Ni,[1] Qi Lin ,[1,2] Jing Fang,[1] Qian Chen,[1] Xiaodong Shen,[3] and Liping Lou[1,2]

[1]*Department of Environmental Engineering, Zhejiang University, Hangzhou 310058, China*
[2]*Key Laboratory of Water Pollution Control and Environmental Safety of Zhejiang Province, Hangzhou, China*
[3]*Institute of Hangzhou Environmental Science, Hangzhou 310014, China*

Correspondence should be addressed to Qi Lin; linqi@zju.edu.cn

Received 5 January 2018; Accepted 13 February 2018; Published 3 April 2018

Academic Editor: Xiao-San Luo

Fe-loaded adsorbents have received increasing attention for the removal of arsenic in contaminated water or soil. In this study, Fe-loaded biochar was prepared from iron-impregnated corn straw under a pyrolysis temperature of 600°C. The ratio of crystalline Fe oxides including magnetite and natrojarosite to amorphous iron oxyhydroxide in the composite was approximately 2 : 3. Consisting of 24.17% Fe and 27.76% O, the composite exhibited a high adsorption capacity of 14.77 mg g^{-1} despite low surface areas (4.81 m^2 g^{-1}). The pH range of 2.0–8.0 was optimal for arsenate removal and the adsorption process followed the Langmuir isotherms closely. In addition, pseudo-second-order kinetics best fit the As removal data. Fe oxide constituted a major As-adsorbing sink. Based on the X-ray diffraction spectra, saturation indices, and selective chemical extraction, the data suggested three main mechanisms for arsenate removal: sorption of arsenate, strong inner-sphere surface complexes with amorphous iron oxyhydroxide, and partial occlusion of arsenate into the crystalline Fe oxides or carbonized phase. The results indicated that the application of biochar prepared from iron-impregnated corn straw can be an efficient method for the remediation of arsenic contaminated water or soil.

1. Introduction

With the rapid development of urban space and intensification of agricultural and industrial activities, chemical pollution has become a serious environmental issue, particularly in China [1, 2]. Arsenic, as a potential carcinogen, is associated with a variety of human diseases, such as cardiovascular diseases, liver fibrosis, kidney disorders, blood toxicity, and chronic lung disease [3]. Arsenic's potential to pose a hazard to human health has prompted the establishment of more stringent environmental regulations and hence the development of innovative and cost-effective technologies for the treatment of arsenic in the environment. [4–7]. Recently, the thermochemical conversion of agricultural waste has received increasing attention in the last decades due to its potential application in pollutant removal [8]. Samsuri et al. [9] reported that the maximum adsorption capacity for biochars prepared from empty fruit bunch and rice husk is 5.5 and 7.1 mg/g for As (V), respectively. Agrafioti et al. [10] reported that the removal efficiency of As (V) was about 25% in rice husk-derived biochars, lower than 65% in soils. Similar results were also observed in biochars prepared from pine needle and straws [11]. A search for improved and inexpensive materials is still underway [12]. Yao et al. [13] reported that Fe-loaded activated carbon had the removal rate of more than 95% for As (V). Using iron-impregnated sawdust, Liu et al. [4] successfully synthesized Fe_3O_4-loaded biochar for both arsenate removal and magnetic separation. Fe-loaded biochars from empty fruit bunch and rice husk achieved the maximum adsorption capacity of 45.2 and 16.0 mg/g for As (V), almost 2~8 times of that in the companion biochar without iron loaded [9]. The results indicated that the effectiveness of arsenic removal was closely related to the amount of iron loaded, characteristics of the media supporting the iron oxide, and synthetic conditions [4, 14]. The characteristics of biochars derived from agricultural residues vary greatly depending on the type of feedstock used, pyrolysis temperature, pyrolysis atmosphere, and activation

treatment [15]. We leveraged this variability to find and optimize a suitable and cheap material with the desired properties for supporting iron oxide.

In this study, biochar derived from iron-impregnated corn straw was prepared and utilized as a potential green adsorbent for arsenate removal. The produced composite was characterized by Fourier transform infrared (FTIR), X-ray diffraction (XRD), BET-N_2 surface area, and elemental analyses combined with chemical extractions. We report equilibrium and kinetic experiments of As(V) absorption and illustrate the mechanisms of As(V) removal through the interpretation of the adsorption data, determination of arsenic speciation using the sequential chemical extraction method, and calculation of the saturation indices for the different arsenic precipitation phases.

2. Materials and Methods

2.1. Materials. The maize straws used in this study were obtained from Tongxiang in Zhejiang province. As(V) standard stock solution (1000 mg L^{-1}) was prepared from $Na_2HAsO_4{\cdot}7H_2O$ and preserved in a brown reagent bottle.

2.2. Preparation of Biochars. The corn straws were dried at 80°C in an oven and ground to pass through 20-mesh sieve. It was mixed with 1.0 mol L^{-1} $FeCl_3$ and 50% H_2SO_4 according to a straw to $FeCl_3$ to H_2SO_4 ratio of 1 : 10 : 5 (g : mL : mL) and then ultrasonicated for 2 h and aged at 60°C for 12 h [4]. After suction separation, the recovered residue was dried at 80°C in an oven for 24 h, packed into a capped-ceramic container, and sealed to exclude as much air as possible. The carbonization was conducted in a temperature-controlled muffle furnace at 600°C for 2 h. Thereafter the furnace was turned off and the retort chamber was allowed to cool to room temperature. The iron-loaded biochar (CS-Fe) was ground to a fine powder and passed through a 0.2 mm sieve. As a control, companion biochar without iron loaded was also prepared and designated as CS.

2.3. Characterization of the Biochars. The total C, H, and N contents in the biochar samples were analyzed with an element analyzer (EA 1112, Italy). The yields of the biochars were measured by the ratio of the biochar's weight before and after pyrolysis. Ash content was determined after heating at 550°C for 3 h in a muffle furnace. The inorganic element composition of the biochars was examined after digestion with a mixture of HNO_3-HCl-$HClO_4$ acids. It was then analyzed for the total K, Ca, Fe, Mn, Cu, Zn, Pb, P, and As contents by inductively coupled plasma-atomic emission spectrometry (ICP-AES) (iCAP6300DUO, Thermo, America). The pH of the biochar was determined using the composite electrode method at the ratio of 1 : 10 water [16]. The point of zero charge (pH_{pzc}) was determined using methods outlined in the literature [17].

The FTIR spectra were carried out by mixing biochar with KBr in a ratio of 1 : 150 and scanning in the wavenumber range of 400–4000 cm^{-1} at a resolution of 4 cm^{-1} (IR PRESTIGE-21, Shimadzu, Japan) [18]. The surface oxygenic functional groups were determined according to the Boehm titration method [19]. XRD patterns of the biochars were determined on a power X-ray diffraction system using Cu Kα (λ = 1.54 Å) radiation at 40 kV and 40 mA (X-pert Powder, PANalytical B.V., Netherlands). The samples were scanned from 10° to 80° with a scan speed of 2° per minute. Surface area and pore size were measured using a BET-N_2 SA analyzer (Tristar ll3020, MIC, America).

2.4. Adsorption Studies. The batch adsorption experiments were performed by mixing 20 mL of a 0.01 M $NaNO_3$ solution containing 0–150 mg L^{-1} As(V) with the desired weight of biochar samples in 100-mL conical flasks. The flasks were then shaken at 200 rpm in a constant temperature mechanical shaker (30°C) for a preset time. The solutions were centrifuged at 3000 rpm for 10 min and filtrated through 0.45 μm filters. The concentrations of As were analyzed by ICP-AES. The effects of the biochars dose (0–10 g L^{-1}), initial solution pH (2.0–12.0), and contact time (0–24 h) were studied. Triplicates were performed for each sorption experiment.

The isotherm data were analyzed by Langmuir and Freundlich equations expressed as follows:

$$\begin{aligned} &\text{Langmuir: } \frac{1}{q_e} = \frac{1}{kq_mC_e} + \frac{1}{q_m}, \\ &\text{Freundlich: } q_e = k_f \cdot {C_e}^{1/n}, \end{aligned} \tag{1}$$

where q_e (mg g^{-1}) is the amount of solute adsorbed per unit weight at equilibrium; C_e (mg L^{-1}) is the equilibrium concentration of As (V) in solution; q_m (mg/g) and k (L mg^{-1}) are the maximum capacities of adsorption for a monolayer coverage and the affinity coefficient, respectively [20]; k_f (mg/g·(L/mg)$^{1/n}$) and $1/n$ are the Freundlich capacity coefficient and intensity constant, respectively.

In order to evaluate the kinetic process, the Lagergren-first-order and pseudo-second-order fits of the experimental data were compared

$$\begin{aligned} &\text{Lagergren-first-order: } \log\left(q_e - q_t\right) \\ &\quad = \log\left(q_e\right) - \frac{k_1 t}{2.303}, \\ &\text{pseudo-second-order: } \frac{t}{q_t} = \frac{1}{k_2 {q_e}^2} + \frac{t}{q_e}, \end{aligned} \tag{2}$$

where q_t and q_e (mg g^{-1}) are the amounts of arsenic adsorbed at time t and equilibrium time, respectively; k_1 and k_2 are the pseudo-first-order rate constant (1/h) and pseudo-second-order rate constant (g mg^{-1} h^{-1}), respectively.

2.5. Arsenic Speciation in the Adsorbent. Samples for speciation analysis were prepared by reacting 1 g of CS-Fe with 200 mL of a 0.01 M $NaNO_3$ solution containing 40 mg L^{-1} As(V). The concentrations of K, Na, Ca, Mg, Fe, Mn, P, and S in the solution were determined by ICP-AES. Nitrate-nitrogen (NO_3-N) and chloride (Cl^-) were determined by ultraviolet spectrophotometry and a silver nitrate titration,

Table 1: Characteristics of the biochars.

	Unit	CS	CS-Fe
Element analysis			
C	%	64.14	38.08
H	%	1.92	1.44
O	%	11.44	27.76
N	%	2.09	1.01
H/C[(a)]		0.36	0.45
O/C		0.13	0.55
Ash	%	20.41	31.72
Mineral			
K	%	5.88	3.42
Ca	%	0.72	0.22
Fe	%	0.08	24.17
Mn	%	0.01	0.01
P	%	0.36	0.04
Trace metals			
Cu	$mgkg^{-1}$	21.20	49.58
Zn	$mgkg^{-1}$	96.18	27.01
Pb	$mgkg^{-1}$	9.18	14.3
As	$mgkg^{-1}$	-[(b)]	-
Functional group			
Acid sites	$mequivg^{-1}$	0.28	2.08
Basic sites	$mequivg^{-1}$	1.33	0.027
BET analysis			
Specific surface area	m^2g^{-1}	0.74	4.81
Pore volume	cm^3g^{-1}	0.0011	0.012
Others			
pH		10.89	2.55
pH_{pzc}		2.75	6.93
Yield	%	33.24	25.01

Notes. [(a)]H/C: atomic ratio of hydrogen to carbon; [(b)]-: not detectable.

respectively. The results including pH and anion and cation concentrations were used in the speciation model Visual MINTEQ for calculating the saturation indices (SI) for the different precipitation phases.

A sequential chemical extraction method was used for the determination of arsenic speciation in the adsorbent as proposed by Cances et al. [21]. The four arsenic forms including the sulfate exchangeable, specially adsorbed, bound to amorphous iron oxyhydroxide and residual fractions were studied (Table S1).

3. Results and Discussion

3.1. Characterization of Biochars. Selected properties of the CS and CS-Fe are listed in Table 1. The content of O in the CS-Fe (27.76%) was higher than that in the CS (11.44%), suggesting that the CS-Fe had a large proportion of oxygen-containing functional groups. It was also confirmed by the Boehm titration that the total functional groups in the CS-Fe were higher than that in the CS (Table 1). The lower carbon content and much higher ash content for CS-Fe when compared with the CS were consistent with the introduction of iron oxide in the former. The higher H/C ratio of the CS-Fe over CS indicated that more original organic matter was preserved in the iron-loaded biochar and showed lower overall aromaticity. The higher O/C ratios of the CS-Fe indicated higher polarity when compared to CS [22].

The total P, K, and Ca proportions in CS were 0.36%, 5.88%, and 0.72%, respectively, much higher than those in CS-Fe (0.04%, 3.42%, and 0.22%, resp.). This was likely due to the chemical treatment by H_2SO_4 which caused the leaching of P, K, and Ca in the CS-Fe. The content of Fe in the CS-Fe was 24.17%, 302 times that of Fe in the CS, indicating that CS-Fe was successfully loaded with iron. The BET surface area and pore volume of the CS were 0.74 $m^2\,g^{-1}$ and 0.0011 $cm^3\,g^{-1}$, respectively. Fe-impregnated biochar showed increase of both surface area (4.81 $m^2\,g^{-1}$) and pore volume (0.012 $cm^3\,g^{-1}$), suggesting that activation by sulfuric acid pretreatment was probably beneficial for the development of pore structure, which also increased the specific surface area. A much higher pH_{pzc} value of 6.93 for the CS-Fe versus 2.75 in the CS was observed; therefore, it was expected that the

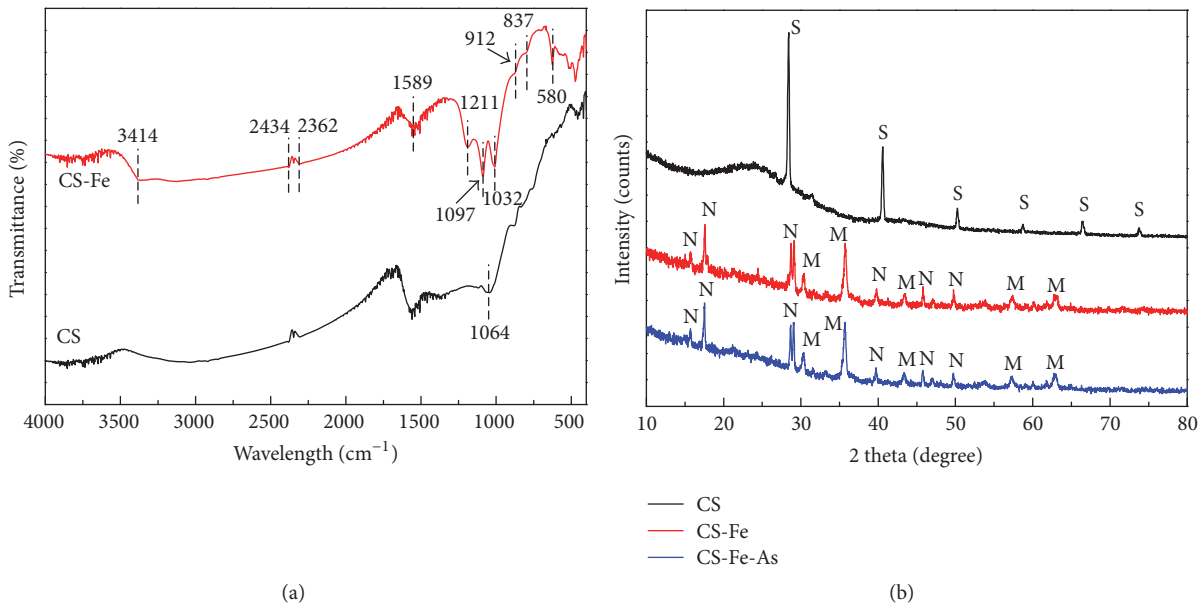

FIGURE 1: The FTIR spectra (a) and the XRD spectra (b) of CS and CS-Fe. The typical peaks of XRD spectra were labeled as follows: S, sylvite; M, magnetite; N, natrojarosite.

CS-Fe would be more conducive to the adsorption of anionic arsenate.

FTIR spectra were obtained for both the CS and CS-Fe samples (Figure 1(a)). The stretching vibration for C≡C corresponds to the peaks at 2362 and 2434 cm^{-1} [18]. The peak at 1589 cm^{-1} is the aromatic ring "breathing" vibrations [18] and the peaks at 837 and 912 cm^{-1} are assigned to the 1,3,5-trisubstituted aromatic ring (δCH out-off-plane) [23]. The new peak that appears at approximately 580 cm^{-1} in the CS-Fe spectrum is characteristic of the Fe-O stretching vibration [24]. The broader absorption band at 3414 cm^{-1} and sharp peaks at 1211 and 1097 cm^{-1} are assigned to the stretching of -OH, epoxy C-O, and C-O-C, respectively, which differed greatly in the CS and CS-Fe. This was likely due to the preservation of the original structure in the pyrolysis process in the presence of iron oxide.

The XRD patterns of CS and CS-Fe are compared in Figure 1(b). The presence of sylvine in the CS pattern was confirmed by peaks at 28.4°, 40.5°, 50.2°, 58.7°, 66.5°, and 73.7° (2θ). The peaks at 28.4°, 40.5°, 66.5°, and 73.7° disappeared in the CS-Fe pattern due to the pretreatment with sulfuric acid. The strong peaks of magnetite (Fe_3O_4) at 30.4°, 35.7°, 43.6°, 57.3°, and 62.9° (2θ) and natrojarosite ($NaFe_3(SO_4)_2(OH)_6$) at 15.8°, 17.5°, 29.1°, 40.2°, 45.8°, and 49.7° (2θ) were clearly observed in the CS-Fe patterns in both the presence and absence of As loading, suggesting that iron oxides with good crystalline structure were formed and loaded on the biochar.

3.2. Adsorption of As(V)

3.2.1. Adsorbent Dosage and Solution pH. The influence of additive dosage of CS-Fe (0 to 10 g L^{-1}) on As adsorption was studied (Figure S1). The removal efficiency of As (V) by CS-Fe increased rapidly from 2.2% to 96% as the adsorbent dose was increased from 0.4 to 5 g L^{-1}. Further increase in the adsorbent dosage had no significant effect on the removal of As (V). Therefore, the dosage of 5 g L^{-1} was selected as the optimum adsorbent dosage for the adsorption experiments.

The solution pH plays a key role in the removal of arsenic, as it influences the surface charge of the adsorbent and the forms of arsenic in solution [25]. Effects of pH on As (V) adsorption by CS and CS-Fe were investigated in the pH range from 2.0 to 12.0, with the initial As (V) concentration of 40 mg L^{-1}. It can be seen in Figure 2 that the removal efficiency of As (V) by CS and CS-Fe varied greatly in the pH range studied which clearly indicated the influence of solution pH on the adsorption process. In the case of CS, pH 4 was more suitable for As (V) removal from solution, while CS-Fe was effective with a larger pH range of 2.0–8.0. These results are similar to that of Zhu et al. [14] for As(V) adsorption on Fe_3O_4-loaded honeycomb briquette cinders, but slightly different from that of Liu et al. [4] who reported that the maximum As(V) removal efficiency was achieved at pH 8.0 by Fe_3O_4-loaded sawdust biochar. The main factors influencing the adsorption process are As (V) species and the surface charge of the adsorbents. Due to the increase in the pH_{pzc} value, the surface of CS-Fe was positively charged at pH < pH_{pzc} 6.93 for the CS-Fe and conducive to the adsorption of $H_2AsO_4^-$ (Figure S2). In an alkaline medium, however, the surface of CS-Fe is negatively charged and most As (V) species exist as $HAsO_4^{2-}$ and AsO_4^{3-} (Figure S2). The adsorption of As (V) thus decreased as a result of enhanced electrostatic repulsion [4]. Similarly, the higher As (V) removal efficiency that occurred at pH 4 for the control biochar (CS) can also be illustrated by the As (V) species and pH_{pzc}. As showed in Table 1, the surface of CS was negatively charged at pH > pH_{pzc} 2.75 and not conducive to the adsorption of $H_2AsO_4^-$ (Figure S2) at the higher pH,

Table 2: Regression parameters of isotherms of As (V).

Sample	Langmuir			Freundlich		
	q_m (mg g^{-1})	k (L mg^{-1})	R^2	k_f ((L mg^{-1})$^{1/n}$ · mg g^{-1})	$1/n$	R^2
CS-Fe	14.77	2.97	0.9968	7.95	0.31	0.8358
CS	2.86	0.01	0.9492	6.16	1.18	0.9041

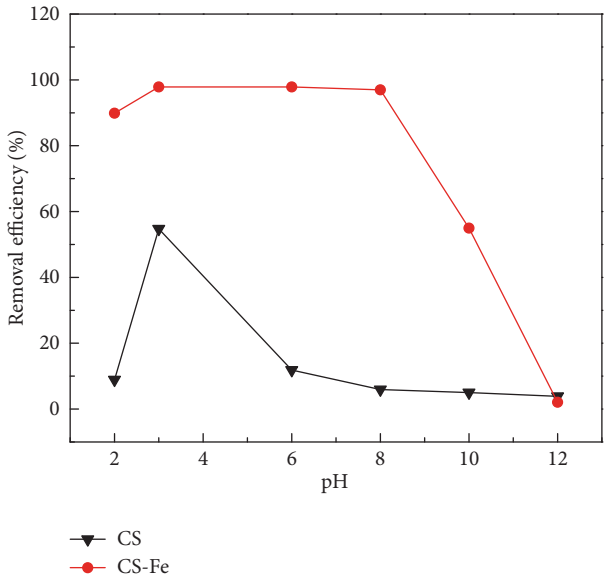

Figure 2: Effect of solution pH on the adsorption of As(V) for CS and CS-Fe (adsorbent dose 5 g L^{-1}; temperature 30°C; As(V) concentration 40 mg L^{-1}).

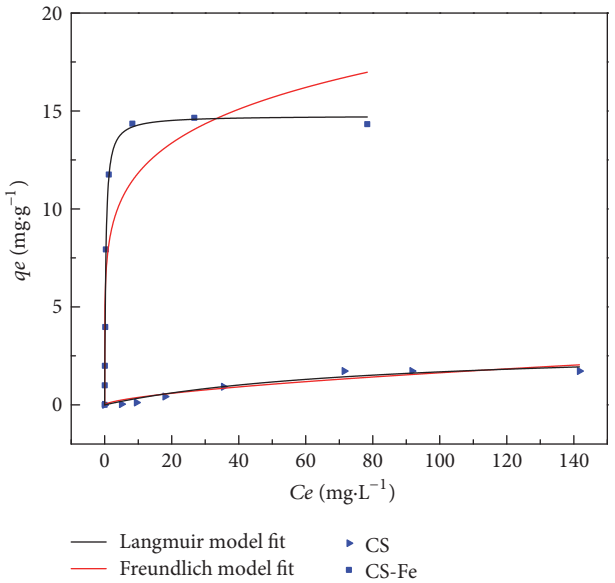

Figure 3: Adsorption isotherms of As(V) on CS-Fe and CS (adsorbent dose 5 g L^{-1}; pH 3.0; temperature 30°C).

while at pH 2, the surface was positively charged but As (V) species exist as H_3AsO_4.

3.2.2. Adsorption Isotherms. Adsorption isotherms of As by CS-Fe and CS were compared (Figure 3). Adsorption potentials of CS-Fe were much higher than that of CS, indicating a positive role of iron oxides for enhanced adsorption of As (V). The regression parameters of isotherms are listed in Table 2. It is clear that both the CS-Fe and CS followed the Langmuir-type isotherm with correlation coefficients R^2 in the range from 0.9492 to 0.9968. The Langmuir model assumes that the adsorption of the molecule occurs on a homogeneous surface as a monolayer, while the Freundlich model is an empirical equation based on a heterogeneous surface [4]. The data fit best to the Langmuir-type, implying that the adsorption of As occurs on a homogeneous surface by monolayer adsorption [14]. Conversely, using Fe_3O_4-loaded biochar prepared from sawdust, Liu et al. [4] reported that the adsorption process followed the Freundlich isotherm model at pH 8.

CS-Fe exhibited excellent immobilization capacities for As (V). The maximum adsorption capacity estimated by the Langmuir model was 14.77 mg g^{-1}, almost fivefold larger than that of CS (2.86 mg g^{-1}). The affinity coefficient of adsorption, k, varied greatly with a value of 2.97 L mg^{-1} for the CS-Fe, about 300 times that of the CS. A comparison between CS-Fe and other Fe-loaded adsorbents showed that the maximum adsorption capacity of As(V) by CS-Fe was moderately greater than iron-containing granular activated carbon (6.57–10.5 mg g^{-1}) [12], iron-containing mesoporous carbon (5.2 mg g^{-1}), and Fe_3O_4-loaded honeycomb briquette cinders (2.42 mg g^{-1}) [14], but much lower than Fe_3O_4-loaded sawdust biochar, which had the adsorption capacity of 204.2 mg g^{-1} [4]. Factors such as iron oxide species, amount of iron loaded, and dispersion and surface accessibility of iron within the carbon likely affected the As(V) removal [26]. Due to the high content of oxygen in CS-Fe (27.76%), the biochar swells in water and permits sorption inside the solid as well as on its pore surfaces, leading to high sorption capacities at low surface areas [18].

3.2.3. Kinetic Study. The adsorption of As (V) onto CS-Fe was quite rapid. At the initial concentration of 25 and 40 mg L^{-1}, 94–97% of As was removed within the first 15 min (Figure 4).

Table 3 shows the Lagergren-first-order and pseudo-second-order rate constants for As (V) on CS-Fe. With correlation coefficient $R^2 > 0.999$, the adsorption kinetics for As (V) onto CS-Fe are best described by pseudo-second-order model. The higher the initial As concentration, the lower the pseudo-second-order rate constant. Since the pseudo-second-order model usually assumes that chemisorption of an adsorbate on an adsorbent is the rate-limiting step [27], it

Table 3: Parameters of kinetic models for As(V) onto CS-Fe.

Kinetic models	Parameters	25 mg L^{-1}	40 mg L^{-1}
Lagergren-first-order	q_e (mg g^{-1})	5.67	7.87
	k_1 (h^{-1})	3.29	3.34
	R^2	0.9993	0.9953
Pseudo-second-order	q_e (mg g^{-1})	5.68	7.93
	k_2 (g mg^{-1} h^{-1})	9.12	5.13
	R^2	0.9999	0.9999

Table 4: Calculation of saturation indices (SI) for precipitation phases using the equilibrium concentrations in solution at the initial As (V) of 40 mg L^{-1} in the CS-Fe.

Phase	Reaction	log Ksp	SI[(a)]
$FeAsO_4{\cdot}2H_2O$	$FeAsO_4{\cdot}2H_2O = Fe^{3+} + AsO_4^{3-} + 2H_2O$	−20.2	−3.525
$AlAsO_4{\cdot}2H_2O$	$AlAsO_4{\cdot}2H_2O = Al^{3+} + AsO_4^{3-} + 2H_2O$	−15.8	−9.275
$Ca_3(AsO_4)_2{\cdot}4H_2O$	$Ca_3(AsO_4)_2{\cdot}4H_2O = 3Ca^{2+} + 2AsO_4^{3-} + 4H_2O$	−18.9	−33.105
$Ca_5(AsO_4)_3OH$	$Ca_5(AsO_4)_3OH = 5Ca^{2+} + 3AsO_4^{3-} + OH^-$	−40.12	−51.179
$Ca_4(OH)(AsO_4)_2{\cdot}4H_2O$	$Ca_4(OH)(AsO_4)_2{\cdot}4H_2O = 4Ca^{2+} + 2AsO_4^{3-} + OH^- + 4H_2O$	−27.49	−51.098

Notes. [(a)]Calculations performed using the Visual MINTEQ speciation model.

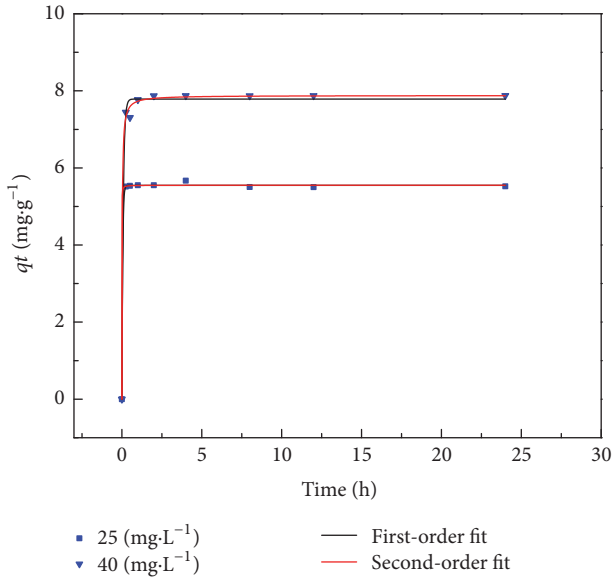

Figure 4: Adsorption kinetics of As(V) by CS-Fe (adsorbent dose 5 g L^{-1}; temperature 30°C).

is inferred that As (V) was likely adsorbed on the surface of CS-Fe via chemical interaction.

3.3. Possible Mechanism for Arsenate Removal

3.3.1. As Precipitation. Table 4 presents the saturation indices (SI) of As precipitates using equilibrium concentrations in solution at the initial As (V) concentration of 40 mg L^{-1} in the CS-Fe. The solution is undersaturated with $FeAsO_4{\cdot}2H_2O$, $AlAsO_4{\cdot}2H_2O$, $Ca_3(AsO_4)_2{\cdot}4H_2O$, $Ca_5(AsO_4)_3{\cdot}OH$, and $Ca_4(OH)(AsO_4)_2{\cdot}4H_2O$, which suggests that the formation of precipitates in the CS-Fe is thermodynamically unfavorable. Using vibrational spectroscopy, Goldberg and Johnston [28] observed that the IR and Raman spectra of As (V) adsorbed to Fe oxide samples are distinct from that of Fe arsenate salts, indicating that As (V) is bound as a surface complex and not as a precipitated solid phase. In this study, the XRD spectra for CS-Fe before and after As addition are shown in Figure 1(b). No new crystalline peak emerged in the As-loaded CS-Fe, suggesting the absence of crystalline arsenic precipitates.

3.3.2. Surface Adsorption Mechanism. Selective chemical extractions were performed on the As-loaded CS-Fe. The sulfate solution is involved in the extraction of exchangeable arsenic, the phosphate solution is typically used to remove specifically adsorbed arsenic, and the oxalate solutions involved in the extraction of arsenic associated with amorphous iron oxides. As shown in Figure 5, most of the Fe was released in the oxalate solution, accounting for about 60% of the Fe in the CS-Fe, which suggested that amorphous iron oxyhydroxide was the dominant species in the iron oxide-loaded biochar. Crystalline Fe oxides including magnetite and natrojarosite likely composed less than 40% of the CS-Fe biochar. The majority of As in the CS-Fe was also associated with amorphous iron oxyhydroxide, accounting for 52.26% of the total, suggesting the strong inner-sphere complexes that arsenate forms with iron oxide surfaces were a major mechanism for As adsorption by CS-Fe. The specifically adsorbed form was 28.23% of total arsenic, indicating that the specific anion exchange mechanism was also important in this system, and the presence of other anions such as PO_4^{3-} may inhibit the removal of As. In a study on the effect of interfering ion on the As (V) removal, Zhu et al. [14] observed that PO_4^{3-} with a concentration range of 0.1–10 mM resulted in a reduction of arsenic removal efficiency by 66.8–86.2%. Residual As comprised 18.38% of total arsenate, which likely represents the arsenate incorporated into the structures of crystalline Fe oxides [29] or the carbonized phase. These

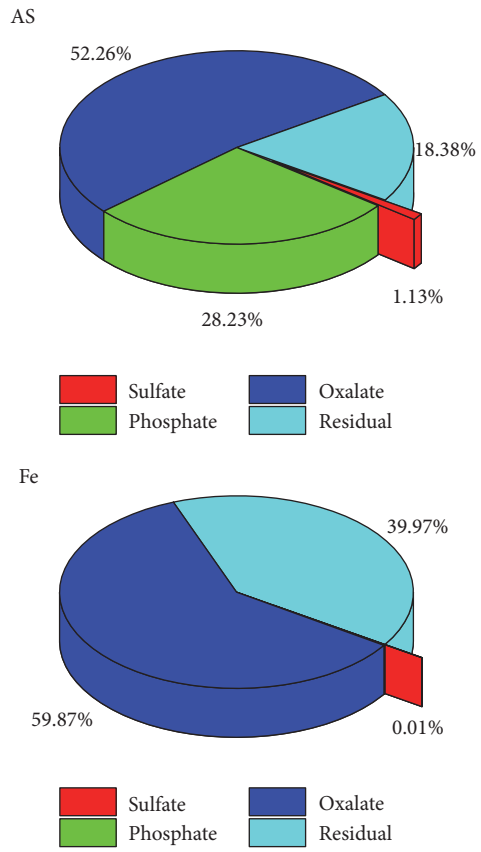

Figure 5: Distribution of As and Fe in the selective extractions.

results demonstrated that crystalline Fe oxides or carbonized phase is more efficient than amorphous iron oxyhydroxide in retaining arsenate in such irreversibly occluded forms. Only small amounts of As were present in the exchangeable fraction (1.13%), indicating that anion exchange from outer-sphere complexes was negligible. The regeneration of adsorbent is important in treating contaminated water for reducing the overall cost. The high proportion of As (70.64%) in the CS-Fe is associated with amorphous iron oxyhydroxide and in the residual, suggesting that CS-Fe does not have the advantage of regeneration ability. On the contrary, the less in the exchangeable and specifically adsorbed form, the better for the stabilization of As contaminated soil.

In summary, there are three mechanisms for arsenate sorption to the CS-Fe. First, a fraction of the arsenate is specifically adsorbed to the surface of both amorphous and crystalline Fe oxides. Second, substantial amounts of arsenate are strongly bound to amorphous iron oxyhydroxide via inner-sphere surface complexes. Third, partial occlusion of arsenate occurs on the crystalline Fe oxides or carbonized phase.

4. Conclusion

In the present study, iron-loaded biochar was successfully synthesized for arsenate removal. The maximum adsorption capacity estimated by the Langmuir model was 14.77 mg g^{-1}, which was comparable to and even moderately higher than many other iron-containing materials. The optimum pH range for arsenate removal was found to be between 2.0 and 8.0. Fe oxides including magnetite, natrojarosite, and amorphous iron oxyhydroxide constituted major As-adsorbing sinks. Further investigation into As speciation in the solid phase suggested that three mechanisms were involved in arsenate removal: sorption, strong inner-sphere surface complexes, and partial occlusion into the crystalline Fe oxides or carbonized phase. The biochar prepared from iron-impregnated corn straw may show better effects of remediation toward arsenic contaminated water or soil.

Conflicts of Interest

The authors declare that they have no conflicts of interest.

Acknowledgments

This project was financially supported by the National Natural Science Foundation of China (no. 41371320, no. 41371447, and no. 21677123).

Supplementary Materials

Table S1: sequential chemical extraction method for As-load biochar [21]. Figure S1: effect of CS-Fe dose on the adsorption of As(V) (experiment condition: the initial concentration of As(V) was 40 mg L^{-1}; the solid-to-liquid ratio was 5.0 g L^{-1} and stirred with 200 r min^{-1} at 30°C for 6 h). Figure S2: diagrams of As (V) species versus pH. *(Supplementary Materials)*

References

[1] X. Hu, Y. Zhang, J. Luo, M. Xie, T. Wang, and H. Lian, "Accumulation and quantitative estimates of airborne lead for a wild plant (Aster subulatus)," *Chemosphere*, vol. 82, no. 10, pp. 1351–1357, 2011.

[2] X. Bi, X. Feng, Y. Yang et al., "Allocation and source attribution of lead and cadmium in maize (Zea mays L.) impacted by smelting emissions," *Environmental Pollution*, vol. 157, pp. 834–839, 2009.

[3] T. Y. Lin, C. C. Wei, C. W. Huang, C. H. Chang, F. L. Hsu, and V. H. C. Liao, "Both phosphorus fertilizers and indigenous bacteria enhance arsenic release into groundwater in arsenic-contaminated aquifers," *Journal of Agricultural and Food Chemistry*, vol. 64, pp. 2214–2222, 2016.

[4] Z. Liu, F. S. Zhang, and R. Sasai, "Arsenate removal from water using Fe_3O_4-loaded activated carbon prepared from waste biomass," *Chemical Engineering Journal*, vol. 160, pp. 57–62, 2010.

[5] M. L. Sangyang, W. A. W. A. K. Ghani, A. Idris, and M. B. Ahmad, "Hydrogel biochar composite for arsenic removal from wastewater," *Desalination Water Treatment*, vol. 57, pp. 3674–3688, 2016.

[6] J. Zhu, Z. Lou, Y. Liu, R. Fu, S. A. Baig, and X. Xu, "Adsorption behavior and removal mechanism of arsenic on graphene modified by iron–manganese binary oxide (FeMnOx/RGO) from

aqueous solutions," *The Royal Society of Chemistry Advances*, vol. 5, pp. 67951–67961, 2015.

[7] N. Zhu, T. Yan, J. Qiao, and H. Cao, "Adsorption of arsenic, phosphorus and chromium by bismuth impregnated biochar: Adsorption mechanism and depleted adsorbent utilization," *Chemosphere*, vol. 164, pp. 32–40, 2016.

[8] T. Budinova, D. Savova, B.Tsyntsarski et al., "Biomass waste-derived activated carbon for the removal of arsenic and manganese ions from aqueous solutions," *Applied Surface Science*, vol. 255, no. 8, pp. 4650–4657, 2009.

[9] A. W. Samsuri, F. Sadegh-Zadeh, and B. J. Seh-Bardan, "Adsorption of As(III) and As(V) by Fe coated biochars and biochars produced from empty fruit bunch and rice husk," *Journal of Environmental Chemical Engineering (JECE)*, vol. 1, no. 4, pp. 981–988, 2013.

[10] E. Agrafioti, D. Kalderis, and E. Diamadopoulos, "Arsenic and chromium removal from water using biochars derived from rice husk, organic solid wastes and sewage sludge," *Journal of Environmental Management*, vol. 133, pp. 309–314, 2014.

[11] L. Z. Guan, J. J. Zhou, Y. Zhang, G. C. Zhang, J. H. Zhang, and Z. X. Chan, "Effects of biochars produced from different sources on arsenic adsorption and desorption in soil," *Chinese Journal of Applied Ecology*, vol. 24, no. 10, pp. 2941–2946, 2013.

[12] M. Jang, W. Chen, and F. S. Cannon, "Preloading hydrous ferric oxide into granular activated carbon for arsenic removal," *Environmental Science & Technology*, vol. 42, no. 9, pp. 3369–3374, 2008.

[13] S. Yao, Z. Liu, and Z. Shi, "Arsenic removal from aqueous solutions by adsorption onto iron oxide/activated carbon magnetic composite," *Journal of Environmental Health Science and Engineering*, vol. 12, no. 1, p. 58, 2014.

[14] J. Zhu, S. A. Baig, T. Sheng, Z. Lou, Z. Wang, and X. Xu, "Fe_3O_4 and MnO_2assembled on honeycomb briquette cinders (HBC) for arsenic removal from aqueous solutions," *Journal of Hazardous Materials*, vol. 286, pp. 220–228, 2015.

[15] Y. Jin, X. Liang, M. He, Y. Liu, G. Tian, and J. Shi, "Manure biochar influence upon soil properties, phosphorus distribution and phosphatase activities: A microcosm incubation study," *Chemosphere*, vol. 142, pp. 128–135, 2016.

[16] J. W. Gaskin, C. Steiner, K. Harris, K. C. Das, and B. Bibens, "Effect of low-temperature pyrolysis conditions on biochar for agricultural use," *Transactions of the Asabe*, vol. 51, no. 6, pp. 2061–2069, 2008.

[17] S. J. Lu, W. F. Tan, and L. Fan, "Point of zero charge (PZC) of manganese oxides determined with an improved salt titration method," *Acta Pedologica Sinica*, vol. 43, p. 763, 2006.

[18] D. Mohan, P. Singh, A. Sarswat, P. H. Steele, and C. U. Pittman, "Lead sorptive removal using magnetic and nonmagnetic fast pyrolysis energy cane biochars," *Journal of Colloid and Interface Science*, vol. 448, pp. 238–250, 2015.

[19] A. Contescu, C. Contescu, K. Putyera, and J. A. Schwarz, "Surface acidity of carbons characterized by their continuous pK distribution and Boehm titration," *Carbon*, vol. 35, no. 1, pp. 83–94, 1997.

[20] T. Sheng, S. A. Baig, Y. Hu, X. Xue, and X. Xu, "Development, characterization and evaluation of iron-coated honeycomb briquette cinders for the removal of As(V) from aqueous solutions," *Arabian Journal of Chemistry*, vol. 7, no. 1, pp. 27–36, 2014.

[21] B. Cances, F. Juillot, G. Morin et al., "XAS evidence of As (V) association with iron oxyhydroxides in a contaminated soil at a former arsenical pesticide processing plant," *Environmental Science & Technology*, vol. 39, pp. 9398–9405, 2005.

[22] D. Xu, Y. Zhao, K. Sun et al., "Cadmium adsorption on plant- and manure-derived biochar and biochar-amended sandy soils: impact of bulk and surface properties," *Chemosphere*, vol. 111, pp. 320–326, 2014.

[23] Y. Mikhaylova, G. Adam, L. Häussler, K. J. Eichhorn, and B. Voit, "Temperature-dependent FTIR spectroscopic and thermoanalytic studies of hydrogen bonding of hydroxyl (phenolic group) terminated hyperbranched aromatic polyesters," *Journal of Molecular Structure*, vol. 788, pp. 80–88, 2006.

[24] S. Y. Wang, Y. K. Tang, K. Li, Y. Y. Mo, H. F. Li, and Z. Q. Gu, "Combined performance of biochar sorption and magnetic separation processes for treatment of chromium-contained electroplating wastewater," *Bioresource Technology*, vol. 174, pp. 67–73, 2014.

[25] D. Bulgariu and L. Bulgariu, "Equilibrium and kinetics studies of heavy metal ions biosorption on green algae waste biomass," *Bioresource Technology*, vol. 103, no. 1, pp. 489–493, 2012.

[26] W. Chen, R. Parette, J. Zou, F. S. Cannon, and B. A. Dempsey, "Arsenic removal by iron-modified activated carbon," *Water Research*, vol. 41, no. 9, pp. 1851–1858, 2007.

[27] M. Li, Q. Liu, L. Guo et al., "Cu(II) removal from aqueous solution by Spartina alterniflora derived biochar," *Bioresource Technology*, vol. 141, pp. 83–88, 2013.

[28] S. Goldberg and C. T. Johnston, "Mechanisms of arsenic adsorption on amorphous oxides evaluated using macroscopic measurements, vibrational spectroscopy, and surface complexation modeling," *Journal of Colloid and Interface Science*, vol. 234, no. 1, pp. 204–216, 2001.

[29] A. Violante, S. D. Gaudio, M. Pigna, M. Ricciardella, and D. Banerjee, "Coprecipitation of arsenate with metal oxides. 2. Nature, mineralogy, and reactivity of iron (III) precipitates," *Environmental Science & Technology*, vol. 41, pp. 8275–8280, 2007.

Hindawi
Journal of Chemistry
Volume 2018, Article ID 2914313, 10 pages
https://doi.org/10.1155/2018/2914313

Research Article

Chemical Characteristics of Precipitation in a Typical Urban Site of the Hinterland in Three Gorges Reservoir, China

Liuyi Zhang,[1,2,3] **Baoqing Qiao**,[1,2] **Huanbo Wang**,[1] **Mi Tian**,[1] **Jian Cui**,[1,3] **Chuan Fu**,[3] **Yimin Huang**,[3] **and Fumo Yang**[1,2,3,4]

[1] *CAS Key Laboratory of Reservoir Environment, Chongqing Institute of Green and Intelligent Technology, Chinese Academy of Sciences, Chongqing 400714, China*
[2] *University of Chinese Academy of Sciences, Beijing 100049, China*
[3] *Key Laboratory of Water Environment Evolution and Pollution Control in Three Gorges Reservoir, Chongqing Three Gorges University, Wanzhou 404100, China*
[4] *CAS Center for Excellence in Regional Atmospheric Environment, Institute of Urban Environment, Chinese Academy of Sciences, Xiamen 361021, China*

Correspondence should be addressed to Fumo Yang; fmyang@cigit.ac.cn

Received 26 October 2017; Revised 5 January 2018; Accepted 18 February 2018; Published 19 March 2018

Academic Editor: Franco Tassi

Major water-soluble ions were analyzed for two-year precipitation samples in Wanzhou, a typical urban site of the hinterland of Chinese Three Gorges Reservoir. The pH values of the precipitation were in the range of 4.0 to 8.3, and the volume-weighted mean (VWM) value was 5.0. The concentration order of anions and cations was as follows: $SO_4^{2-} > NO_3^- > Cl^- > F^-$ and $NH_4^+ > Ca^{2+} > Na^+ > K^+ > Mg^{2+}$, respectively. Good correlations were found between SO_4^{2-} and NH_4^+, SO_4^{2-} and Ca^{2+}, NO_3^- and NH_4^+, and NO_3^- and Ca^{2+}, implying their co-occurrence in the precipitation, most likely as $(NH_4)_2SO_4$, $(NH_4)HSO_4$, NH_4NO_3, $CaSO_4$, and $Ca(NO_3)_2$. The sum of all measured ions was 416.4 μeq L^{-1}, indicating serious air pollution in Wanzhou. NH_4^+ and Ca^{2+} were the most important ions neutralizing the acidic compounds in the precipitation; their major sources included agricultural activity and crustal dust. Local anthropogenic activities, for example, coal burning and traffic related sources, contributed most of SO_4^{2-} and NO_3^-. The equivalent concentration ratio of SO_4^{2-}/NO_3^- was 4.5, indicating that excessive emission of sulfur was the main reason leading to the precipitation acidity in Wanzhou. However, this ratio was lower than the ratio (5.9) in 2000s in Wanzhou, indicating that the contribution of nitric acid to the acidity of precipitation was strengthening.

1. Introduction

Precipitation is an important means of scavenging airborne pollutants, including in-cloud scavenging (rainout) and below-cloud scavenging (washout) [1]. With the accelerated urbanization and industrialization, excessive pollutants have emitted into the atmosphere in China, for example, nitrogen oxides (NO_x), sulfur dioxide (SO_2), and particulate matter (PM). These pollutants can dissolve in precipitation and then return to surface through wet deposition. Precipitation that contains a large amount of pollutants would cause a series of negative ecological effects on the surface ecosystem, for example, soil acidification, eutrophication, and biodiversity reduction.

It has been observed that precipitation was contaminated worldwide because of the excessive emission of atmospheric pollutants. These pollutants can change the chemical characteristics of precipitation during the scavenging process depending on the solubility [2]. Chemical compositions of precipitation were influenced by the type of pollutant, meteorology, and topographic structure. Therefore, different regions have very different chemical composition in precipitation. Generally, Na^+ and Cl^- are abundant along coastal areas [3]; Ca^{2+} and Mg^{2+} are abundant in inland areas [4];

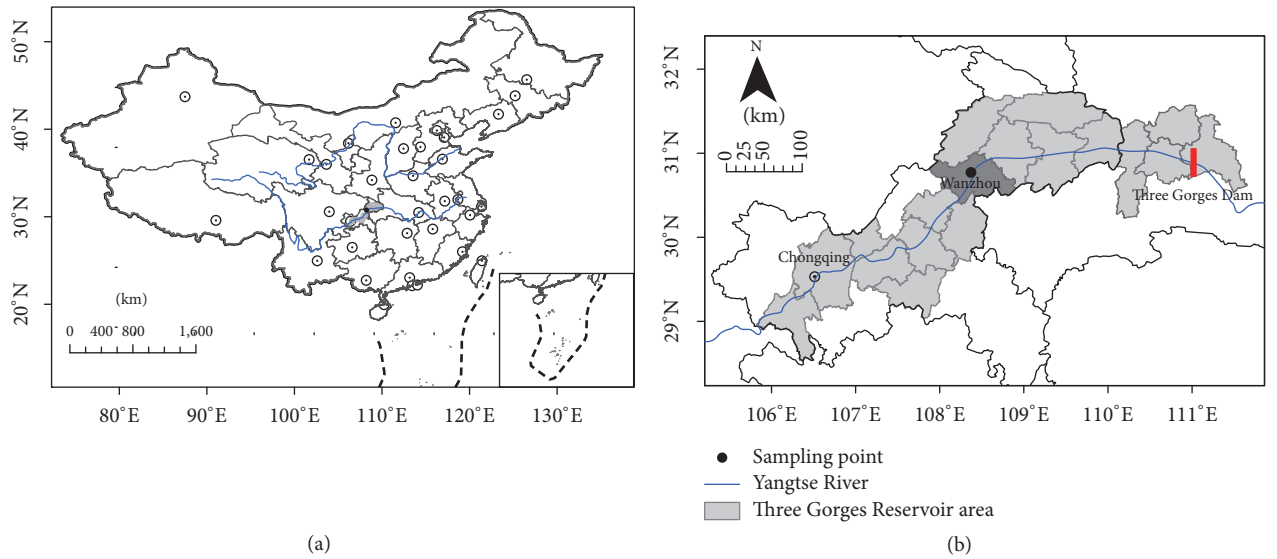

Figure 1: The sampling site in Wanzhou.

SO_4^{2-} and NO_3^- are abundant in industrial or urban areas [5, 6].

Because large amount of coal combustion increased the SO_2 concentration in the atmosphere over the past 30 years, China has become the largest acid rain region in the word [7]. Extensive acid rain was observed in the southern and southwest China in the 1990s, and it has extended to the eastern and central areas [5]. Northern China had a higher concentration of acidic ions in the precipitation than that in the south, but the pH of precipitation was almost higher than the threshold value of acid rain (pH = 5.6) in Northern China, because there were enough alkaline substances (e.g., alkaline particles and NH_3) which can neutralize the acidic components. It was estimated that the pH of precipitation would decrease by a factor of 1.85 pH units in the absence of alkaline neutralization in Northern China [8]. Acid precipitation would cause huge damage to environment, including acidification of soil and water, death of animals and plants, and weathering of buildings and artifacts [9]. The sum of economic loss resulting from acid deposition in China reached RMB 176.42 billion yuan in 2000 according to the evaluation from Chinese Research Institute of Environment [10].

Chongqing has been one of the most serious acid rain polluted regions in China since the late 1970s. Simian Mountain and Jinyun Mountain in Chongqing were believed to be relatively clean in the sense of air pollution, but the average pH values of precipitation in the two areas were 4.3 and 4.8 in 1991-1992, respectively [11]. As the stringent national air pollution regulations were established to decrease the emission of SO_2, the SO_4^{2-} concentration in precipitation in Chongqing has been decreasing since 2007 [12]. However, the alleviation of the acid rain pollution was not so evident, likely due to the increase of NO_x emission [13].

Wanzhou is located in the northeastern Chongqing and is the biggest city in the hinterland of the Three Gorges Reservoir Area (TGRA), being 327 kilometers away from downtown Chongqing and 283 kilometers away from Three Gorges Dam. In the light of the important and sensitive location in the Three Gorges Reservoir, two-year precipitation samples were collected in urban Wanzhou and the major ions were analyzed. The aim of this paper is to gain better understanding of precipitation chemistry in the hinterland of TGRA and to identify its major sources.

2. Experiments

2.1. Descriptions of Sampling Site. Wanzhou lies at the east of Sichuan Basin with a population about one million. The urban area of the city is basically built along the two mountainous banks of Yangtze River. Wanzhou has a subtropical monsoon wet climate with four distinct seasons. The average annual temperature is 18.6°C. In Wanzhou, there is a mild climate with an annual average precipitation amount of ~1200 mm, among which ~70% are concentrated in the period between May and September. Because of the topographic condition, Wanzhou is the region with the lowest wind speed in China, and the average wind speed is 0.81 m s^{-1} between 2014 and 2015 (automatic weather station's data at the sampling point).

Sampling of atmospheric precipitation was performed on the rooftop of a teaching building with nine floors in Chongqing Three Gorges University (Figure 1). This sampling site is surrounded by residential areas, and three kilometers away from the downtown Wanzhou and about 600 m away from Yangtze River. To the west of the sampling site, there is a hill with dense vegetation and a few cultivated lands. To the east, there is a major street road (about 100 m away). Next to the sampling site, a weather station (Lufft WS500-UMB, Germany) and atmospheric particle monitor (Thermo TEOM1405, USA) were equipped to obtain meteorological data and particle data, respectively, including wind speed and

direction, temperature, air pressure, relative humidity, total solar radiation, and mass concentrations of $PM_{2.5}$ and PM_{10}.

2.2. Sample Collection and Analyses. The samples of precipitation were collected with a dry-wet deposition autosampler (APS-3A, Changsha Xianglan Scientific Instrument Co., Ltd.). There is a movable lid which can be stimulated by a wetness sensor to open the funnel of 300 mm in diameter for collection of precipitation during precipitation. Precipitation samples were collected on each rainy/snowy day between 9:00 a.m. and 9:00 a.m. the next day. After the samples were taken to the laboratory, 10 mL of each sample was taken to determine pH value (pHS-3C, Shanghai Leici Instrument Factory, China) and electrical conductivity (EC) value (sensION5, Hach, USA). Before each measurement, standard buffer and standard NaCl solution were used to calibrate the pH meter and conductivity meter. The remaining solution of samples was filtered with 0.45 μm pore diameter membrane filter and then kept in 4°C for subsequent testing.

The anion components, including F^-, Cl^-, NO_3^-, and SO_4^{2-}, were analyzed by using ion chromatography (ICS-900, Dionex Company, USA), with an IonPac AS19-HC column, 25 mM NaOH eluent, and ASRS300 suppresser. The detection limits for these anions are 0.03 mg L^{-1}, 0.03 mg L^{-1}, 0.1 mg L^{-1}, and 0.1 mg L^{-1}, respectively. K^+, Na^+, Ca^{2+}, and Mg^{2+} were analyzed by flame atomic absorption spectrophotometer. To eliminate spectral interference, cesium nitrate and lanthanum nitrate as deionizing agents were added to the potassium and sodium calibration solutions and the calcium and magnesium calibration solutions, respectively. The detection limits for K^+, Na^+, Ca^{2+}, and Mg^{2+} were 0.013 mg L^{-1}, 0.008 mg L^{-1}, 0.02 mg L^{-1}, and 0.0025 mg L^{-1}, respectively. NH_4^+ were analyzed by Spectrophotometry Method of Sodium Hypochlorite-Salicylic Acid in accordance with the national standard method of China (GB 13580.11-92). In this method, NH_4^+ reacted with hypochlorite and salicylic acid to produce stable blue compound, whose absorbance was determined at the wavelength of 698 nm by using UV-visible spectrophotometer (T6, Purkinje General Instrument Co. Ltd., China). The lowest concentration detected by this method for NH_4^+ was 0.01 mg L^{-1}. The recoveries for all ions detected here were in the range of 80%–120% and the relative standard deviation was less than 5% for reproducibility test. A total of 207 valid samples were analyzed. After statistical analyses described in Section 2.4, the monthly data included meteorological factors, $PM_{2.5}$, PM_{10}, precipitation amount, pH, anions, and cations, which are presented in the supplementary material (available here).

2.3. Quality Control and Assurance. In the process of ion analysis, Standard Reference Materials, produced by National Research Center for Certified Reference Materials, China, were routinely analyzed to guarantee the data quality. Six samples were removed because their data were outside the range of $(m - 3\delta, m + 3\delta)$, which was often used to exclude outliers [22], and where m denotes averaged value; δ means standard deviation. The Pearson correlation between anions and cations was 0.97 ($p < 0.01$), suggesting credible data quality. And the data were also considered acceptable because the ratio of total cations (H^+, Na^+, K^+, Ca^{2+}, Mg^{2+}, and NH_4^+) and total anions (F^-, Cl^-, NO_3^-, and SO_4^{2-}) is 1.05, which is within the range of 1 ± 0.25 [23].

2.4. Statistical Analysis. The volume-weighted mean (VWM) pH value was calculated by

$$\overline{\mathrm{pH}} = -\log\left[\mathrm{H}^+\right] = -\log\left[\frac{\sum_{j=1}^{n} 10^{-\mathrm{pH}_j} \cdot Q_j}{\sum_{j=1}^{n} Q_j}\right], \quad (1)$$

where $\overline{\mathrm{pH}}$ is the VWM pH value in a month/season/year, pH_j is the pH value of jth precipitation, and Q_j (mm) is the amount of jth precipitation. The ionic concentration of precipitation was calculated by

$$\overline{C_i} = \frac{\sum_{j=1}^{n} C_{ij} \cdot Q_j}{\sum_{j=1}^{n} Q_j}, \quad (2)$$

where $\overline{C_i}$ (μeq L^{-1}) is the VWM concentration of ith ion in a month/season/year and C_{ij} (μeq L^{-1}) is the concentration of ith ion in jth rainfall.

The non-sea salt (nss) values of any particular ion were calculated from the measured concentrations of the ions of interest using sodium ion as the reference element. This process was implemented under the assumption that all sodium is derived from marine sources [23]. The equation for the non-sea salt contribution can be written as

$$[\text{nss-}X]_i = \left[X_i\right] - \left[\mathrm{Na}^+\right]_i \times \left[\frac{[X]}{\left[\mathrm{Na}^+\right]}\right]_{\text{sea salt}}, \quad (3)$$

where $[\text{nss-}X]_i$ (μeq L^{-1}) is the concentration of nss concentration of species X in sample i, $[X_i]$ is the total measured concentration of chemical species X in sample i, $[Na^+]_i$ (μeq L^{-1}) is the concentration of Na^+ in sample i, and $\{[X]/[Na^+]\}_{\text{sea salt}}$ is the ratio of these species as measured in seawater [23].

2.5. Back Trajectories and PSCF Analysis. Cluster analysis of backward air-mass trajectories and potential source contribution function (PSCF) analysis were performed using TrajStat software on the sample date during this study period [24]. The meteorological data used for the analysis were from the Global Data Assimilation System (GDAS) of National Centers for Environmental Prediction (NCEP). The 72-hour backward trajectories of the air parcels arriving at 00:00 UTC at 1200 m elevation above the ground level were clustered. The PSCF values corrected by a weight factor were then calculated using the mean concentration for three anthropogenic ions (SO_4^{2-}, NH_4^+, and NO_3^-) [25]. The results were displayed as maps with each grid cell equal to 0.5° latitude by 0.5° longitude in size.

3. Results and Discussion

3.1. Precipitation Amount, EC, and pH Distribution. The annual precipitation amounts were 1189.2 mm and 1081.1 mm

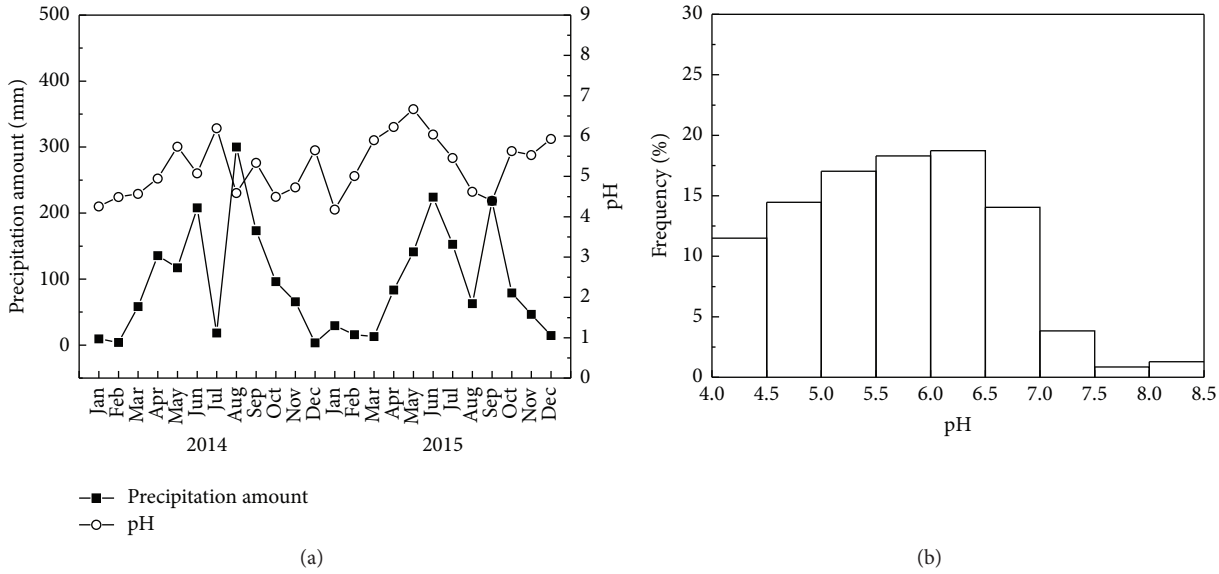

Figure 2: (a) Monthly precipitation amount, VWM pH, and (b) pH frequency distribution of the precipitation in Wanzhou.

in 2014 and 2015, respectively. As shown in Figure 2(a), monthly mean precipitation amount varied markedly with a peak in the summer and about 70% of the precipitation occurred during the period from May to September. These results were consistent with the long-term average precipitation levels and seasonal variations in Wanzhou [26].

The EC values of single precipitation varied in the range of 3.4 μS cm^{-1} to 234.0 μS cm^{-1} with an average of 35.9 μS cm^{-1}, which was larger by a factor of 2.5 than that (14.6 μS cm^{-1}) measured at the global atmospheric background site in Mt. Waliguan Mountain [27]. However, this value was comparable to those measured in many other cities, such as 42.2 μS cm^{-1} in Shenzhen [28] and 66.5 μS cm^{-1} in Beijing [6], indicating that anthropogenic impacts on the atmospheric environment in Wanzhou could not be neglected.

The pH values of a single precipitation sample ranged from 4.0 to 8.3 with a VWM value of 5.0, lower than the pH of typical natural rainwater (5.6). As for the frequency of acid precipitation (Figure 2(b)), there were 46.9% of precipitation with the pH lower than 5.6. Additionally, 26.1% of precipitations had pH lower than 5.0, and 11.6% were strongly acidic with pH lower than 4.5. It is worth noting that the arithmetic mean pH value of precipitation was 5.7 during the two-year study period, which was a little higher than the average (5.5) observed during the period of 2001–2009 [15]. This is an indication of the mitigation trend in acidification of precipitation in Wanzhou.

3.2. Chemical Composition of the Precipitation. Figure 3 presented the statistical results of ion concentrations and percentage share of each ion. The most abundant ions were SO_4^{2-}, Ca^{2+}, NH_4^+, and NO_3^-. The average concentration of NH_4^+ together with Ca^{2+} reached 151.6 μeq L^{-1} and accounted for 68.4% of the total cations. The average concentration of SO_4^{2-} plus NO_3^- was 246.51 μeq L^{-1} which occupied 91.3% of all anions. Among the precipitation components, SO_4^{2-} was the most abundant single ion, accounting for 36.3% of the total ions, followed in decreasing order by, NO_3^-, Cl^-, and F^-. For the cations, NH_4^+ and Ca^{2+} were followed in decreasing concentration by Na^+, K^+, H^+, and Mg^{2+}. The total VMW concentration of the measured ions was 416.4 μeq L^{-1} in Wanzhou, indicating the serious air pollution in the hinterland of TGRA.

The sum of SO_4^{2-}, NO_3^-, and NH_4^+, which were the main anthropogenic ions in precipitation, accounted for 71.4% of the total ionic equivalents, while H^+ accounted for 3.6%, demonstrating that anthropogenic sources predominated in the contributions to precipitation ions. Ca^{2+} and Mg^{2+}, regarded as two kinds of main crustal-related ions, occupied together 32.5% of total ionic equivalents, indicating that crustal-derived elements had key contribution to the neutralization of the acid precipitation. Nss-SO_4^{2-} and nss–Ca^{2+} accounted for 96.1% and 98.5% of the total sulfate and total calcium, respectively. Thus, the impact of sea salt on the wet deposition in Wanzhou was negligible.

The equivalent ratio of ($[Ca^{2+}]$ + $[NH_4^+]$)/($[SO_4^{2-}]$ + $[NO_3^-]$) was further used to evaluate the degree of influence by the anthropogenic activities. The ratio of ($[Ca^{2+}]$ + $[NH_4^+]$)/($[SO_4^{2-}]$ + $[NO_3^-]$) in the precipitation in this study reached 0.79, which conformed with the ratio (0.80) in the period between 2001 and 2009 in Wanzhou [15]. It is noted that this ratio was lower than that measured in Lin'an (0.97), Longfengshan (1.27), and Shangdianzi (0.96), three regional background atmospheric stations of World Meteorological Organization (WMO) in Yangtze River Delta, Northeast China, and North China, respectively [29]. This comparison reflected that there was more influence from anthropogenic activities on the precipitation in Wanzhou.

As compared in Table 1, the concentration levels of the ions associated with human activities (SO_4^{2-}, NO_3^-,

Table 1: VWM concentrations of major inorganic ions in the precipitation in Wanzhou and some selected areas (unit: μeq L^{-1}).

Areas	Periods	pH	F^-	Cl^-	NO_3^-	SO_4^{2-}	NH_4^+	Ca^{2+}	Na^+	K^+	Mg^{2+}	SO_4^{2-}/NO_3^-	References
Wazhou	2014-2015	5.0	3.2	15.1	35.1	156.9	89.6	62.1	24.4	20.1	9.9	4.5	This study
Zigui	2009	4.9	ND[b]	11.8	63.2	177.2	90.6	142.6	11.7	7.5	18.3	2.8	[14]
Wanzhou	2001–2009	5.5[a]	8.4	25.3	43.7	258.3	126.6	114.4	27.0	12.7	29.2	5.9	[15]
Okinawa, Japan	2003–2005	4.9	ND[b]	351	7.0	53.9	9.5	25.2	308	9.4	63.9	7.7	[16]
New Jersey, USA	2006-2007	4.6	1.1	10.7	14.3	19.0	24.4	3.0	10.9	1.3	1.6	1.3	[17]
Delhi, India	2011–2013	6.4	10.7	42.9	50.5	91.6	23.7	198.6	26.8	5.3	69.2	1.8	[4]
Beijing	2001–2005	6.0	15.4	34.9	106.0	314.0	236.0	209.0	22.5	13.8	48.4	3.0	[6]
Guiyang	2008-2009	4.2	14.5	20.7	7.3	265.6	112.8	182.9	13.9	9.6	10.5	36.4	[5]
Guangzhou	2005-2006	4.5	12.0	21.0	51.8	202	66.2	131.0	18.0	9.0	9.0	3.9	[18]
Lijiang	1989–2006	6.1	ND[b]	11.6	3.6	32.6	11.4	50.2	2.5	ND[b]	7.7	9.1	[19]
Shenzhen	1986–2006	5.0	4.5	37.9	22.1	74.3	35.2	77.7	40.3	7.2	9.7	3.4	[20]
Chengdu	2008	5.1	6.2	8.9	156.2	212.8	150.5	196.6	1.4	6.6	16.2	1.4	[21]

[a]Arithmetic mean value; [b]not determined.

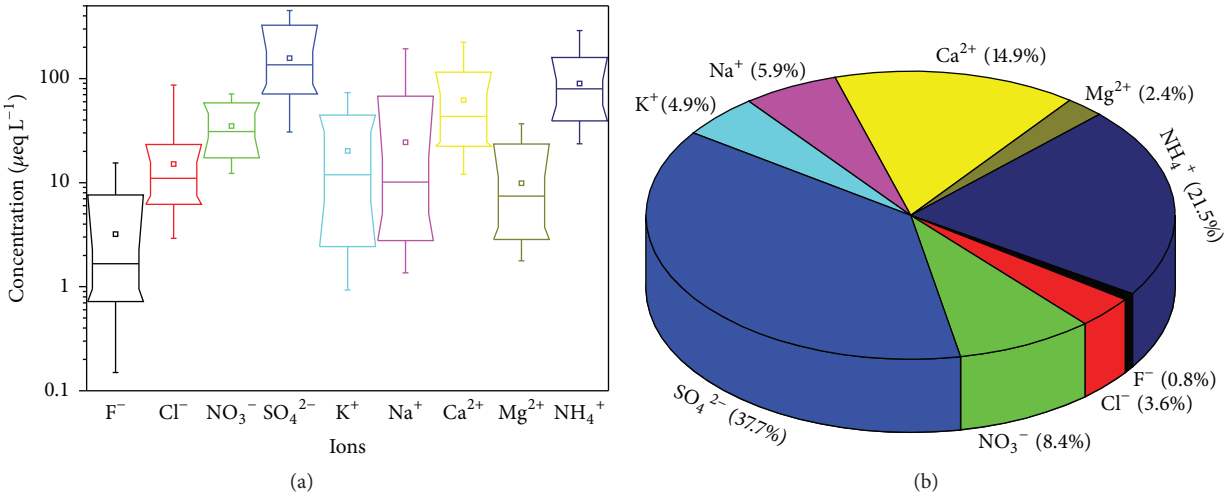

Figure 3: (a) Statistics of ions' concentration and (b) percentages of ions' VWM concentration (μeq L^{-1}) in the precipitation in Wanzhou. The box plots indicate the minimum, 10th and 25th percentiles, median, 75th and 90th percentiles, maximum, and average (square) of each ion.

and NH_4^+) in Wanzhou were lower than those in Beijing, Guiyang, Guangzhou, but significantly higher than those reported in Japan, India, and North America. In the case of the soil derived calcium, Wanzhou had much lower values than Beijing, Guiyang, Guangzhou, and Chengdu. In comparison with Zigui, which is located in the head region of TGRA, the concentrations of SO_4^{2-} and NH_4^+ were very similar in the two areas, whereas NO_3^- presented much low concentration in Wanzhou. It is noted that K^+ concentration was much higher in this study compared to other areas and the historical value, likely due to enhanced biomass burning in the immediate vicinity of the site.

Compared to the period from 2001 to 2009, all the ions except K^+ in this study exhibited decreasing trends. This was likely attributed to the implementation of industrial restructuring and emission reduction policies by local government. A typical example was that the emission amount of sulfur dioxide had been decreased from 26,400 t in 2008 to 17,388 t in 2015 [30], about one-third reduction within seven years.

3.3. Temporal Variations of pH and Major Ionic Concentration. Figure 4 showed the seasonal variations of the EC, pH, and precipitation amount in Wanzhou. In winter, the pH was 4.9 and the precipitation amount was 12.8 mm; both were the lowest, while the EC was the highest with the value of 55.9 μS cm^{-1}. By contrast, the lowest EC and highest precipitation amount occurred in summer and were 18.5 μS cm^{-1} and 161.1 mm, respectively. This indicated that the dilution effect played an important role in determining analyte concentrations in the precipitation. The seasonal variation of pH was significant in the following order with a decrease trend: spring > summer > autumn > winter. The enhanced fugitive dust, which contained many alkaline substances because of the windy weather, and local farming

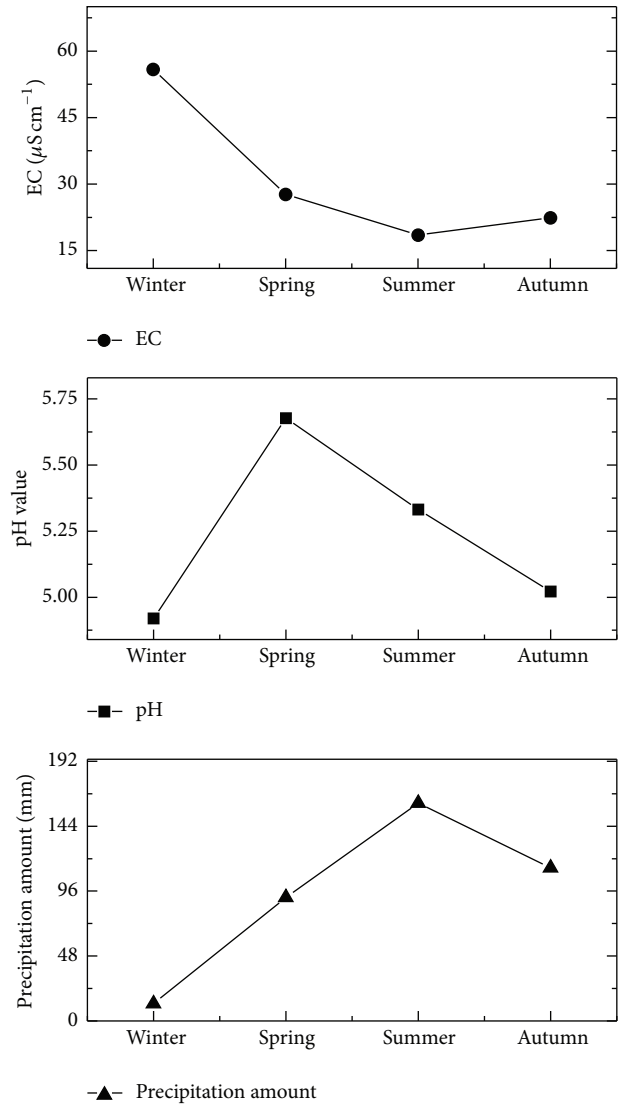

Figure 4: Seasonal variations of the two-year average EC, pH, and precipitation amount in Wanzhou.

might be responsible for the highest precipitation pH in spring.

Figure 5 showed the monthly and seasonal variations in VWM concentration of ions in the precipitation in Wanzhou; both monthly and seasonal concentrations of each ion were subject to large variability. Both higher loadings of crustal-related and anthropogenic ions usually appeared during the dry months from November to April, while lower loadings appeared in rainy months. This variation of ionic concentration might be related to the seasonal distribution of air-mass origins, precipitation intensity, and emissions of pollutants. In the dry months, enhanced coal combustion caused the anthropogenic emissions of gaseous pollutants and particles. Taking SO_4^{2-} as an example, the seasonal variation was completely consistent with the variation of its gaseous precursor, SO_2 [31]. Additionally, atmospheric particles might play an important role in contribution of ions in precipitation, since the sum of monthly ionic concentrations was well correlated ($r = 0.59, p < 0.01$) with the PM_{10} concentration in Wanzhou. Furthermore, the plentiful rains during rainy periods enhanced dilution effect of precipitation on ionic mass, as indicted by the negative correlations with precipitation volume (correlation coefficient $r = -0.15$ to -0.37).

3.4. Acid Neutralization and the Form of Acidity. The neutralization between the acidic components and basic components determines the pH value of the precipitation. Balasubramanian et al. presented an equation for calculation of fractional acidity (FA = $[H^+]/([SO_4^{2-}] + [NO_3^-])$ in precipitation [32]. On the other hand, neutralization factor (NF) was widely used to evaluate the acid neutralization efficiency by alkaline ions in precipitation: $NF_{Xi} = [X_i]/([SO_4^{2-}] + [NO_3^-])$, where X_i is the chemical component of interest and all of the ion concentrations are expressed in μeq L^{-1} [8, 33]. In Wanzhou, the *FA* value was 7.3%, which means 92.7% of the acidity had been neutralized. The NF values for NH_4^+, Ca^{2+}, Na^+, K^+, and Mg^{2+} during the 2-year period were 0.46, 0.32, 0.13, 0.11, and 0.05, respectively, revealing that NH_4^+ and Ca^{2+} were the major basic ions for the neutralization of the acidity. Nevertheless, the neutralization effect of NH_4^+ and Ca^{2+} in precipitation in Wanzhou was much lower than that in Northern China, where the NF values accounted for 0.71 and 0.72, respectively [8].

In this paper, the equivalent ratio of $[SO_4^{2-}]/[NO_3^-]$ was utilized to assess relative contributions of SO_4^{2-} and NO_3^- in the acidity of precipitation. As shown in Table 1, the SO_4^{2-}/NO_3^- ratio (4.5) in this study was much higher than those in all other Chinese cities except Guiyang, which is the capital city of Guizhou province suffering serious acid rain since late 1970s. This suggested that the precipitation acidity in Wanzhou was dominantly from excessive emission of sulfur. On the other hand, the ratio was lower than that determined during 2001–2009 in Wanzhou [15], indicating the relatively reinforced contribution of nitric acid to precipitation acidity.

3.5. Air-Mass Back Trajectories and PSCF Analysis. Figure 6(a) showed the five air-mass clustering trajectories arriving at the sampling site and Table 2 showed the VWM concentrations of NH_4^+, SO_4^{2-}, and NO_3^- of each cluster. It can be seen that all air masses converged to southern Wanzhou and finally entered Wanzhou. Cluster 1 and cluster 2, two short-distance transport trajectories, were the most important air-mass trajectories, which accounted for 39.8% and 35.7% of all the trajectories, respectively. The concentrations of NH_4^+, SO_4^{2-}, and NO_3^- in cluster 1 and cluster 2 were lower than that in cluster 3, cluster 4, and cluster 5. The trajectories in cluster 3, moving from the Yunnan Province to Wanzhou via Guizhou province, represented for 11.2% of air masses, and the precipitation in this cluster contained moderate concentrations of NH_4^+, SO_4^{2-}, and NO_3^-.

Precipitation in cluster 4 and cluster 5 occurred mainly in winter and spring, respectively. The trajectories accounted

Table 2: VWM concentrations of NH_4^+, SO_4^{2-}, and NO_3^- in precipitation for the six trajectory clusters during 2014-2015 in Wanzhou (unit: μeq L^{-1}).

Cluster	NH_4^+	SO_4^{2-}	NO_3^-
(1) 39.8%	85.29	134.19	24.65
(2) 35.7%	83.37	118.81	25.98
(3) 11.2%	92.97	145.66	29.19
(4) 9.2%	97.62	206.74	56.51
(5) 4.1%	90.34	184.53	40.63

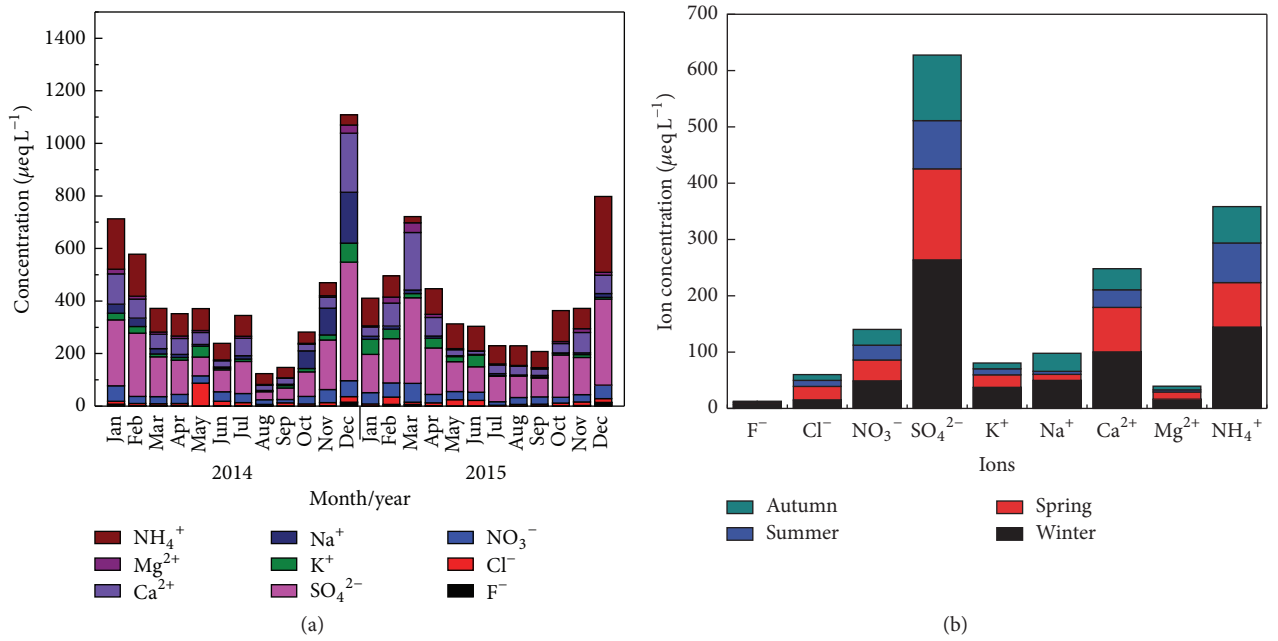

Figure 5: (a) Monthly variations and (b) seasonal variations in the VWM concentration of ions in the precipitation in Wanzhou.

for only 9.2% and 4.1% of the total trajectories, respectively, while the cluster-mean concentrations of NH_4^+, SO_4^{2-}, and NO_3^- were the highest in the five clusters. This could have been due to the low precipitation amount and to the traversal of the clusters through high-emission areas. For example, cluster 4 and cluster 5 passed over Chongqing city and Xi'an city, respectively, both of which suffered severe air pollution [34, 35]. The potential source contribution areas of SO_4^{2-}, NH_4^+, and NO_3^- were shown in Figures 6(b)–6(d). SO_4^{2-}, NH_4^+, and NO_3^- possessed similar potential areas of source contribution. These areas were predominately concentrated on the southeast of Wanzhou, the junction region of Chongqing, Hubei province, and Hunan province. In addition, the areas in the northeast of Wanzhou had some contributions as well. Therefore, it can be concluded that the anthropogenic ions in the precipitation in Wanzhou were mostly from local sources and surrounding areas. In winter and spring, however, there was a small amount of pollutants input into Wanzhou through long distance.

3.6. Factor Analysis of Ions in Precipitation. Varimax-rotated factor analysis was utilized for the investigation of the major sources of chemical species in the precipitation (Table 3). Three factors were identified with the cumulative variance more than 85%. And the communalities of all the ions are no less than 0.60, indicating that these extracted factors are reasonable. There was a strong correlation between Mg^{2+}, Ca^{2+}, and Na^+ with factor 1 accounting for 34% of the total variance, pointing to the common occurrence of these ions from crustal origin. Additionally, factor 1 had a moderate relation with SO_4^{2-}, NO_3^-, and F^-, implying that this factor was also likely associated with certain anthropogenic sources, such as industrial emissions, fossil fuel combustion, and fugitive dust. Factor 2 accounted for 31% of the total variance with high loadings for SO_4^{2-}, NO_3^-, NH_4^+, and F^-, suggestive of the secondary pollution formed from their precursors in the atmosphere. The correlation coefficients were significant in statistics ($p < 0.01$) between the following ions: SO_4^{2-} and NH_4^+ (0.68), SO_4^{2-} and Ca^{2+} (0.59), NO_3^- and NH_4^+ (0.53), and NO_3^- and Ca^{2+} (0.70). Therefore, these ions in the precipitation mainly existed as the compounds of $CaSO_4$, $(NH_4)_2SO_4$, $(NH_4)HSO_4$, NH_4NO_3, and $Ca(NO_3)_2$. Therefore, SO_4^{2-} and NO_3^- were always in neutralized forms [36]. In addition, factor 3 was indicated by high loading

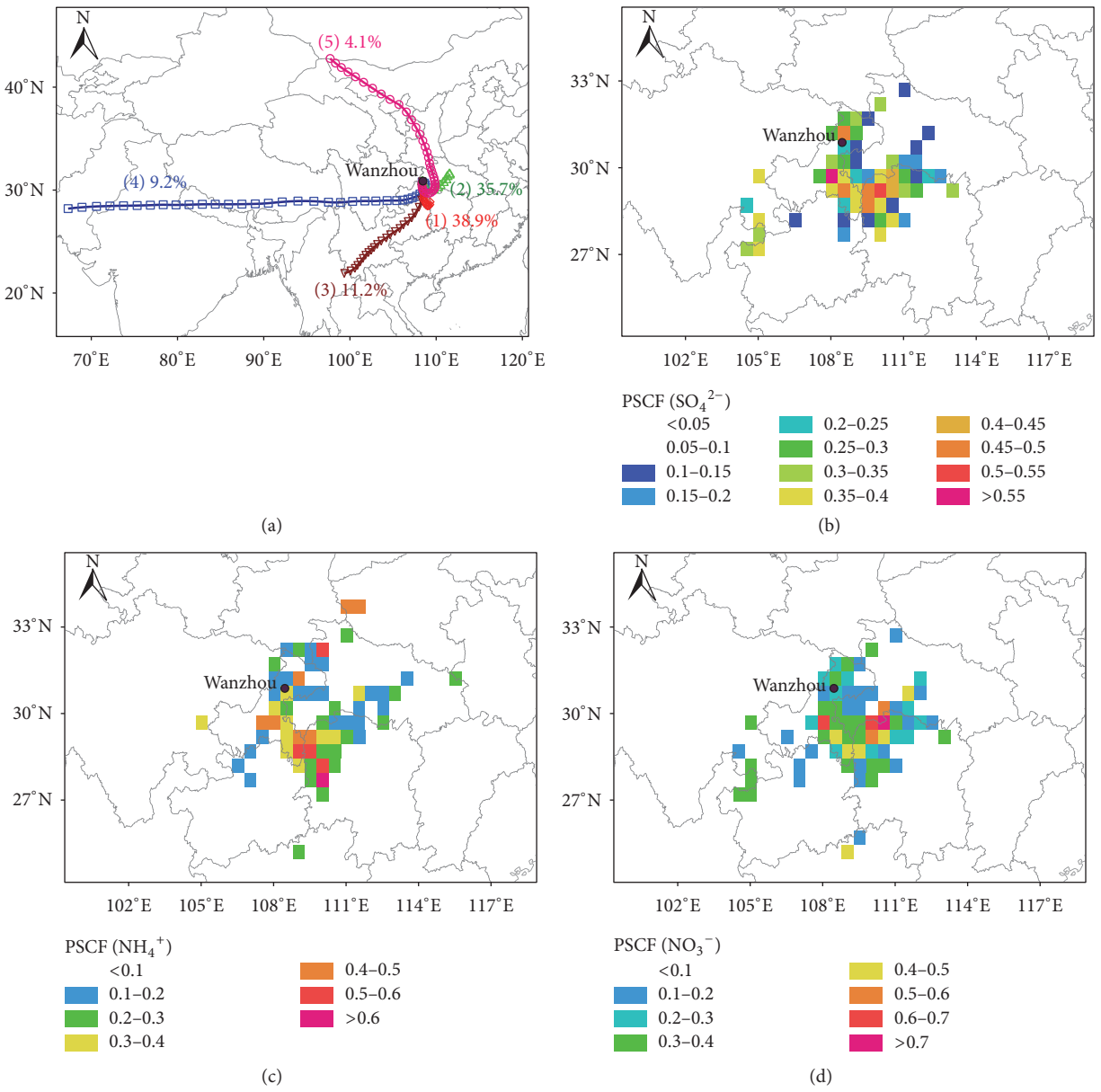

Figure 6: Cluster analysis (a) and potential source areas for SO_4^{2-} (b), NH_4^+, (c) and NO_3^- (d) in Wanzhou.

for Cl^- and K^+, implying the sources of biomass burning [37].

4. Conclusions

The chemical compositions of daily precipitation in Wanzhou, a typical urban area located in the hinterland of the TGRA, were investigated during the period of January 2014 to December 2015. The main findings can be summarized as follows:

(1) The pH of two-year precipitation samples in Wanzhou ranged from 4.0 to 8.3 with a volume-weighted mean (VWM) value of 5.0. About 46.9% of the precipitation samples had a pH lower than 5.6 and 26.1% samples had a pH lower than 5.0, and 11.6% of precipitation was strong in acidity with the pH below 4.5. EC ranged from 3.4 to 234.0 μS cm^{-1}, with the VWM value of 35.9 μS cm^{-1}.

(2) SO_4^{2-} was the most abundant ion with the VWM concentration of 156.9 μeq L^{-1}, accounting for 74.6% of total anions, followed in decreasing order by NO_3^-, Cl^-, and F^-. The precipitation acidity was predominantly neutralized by NH^+ and Ca^{2+}, whose sum contributed 68.4% to the total cations. There were good relations between the following pairs of ions: SO_4^{2-} and NH_4^+, SO_4^{2-} and Ca^{2+}, NO_3^- and NH_4^+, and NO_3^- and Ca^{2+}, indicating their coexistence in precipitation, mostly as $(NH_4)_2SO_4$, $(NH_4)HSO_4$, $CaSO_4$, NH_4NO_3, and $Ca(NO_3)_2$.

(3) Long-distance inputs of air pollutants were less in Wanzhou. NH_4^+ and Ca^{2+} were mainly originated from local

Table 3: Varimax-rotated principal factor analysis of ions in the precipitation of Wanzhou.

Variable	Factor 1	Factor 2	Factor 3	Communality
Cl^-	0.08	0.15	0.89	0.83
K^+	0.15	−0.01	0.92	0.87
Mg^{2+}	0.95	0.15	0.29	0.94
Na^+	0.54	0.44	0.37	0.72
NH_4^+	−0.01	0.91	0.07	0.84
SO_4^{2-}	0.45	0.81	0.06	0.86
NO_3^-	0.59	0.65	0.16	0.80
Ca^{2+}	0.92	0.26	0.13	0.93
F^-	0.47	0.72	0.07	0.74
Variance (%)	33.6	31.3	20.5	
Cumulative (%)	33.6	64.9	85.4	

agricultural activities and crust fraction, respectively. Cl^- and K^+ were mainly derived from the biomass burning near the sampling site. SO_4^{2-} and NO_3^- were primarily associated with local anthropogenic activities, such as coal burning and traffic emissions.

(4) The levels of ionic concentrations in precipitation in Wanzhou were similar to that in the head region of the TGRA. However, most ion concentrations were lower than that in 2000s, revealing the improvement of the air pollution in Wanzhou.

Conflicts of Interest

The authors declare no conflicts of interest.

Acknowledgments

The authors were grateful to Min Gao and Binni Shen for their assistance in sample collection and laboratory work. This study was supported by the West Action Plan of the Chinese Academy of Science (no. KZCX2-XB3-14), the National Natural Science Foundation of China (no. 31670467), Science and Technology Commission of Chongqing Projects (nos. cstc2015jcyjB0332 and cstckjcxljrc13) and Wanzhou Project (no. wzstc-042017105), Chongqing Municipality Education Commission (KJ1501006), and the open fund of CAS Key Laboratory from Reservoir Aquatic Environment.

Supplementary Materials

Table S1: monthly data of ionic concentration of precipitation, mass concentration of particulate matter, and meteorological factors in Wanzhou. *(Supplementary Materials)*

References

[1] M. Kajino and M. Aikawa, "A model validation study of the washout/rainout contribution of sulfate and nitrate in wet deposition compared with precipitation chemistry data in Japan," *Atmospheric Environment*, vol. 117, pp. 124–134, 2015.

[2] Y.-Z. Cao, S. Wang, G. Zhang, J. Luo, and S. Lu, "Chemical characteristics of wet precipitation at an urban site of Guangzhou, South China," *Atmospheric Research*, vol. 94, no. 3, pp. 462–469, 2009.

[3] S. Park, B. Seo, G. Lee, S. Kahng, and Y. Jang, "Chemical composition of water soluble inorganic species in precipitation at shihwa basin, Korea," *Atmosphere*, vol. 6, no. 12, pp. 732–750, 2015.

[4] P. S. P. Rao, S. Tiwari, J. L. Matwale et al., "Sources of chemical species in rainwater during monsoon and non-monsoonal periods over two mega cities in India and dominant source region of secondary aerosols," *Atmospheric Environment*, vol. 146, pp. 90–99, 2016.

[5] H.-W. Xiao, H.-Y. Xiao, A.-M. Long, Y.-L. Wang, and C.-Q. Liu, "Chemical composition and source apportionment of rainwater at Guiyang, SW China," *Journal of Atmospheric Chemistry*, vol. 70, no. 3, pp. 269–281, 2013.

[6] F. Yang, J. Tan, Z. B. Shi et al., "Five-year record of atmospheric precipitation chemistry in urban Beijing, China," *Atmospheric Chemistry and Physics*, vol. 12, no. 4, pp. 2025–2035, 2012.

[7] W. X. Wang and P. J. Xu, "Research progress in precipitation chemistry in China," *Progress in Chemistry*, vol. 21, pp. 266–281, 2009 (Chinese).

[8] Y. Wang, W. Yu, Y. Pan, and D. Wu, "Acid neutralization of precipitation in Northern China," *Journal of the Air & Waste Management Association*, vol. 62, no. 2, pp. 204–211, 2012.

[9] S. Eyssautier-Chuine, B. Marin, C. Thomachot-Schneider et al., "Simulation of acid rain weathering effect on natural and artificial carbonate stones," *Environmental Earth Sciences*, vol. 75, no. 9, article no. 748, 2016.

[10] C.-F. You and X. C. Xu, "Coal combustion and its pollution control in China," *Energy*, vol. 35, no. 11, pp. 4467–4472, 2010.

[11] F. Zhang, J. Zhang, H. Zhang, N. Ogura, and A. Ushikubo, "Chemical composition of precipitation in a forest area of Chongqing, Southwest China," *Water, Air, & Soil Pollution*, vol. 90, no. 3-4, pp. 407–415, 1996.

[12] Y. Peng, F. Zhou, J. Cui et al., "Impact of socioeconomic and meteorological factors on reservoirs' air quality: a case in the Three Gorges Reservoir of Chongqing (TGRC), China over a 10-year period," *Environmental Science and Pollution Research*, vol. 24, no. 19, pp. 16206–16219, 2017.

[13] L. Duan, Q. Yu, Q. Zhang et al., "Acid deposition in Asia: emissions, deposition, and ecosystem effects," *Atmospheric Environment*, vol. 146, pp. 55–69, 2016.

[14] Q. Wu and G. Han, "Sulfur isotope and chemical composition of the rainwater at the three gorges reservoir," *Atmospheric Research*, vol. 155, pp. 130–140, 2015.

[15] Q. M. Lu, L. Zhao, L. Li et al., "Chemical composition of precipitation and its spatiotemporal variations in the Three Gorges Reservoir Region," *Acta Scientiae Circumstantiae*, vol. 33, pp. 1682–1689, 2013 (Chinese).

[16] H. Sakihama, M. Ishiki, and A. Tokuyama, "Chemical characteristics of precipitation in Okinawa Island, Japan," *Atmospheric Environment*, vol. 42, no. 10, pp. 2320–2335, 2008.

[17] F. Song and Y. Gao, "Chemical characteristics of precipitation at metropolitan Newark in the US East Coast," *Atmospheric Environment*, vol. 43, no. 32, pp. 4903–4913, 2009.

[18] D.-Y. Huang, Y.-G. Xu, P. Peng, H.-H. Zhang, and J.-B. Lan, "Chemical composition and seasonal variation of acid deposition in Guangzhou, South China: Comparison with precipitation in other major Chinese cities," *Environmental Pollution*, vol. 157, no. 1, pp. 35–41, 2009.

[19] N. Zhang, Y. He, J. Cao, K. Ho, and Z. Shen, "Long-term trends in chemical composition of precipitation at Lijiang, southeast Tibetan Plateau, southwestern China," *Atmospheric Research*, vol. 106, pp. 50–60, 2012.

[20] Y. Huang, Y. Wang, and L. Zhang, "Long-term trend of chemical composition of wet atmospheric precipitation during 1986-2006 at Shenzhen City, China," *Atmospheric Environment*, vol. 42, no. 16, pp. 3740–3750, 2008.

[21] H. Wang and G. Han, "Chemical composition of rainwater and anthropogenic influences in Chengdu, Southwest China," *Atmospheric Research*, vol. 99, no. 2, pp. 190–196, 2011.

[22] Y. W. Liu, X. R. Xu-Ri, Y. S. Wang, Y. P. Pan, and S. L. Piao, "Wet deposition of atmospheric inorganic nitrogen at five remote sites in the Tibetan Plateau," *Atmospheric Chemistry and Physics*, vol. 15, no. 20, pp. 11683–11700, 2015.

[23] W. C. Keene, A. A. P. Pszenny, J. N. Galloway, and M. E. Hartley, "Sea-salt corrections and interpretation of constituents ratios in marine precipitation," *Journal of Geophysical Research: Atmospheres*, vol. 91, pp. 6647–6658, 1986.

[24] Y. Q. Wang, X. Y. Zhang, and R. R. Draxler, "TrajStat: GIS-based software that uses various trajectory statistical analysis methods to identify potential sources from long-term air pollution measurement data," *Environmental Modeling and Software*, vol. 24, no. 8, pp. 938-939, 2009.

[25] D. Lucey, L. Hadjiiski, P. K. Hopke, J. R. Scudlark, and T. Church, "Identification of sources of pollutants in precipitation measured at the mid-Atlantic US coast using potential source contribution function (PSCF)," *Atmospheric Environment*, vol. 35, no. 23, pp. 3979–3986, 2001.

[26] X. Y. Zhou, S. Y. Xie, and W. Ren, "An analysis of the characteristics of precipitation in the Three Gorges Reservoir Area from 1955 to 2014—a case study of Wanzhou in Chongqing," *Journal of Southwest University*, vol. 39, pp. 102–108, 2017 (Chinese).

[27] J. Tang, H. S. Xue, X. L. Yu et al., "The preliminary study on chemical characteristics of precipitation at Mt. Waliguan," *Acta Scientiae Circumstantiae*, vol. 20, pp. 420–425, 2000 (Chinese).

[28] Y. W. Niu, L. Y. He, and M. Hu, "Chemical characteristics of atmospheric precipitation in Shenzhen," *Journal of Environmental Sciences*, vol. 29, pp. 1014–1019, 2008 (Chinese).

[29] L. Yi, Y. Xiaolan, C. Hongbing, L. Weili, T. Jie, and W. Shufeng, "Chemical characteristics of precipitation at three Chinese regional background stations from 2006 to 2007," *Atmospheric Research*, vol. 96, no. 1, pp. 173–183, 2010.

[30] Bureau of statistics of Wanzhou district, Chongqing, Wanzhou Statistical Yearbook, 2009/2016.

[31] Y. C. Xiang, L. Y. Zhang, F. Gao, N. Zeng, and R. Z. Qian, "Analysis on relationships between sulfur dioxide concentration and dioxide concentration and meteorological factors in Wanzhou," *Journal of Agricultural Catastrophology*, vol. 4, pp. 45–47, 2014 (Chinese).

[32] R. Balasubramanian, T. Victor, and N. Chun, "Chemical and statistical analysis of precipitation in Singapore," *Water, Air, & Soil Pollution*, vol. 130, no. 1-4, pp. 451–456, 2001.

[33] P. C. Mouli, S. V. Mohan, and S. J. Reddy, "Rainwater chemistry at a regional representative urban site: influence of terrestrial sources on ionic composition," *Atmospheric Environment*, vol. 39, no. 6, pp. 999–1008, 2005.

[34] H. Wang, M. Tian, Y. Chen et al., "Seasonal characteristics, formation mechanisms and source origins of $PM_{2.5}$ in two megacities in Sichuan Basin, China," *Atmospheric Chemistry and Physics*, vol. 18, no. 2, pp. 865–881, 2018.

[35] L. Bai and Z.-L. Wang, "Anthropogenic influence on rainwater in the Xi'an City, Northwest China: Constraints from sulfur isotope and trace elements analyses," *Journal of Geochemical Exploration*, vol. 137, pp. 65–72, 2014.

[36] B. Kyoung Lee, S. Hee Hong, and D. Soo Lee, "Chemical composition of precipitation and wet deposition of major ions on the Korean peninsula," *Atmospheric Environment*, vol. 34, no. 4, pp. 563–575, 2000.

[37] H. Wang, G. Shi, M. Tian et al., "Wet deposition and sources of inorganic nitrogen in the Three Gorges Reservoir Region, China," *Environmental Pollution*, vol. 233, pp. 520–528, 2018.

Hindawi
Journal of Chemistry
Volume 2018, Article ID 7172426, 9 pages
https://doi.org/10.1155/2018/7172426

Research Article

Distribution and Identification of Sources of Heavy Metals in the Voghji River Basin Impacted by Mining Activities (Armenia)

A. V. Gabrielyan,[1] G. A. Shahnazaryan ,[1] and S. H. Minasyan[2]

[1] *"Environmental Monitoring and Information Center" SNCO, 0012 Yerevan, Armenia*
[2] *Institute of Chemical Physics, NAS RA, 0014 Yerevan, Armenia*

Correspondence should be addressed to G. A. Shahnazaryan; gayane_shahnazaryan@yahoo.com

Received 23 December 2017; Revised 11 February 2018; Accepted 18 February 2018; Published 18 March 2018

Academic Editor: Xiao-San Luo

The objective of this research is to assess the distribution of heavy metals in the waters and sediments of the Voghji River and its tributaries impacted by mining activity and to reveal the real source of each of the heavy metals in the environment for assessing the pollution level of heavy metals. Voghji River with two main tributaries (Geghi and Norashenik) drain two mining regions. To identify distribution and pollution sources of heavy metals, the water and sediment samples were collected from eight sampling sites. The results of statistical analysis based on data sets of the period 2014–2016 showed that, after the influence of drainage water and wastewater of mining regions, heavy metal contents in the Voghji River basin dramatically increased. The waters of the Voghji River were highly polluted by Mn, Co, Cu, Zn, Mo, Cd, and Pb. The relation of metals content was highly changed due to anthropogenic impact disturbing the geochemical balance of the Voghji River. The water quality based on only heavy metal contents in the source of the Voghji River belongs to "good" chemical status, and in the sources of Geghi and Norashenik Rivers it is "moderate." The water quality of Voghji and Norashenik Rivers is sharply worsening after the influence of mining activity, becoming "bad" chemical status. The research revealed the pollution sources of each metal.

1. Introduction

Impact of mining on aquatic ecosystems became an issue of increasing concern. Mining by its nature consumes, diverts, and seriously pollutes water resources [1–3]. Mining and milling operations, together with grinding, concentrating ores, and disposal of tailings, provide obvious sources of contamination in the surface environment, along with discharge or overflow of wastewater, runoff from rainfall or snowmelt, drainage from the toe of waste piles, and discharge of impacted groundwater to streams and springs. Water pollution problems caused by mining include acid mine drainage, metal contamination, and increased sediment levels in streams [4, 5]. The generation of acidic drainage and the release of water containing high concentrations of dissolved metals from mine wastes constitute an environmental problem of international scale [6–8]. Chemical leaching of metals occurs when precipitation from rainfall or snowmelt infiltrates through ore or waste materials and dissolves or desorbs metals from the solid material. As a consequence, streams transport high contents of toxic trace elements such as As, Cd, Pb, Zn, Cu, Sb, and Se [9].

Heavy metals are an important class of pollutants which can produce considerable harm to the environment when they are above certain concentrations [10–12]. These elements can be leached into the surface water or groundwater, taken up by plants, and can bond semipermanently with soil components such as clay or organic matter, which later affect human health [13]. After heavy metals enter into a water body, they can harm aquatic organisms, and, through the processes of chemical adsorption and physical precipitation, heavy metals can accumulate in the sediments of the water environment [14]. Heavy metal contents of the surface sediments are generally significantly higher compared with those in the water body, so it is very important to explore the heavy metal contents in the surface sediments [15, 16].

Heavy metals are defined as metallic elements that have a relatively high density compared to water. With the assumption that heaviness and toxicity are interrelated, heavy metals also include metalloids, such as arsenic, that are able to induce

Table 1: Summary of sampling sites (water and sediment) of the Voghji River basin.

Site	River	Location description
1	Voghji	Upstream of the Kajaran city before confluence with ZCMC
2	Voghji	Downstream of the Kajaran city, after confluence with ZCMC
3	Voghji	Upstream of the Kapan city, after runoff Geghi River
4	Voghji	Downstream of the Kapan city, after runoff wastewaters of KPM, Kavart, and Geghanush
5	Norashenik	Before confluence wastewater of tailings dam of Artshvanik
6	Norashenik	Mouth
7	Geghi	Source
8	Geghi	Mouth

toxicity at a low level of exposure and nonmetal selenium [17].

The mining industry is developed in the Republic of Armenia (RA). Due to the lack of adequate management and planning, as well as poor operating experience and waste management, this branch of industry is one of the main sources of water pollution and of the environment, in general, with heavy metals (Pb, Cu, Ni, Cd, Mo, As, etc.). Previous studies in the Voghji River basin [18–21] have all found elevated concentrations of heavy metals and trace elements such as As, Cu, Mo, Sb, Cu, Co, Ni, and Zn in the surface waters and sediments. The pollution problems were reported in soils located near kindergarten and schools of the Kapan and Kajaran cities [22, 23].

However, inadequate information is available on the concentrations and distribution of heavy metals and trace elements in the Voghji River basin. The aim of this study was therefore to investigate the distribution of heavy metals (Ti, Fe, Mn, V, Cr, Co, Ni, Cu, Zn, As, Se, Mo, Cd, Sb, Pb) in the waters and sediments of the Voghji River and its tributaries impacted by mining activity; to reveal the source of each of heavy metals in the environment and correlation between parameters, to assess the pollution level of heavy metals; and to estimate the temporal variability influence in concentrations of heavy metals.

2. Materials and Methods

2.1. Study Area. Voghji River is a left tributary of Aras River located in the southeast of Armenia. The sources of Voghji River are mountain springs and small lakes of the Kaputjugh Mountain at an elevation of 3650 m above sea level located in the west-southern part of Armenia. The total length of the River is 82 km (in Armenia 52 km) and the catchment basin area is 2337 km^2 (in Armenia 1240.47 km^2). The largest tributaries are Geghi and Norashenik. On its way, the stream is fed by groundwater, rain, and melting snow and has perennial flow throughout the year. Mean annual water discharges of the Voghji, Norashenik, and Geghi Rivers are estimated to be 334.3, 69.7, and 135.3 million m^3 or 10.6, 2.21, and 4.29 m^3/s, respectively [24].

The Voghji River passes through the two mining districts. One of them is Zangezur copper-molybdenum combine (ZCMC) which is located in the upstream of the Voghji River in the territory of the Kajaran city, in the southeast of Armenia. ZCMC is the largest in the region open pit mine which extracts copper and molybdenum-rich ore, afterwards producing two separate concentrates of copper and molybdenum. ZCMC produces 21 Mt of ore (and the similar amount of waste) annually. Besides the basic elements, a number of valuable associated elements exist in the ore, such as Pb, Zn, Cd, As, Co, and Ni. The slurry tailings, 33% of which is water, are transported from the plant of ZCMC to the tailings dam of Artsvanik by pipeline. The tailings dam of Artsvanik is located in the gorge of the same river. After precipitation of slurry tailings, the surface water of tailings dam flows into the Norashenik River. Besides, drainage waters (surface and ground) from open pit mine also flow into the Voghji River in the territory of Kajaran city.

The second mining district (Kapan Polymetal) is located in the downstream of the Voghji River, 1.5 km east of the town of Kapan in the southeast of Armenia. Kapan Polymetal (KPM) is fully mechanized underground mine with a current capacity of approximately 400 ktpa, a conventional 750 ktpa flotation concentrator, and various infrastructure facilities. The mine produces gold-copper-silver and zinc concentrate. Tailings of KPM are discharged into the tailings dam of Geghanush located in the gorge of the same river. After precipitation of slurry tailings in the tailings dam, the tailing liquid flows into the Geghanush River and then Voghji River. Near the city of Kapan, the abandoned mine of Kavart (not belonging to KPM) is located which is considered a possible source of metal's pollution. The waters of Kavart rich in heavy metals mix with surface and groundwaters in different ways.

2.2. Sample Collection and Analysis. Water and sediment samples were collected at 8 sampling sites of the Voghji River basin in the period 2014–2016 (see Figure 1, Table 1). The sampling sites were selected with the aim of covering the whole stream from its source to its confluence with two mining areas. The sampling sites were categorized in two groups: sampling sites 1, 5, and 7 are located in the source of rivers, which have the minimal anthropogenic influence representing the background state of the river basin; sampling sites 2, 4, and 6 bear the influence of mining activity and untreated wastewater of the cities.

Water samples were collected on a monthly basis. The frequency of sampling in the sources of Voghji (WS-1), Geghi (WS-7), and Artsvanik (WS-5) Rivers was less compared to

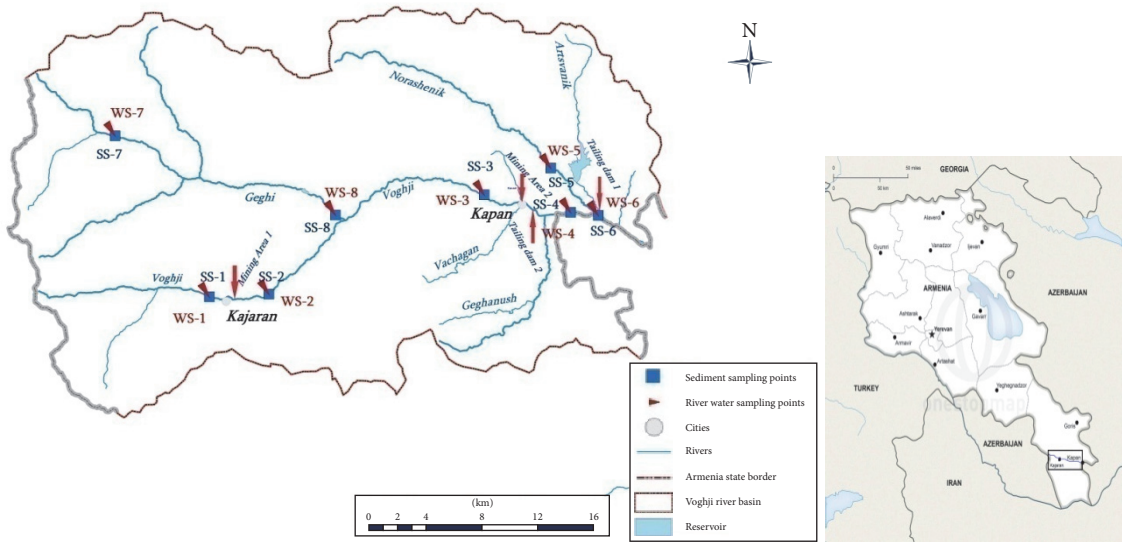

Figure 1: Map of the study area and location of sampling points: (mining area 1) ZCMC; (mining area 2) KPM; (WS) water sampling sites; (SS) sediment sampling sites; red arrows indicate pollution sources.

the other sites. Sediment samples were collected during the summer period in June and August.

Collection and handling of water and sediment samples were conducted in accordance with standard methodology (ISO 5667-3, -6, and -12). Water samples were collected in polypropylene plastic bottles. The water samples were acidified at the time of collection with nitric acid. Double-distilled nitric acid was used for water sample conservation. The samples were stored at 4°C and transported to the laboratory.

Sediment samples were collected using the appropriate sampler. Samples were transported to the laboratory, air-dried in the laboratory at room temperature until stable weights were recorded, and subsequently sieved through 2 mm mesh. Then dried sediments samples were placed into the digestion vessel with 12 mL of HNO_3/HF (3 : 1 v/v) solution and digested in a microwave digestion system (Speedwave MWS-3, Berghof, GmbH).

An inductively coupled plasma-mass spectrometer (ICP-MS, PerkinElmer ELAN 9000, USA) was used to determine the concentrations of Ti, Fe, Mn, V, Cr, Co, Ni, Cu, Zn, As, Se, Mo, Cd, Sb, and Pb in the sediment and water samples.

The standard curves were obtained using separate solutions containing known concentrations of each heavy metal (PerkinElmer, Pure Grade Atomic Spectroscopy Calibration Standard, USA) diluted with deionized water. For the calibration procedure, single element and multielement calibration standard solutions were used. For the preparation of standard solutions, deionized water (18.2 MOhm/cm) purified by Thermo Scientific Barnstead Easypure II and argon gas with the purity of 99.998% were used.

The background interferences from the plasma gases, air entrainment, and solvent were corrected by subtraction of reagent blank signals. The isobaric spectral interferences originating from the polyatomic ion species involving the sample matrix elements eliminated by selecting a suitable isotope were corrected or reduced by applying interference correction equations. To adjust the matrix effect and improve accuracy the internal standard ^{115}In was used.

2.3. Data Analysis. The data was analyzed using descriptive statistics: maximum, minimum, mean, standard deviation, variation coefficient, kurtosis, and skewness are reported. Box-and-whisker plot was used for visualisation kurtosis and skewness. Box-and-whisker provides a powerful tool for the analysis of pattern, which helps to evaluate the sources of changes as well as to assign the parameters that are associated with these sources. The Pearson correlation analysis was used to determine whether there was a linear association between the trace elements. Based on the value of correlation coefficient "*r*," the correlation between two parameters can be termed as positive or negative. Analyses were conducted using SPSS 19.0 (IBM, NYC, USA).

Assessment of pollution level of heavy metals in the Voghji River was done based on national water quality standards [25]. According to these standards, water quality is classified into 5 classes: "excellent" (I class), "good" (II class), "moderate" (III class), "poor" (IV class), and "bad" (V class). The classification system of water quality is based on background concentrations of heavy metals for each water basin management area, and the first class of system corresponds to the background concentration. The classification scheme is given in Table 2.

Since there are no established national sediment quality guidelines in Armenia, the results of heavy metals in sediments have been compared with the Canadian Interim Sediment Quality Guidelines (ISQG) proposed by the Canadian

Table 2: Water quality assessment objectives of heavy metals for Voghji River basin.

Heavy metal	Quality class				
	I	II	III	IV	V
Zn, μg/L	3	100	200	500	>500
Cu, μg/L	4	24	50	100	>100
Cr, μg/L	0.5	10.5	100	250	>250
As, μg/L	0.3	20.3	50	100	>100
Cd, μg/L	0.1	1.1	2.1	4.1	>4.1
Pb, μg/L	0.1	10.1	25	50	>50
Ni, μg/L	0.6	10.6	50	100	>100
Mo, μg/L	15	30	60	120	>120
Mn, μg/L	4	8	16	32	>32
V, μg/L	0.4	10	20	100	>100
Co, μg/L	0.09	0.18	0.36	0.72	>0.72
Fe, mg/L	0.03	0.06	0.5	1.0	>1.0
Sb, μg/L	0.5	1	2	4	>4
Ti, μg/L	1.5	10	20	100	>100
Se, μg/L	1.1	20	40	80	>80

Sediment Quality Guidelines for the Protection of Aquatic Life [26].

3. Results and Discussion

3.1. Heavy Metals in Waters of Voghji River and Its Tributaries. The data in Table 3 show a summary of the descriptive statistics of the heavy metals in waters of the Voghji River and its tributaries. The high CV implies that measured concentrations for all metals varied between stations ($p < 0.05$; ANOVA).

The spatial distribution of some heavy metals in the waters of Voghji, Norashenik, and Geghi Rivers was analyzed as box-and-whisker plots (See Figure 2).

They display batches of data with five values being used to describe the data set. The length of the box represents the interquartile range, which contains 50% of the values, and the heavy horizontal line inside the box indicates the median. The "whiskers" are lines that extend from the box to the highest and lowest values.

Spatial distribution pattern proved to be a powerful tool in identifying the contamination hotspots and possible sources of heavy metals. The comparison of heavy metal contents observed in the sources of rivers and other sites allows distinguishing geological and anthropogenic origins of pollutants.

The highest Cu concentration in the waters of Voghji River and its tributaries (median value 71.3 μg/l) (see Figure 2) was observed at WS-4, approximately 30–60 times higher compared to the background sites WS-1, WS-5, and WS-7 (see map, Figure 1). The Cu concentration is an order of magnitude higher compared to WS-3, too. This phenomenon states that the waters of Voghji River are polluted by Cu in the territory of Kapan city and the pollution source of Cu is the wastewater of KPM. There is also a potential of diffuse pollution with Cu from the abandoned mine of Kavart. Another source of Cu pollution of Voghji River, although not as large as the wastewater of KPM, is ZCMC with its Artsvanik tailings dam which is evident from the increase in the concentration of Cu after Kajaran city and in the mouth of Norashenik compared to the source of Voghji (WS-1) and Norashenik (WS-5) rivers. The Cu concentration variation around the median value also is higher due to the uncontrolled point and nonpoint contamination.

The spatial distribution patterns for Co and Fe are similar to Cu with observed highest concentration values in the WS-4 (see Figure 2 and Table 3).

The median values of Zn and Mn were significantly higher ($p < 0.001$) in WS-6 and WS-4 (see Figure 2). They were about two orders of magnitude higher than the highest concentrations of Zn and Mn measured in the other sites which are connected to the inflow of wastewater both from the Artsvanik tailings dam and KPM. The concentrations of Zn and Mn in WS-6 (mouth of Norashenik) after the influence of wastewater of Artsvanik tailings dam increase 99 and 55 times, respectively. The range of variation in the median value also is higher.

In the case of Sb, Mo, Se, As, and Cd the median values were significantly higher in WS-6, 4.78, 340.1, 4.0, 4.0, and 1.93 μg/l ($n = 29$), respectively (see Figure 2 and Table 3). The concentration increase between WS-6 and WS-5 is about 2-3 orders of magnitude. It is connected to the inflow of wastewater from Artsvanik tailings dam. In spite of observed higher concentrations of Sb and Mo in the mouth of Norashenik (WS-6), the impact on Voghji River is not so big because of differences of water quantity of Norashenik and Voghji Rivers (See Section 2.1). This pattern indicates that wastewater of KPM is not polluted by Sb and Mo. The increase in concentrations of Sb, Cd, and Mo is observed also at the WS-2 due to the point and nonpoint contamination of ZCMC. The concentration of Cd increases at WS-4 due to the impact of wastewater of KPM.

The spatial distribution pattern of Pb has similarity with Cd (See Table 3). The variation of mean concentration Pb within sampling sites is more than 80% indicating that the difference between the concentration of background and influenced sites is large. As observed from the data (Table 3) Pb content in the Voghji River increased due to the impact of wastewater of ZCMC and KPM.

The variability of mean concentrations of Cr, Ni, and Ti between sampling sites is 37%, 49%, and 41%, respectively. A little increase in the content of Cr and Ti was observed only at the WS-2 (0.97 and 5.05 μg/l) (Figure 2). Ni concentration slightly increases at WS-2 and WS-6.

The spatial distribution pattern of V differs from other metals. Under the influence of ZCMC, a small increase in the concentration of V was observed in WS-2 which is much lower than the concentration observed in WS-5. The content of several heavy metals, such as Ti, Cr, Co, Ni, Sb, and Pb, is higher at WS-5 comparing to the other two background sites (WS-1 and WS-7).

Overall, in the Norashenik River, the concentrations of Mn, Mo, Zn, Cd, and Sb were dramatically increased under the influence of wastewater of the Artsvanik tailings dam. In

Table 3: Arithmetic mean (AM) concentrations, standard deviation (SD), and variation coefficient (VC %) of heavy metals in waters of Voghji River and its tributaries during the period 2014–2016 (units are μg/L, except Fe and Mn for which units are mg/L; N represents the number of data).

WS	BS	Fe	Mn	Ti	V	Cr	Co	Ni	Cu	Zn	As	Mo	Cd	Sb	Pb	Se
1 (N = 24)	AM	0.038	0.004	1.82	0.243	0.395	0.082	0.927	3.07	3.21	0.938	5.83	0.045	0.044	0.039	0.765
	SD	0.03	0.002	0.66	0.12	0.24	0.057	0.36	1.51	1.88	0.56	2.85	0.02	0.03	0.03	0.798
	VC	69	54	36	51	60	70	38	49	59	60	49	48	71	87	104
2 (N = 29)	AM	0.183	0.023	5.54	1.06	1.030	0.316	1.67	10.9	4.75	1.79	111.6	0.372	0.39	0.397	7.69
	SD	0.14	0.02	3.12	0.76	0.57	0.24	0.67	5.66	4.77	0.95	94.2	0.34	0.36	0.47	7.94
	VC	74	102	56	72	55	76	40	52	101	53	84	92	92	119	103
3 (N = 29)	AM	0.074	0.004	2.79	1.17	0.559	0.157	1.07	5.62	1.59	1.94	46.3	0.153	0.33	0.463	1.38
	SD	0.05	0.00	2.05	0.42	0.29	0.12	0.46	2.14	1.25	0.77	17.5	0.07	0.19	0.56	1.09
	VC	68	62	74	36	51	73	43	38	78	40	38	46	59	121	79.0
4 (N = 29)	AM	0.376	0.181	3.95	1.36	0.677	2.57	2.92	82.5	105.5	1.51	64.2	1.18	0.778	0.329	1.81
	SD	0.189	0.137	2.38	0.875	0.436	1.95	2.00	51.3	84.6	0.818	65.1	0.779	0.851	0.238	1.36
	VC	50	76	60	64	64	76	68	62	80	54	101	66	109	72	75.3
5 (N = 15)	AM	0.110	0.003	4.14	4.61	0.716	0.227	1.28	1.28	0.94	0.688	1.19	0.009	0.116	0.099	0.728
	SD	0.078	0.00	1.98	1.62	0.50	0.10	0.56	0.44	0.67	0.19	0.48	0.01	0.07	0.10	1.14
	VC	71	56	48	35	69	44	44	34	72	27	40	59	61	100	157
6 (N = 29)	AM	0.236	0.178	6.18	6.90	0.790	0.720	2.150	11.5	82.1	4.59	400.5	1.891	5.87	0.522	4.25
	SD	0.21	0.14	4.68	5.80	0.70	0.51	1.22	7.79	50.4	2.29	217.5	0.78	3.43	0.47	2.57
	VC	88	77	76	84	57	70	57	68	61	50	54	41	58	90	60.6
7 (n = 15)	AM	0.075	0.005	2.12	0.647	0.297	0.126	0.805	1.51	1.39	0.616	7.15	0.036	0.084	0.048	1.57
	SD	0.06	0.01	1.21	0.32	0.25	0.06	0.37	0.47	1.05	0.46	2.95	0.02	0.05	0.04	2.08
	VC	85	99	57	49	86	44	46	31	75	75	41	42	58	93	132
8 (N = 29)	AM	0.077	0.011	2.76	0.840	0.503	0.150	1.025	3.23	2.35	1.14	15.3	0.057	0.166	0.114	1.71
	SD	0.07	0.01	2.40	0.35	0.46	0.07	0.53	1.75	1.79	0.61	12.2	0.04	0.12	0.15	2.09
	VC	86	59	87	42	92	47	52	54	76	53	79	63	69	129	122

the Geghi Rivera little increase in concentration values of Mn, As, Sb, and Pb was observed.

The variation coefficient (VC) was used to investigate the variability of concentrations during the sampling period (2014–2016). The most seasonally variable metals are Pb, Fe, and Se (see Table 2). VC values for Pb were higher than 80% (86–136%) at all sampling sites with the exception of WS-4. At the background sites with the exception of WS-7, VC values are less than 80% (except Se and Pb), indicating less variability of heavy metals at background sites. At WS-7 the variable metals (CV > 80%) are Fe, Mn, Cr, and Pb. The highest values during the year were observed from March to May and partly from October to November. Heavy metal content increases in the spring due to the snowmelt and precipitation in the catchment. Runoff waters from mining area and mine drainage are considered nonpoint pollution source of heavy metals.

To distinguish the pollution sources, heavy metals were also analyzed through Pearson's correlation. The correlation analysis was done for the observed 15 heavy metals based on the data for the period 2014–2016 (See Table 4). Only the strong and positive ($r > 0.7$) correlation among metals were taken into account. Among the metals, the only not-correlated metal is Ni.

At site 2, the number of correlated parameters and values of correlation coefficient increase. A strong correlation was found among 9 metals (Ti, V, Co, Cu, As, Mo, Cd, Pb, and Fe). After the mining and processing molybdenum and copper, the composition of river water has changed. The correlated metals are associated with the composition of local minerals: molybdenum, chalcopyrite, magnetite, and pyrite.

At site 3, the strong correlation was observed for 5 pairs. At site 4, the correlation coefficients were decreased from 0.95 to 0.70 among 13 pairs. The high correlation indicates that these elements shared the same artificial sources.

In the source of Norashenik River (WS-5) the strong correlation was observed only among 3 metals (Fe, Mn, and Ti). These metals are the main components of several common minerals and rocks. At site 6, the number of correlated parameters and values of correlation coefficient increase. The correlation was found among 8 pairs, and the correlation coefficients were changed from 0.76 to 0.7.

At site 7, the correlation coefficients were decreased from 0.87 to 0.70 among 12 pairs. Although WS-7 is considered as background site from the correlated pairs, it is evident that anthropogenic impact exists. The most correlated pairs were observed at the WS-8. At site 8, the correlation coefficients were decreased from 0.93 to 0.70. It indicates that these metal pairs likely originated from the same sources.

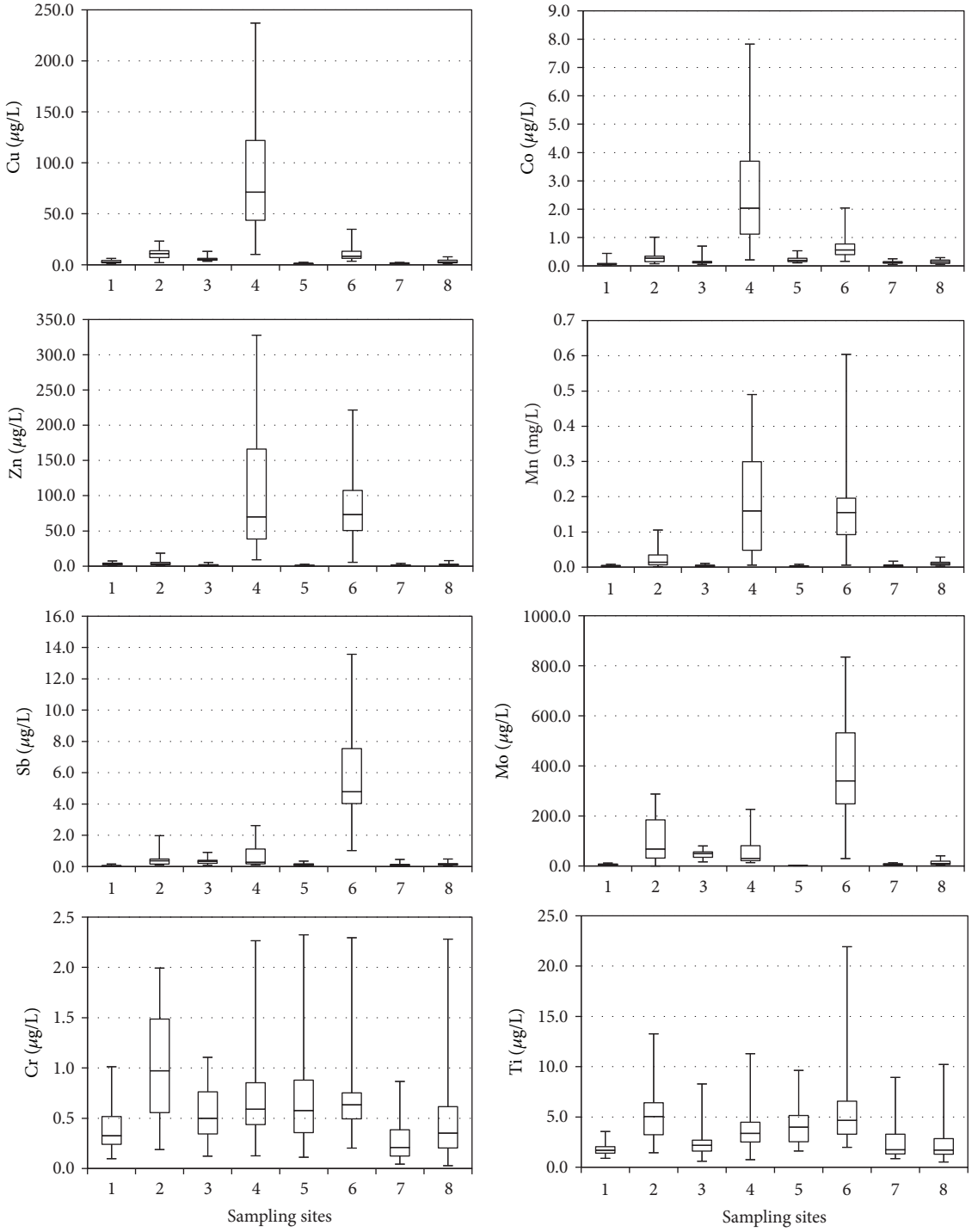

Figure 2: Spatial distribution of concentrations values of some heavy metals in the waters of Voghji River and its tributaries. Median, 25th and 75th percentiles are shown in the box; whiskers indicate the maximums and minimums.

3.2. Spatial Distribution of Heavy Metals in Sediments. The results of the analysis of heavy metals in Voghji, Geghi, and Norashenik Rivers sediments (see Table 5) showed an increase in heavy metal concentrations in the sediments at the downstream of Kajaran (SS-2), with the exception of Ti, Mn, and Fe, compared to SS-1 (source of Voghji River) associated with the drainage of mining territory of ZCMC. The highest concentrations of Cu, Zn, Mo, and Pb were observed at SS-2 and SS-3. At the SS-1, the average content of metals follows the order Fe > Ti > Mn > Cu > Zn > V > Mo > Pb > Ni > Cr > As > Co > Cd > Sb. At the SS-2, the average content of metals follows the order Fe > Ti > Cu > Mn > Mo > Zn > V >

Table 4: Correlation between metals in water of the Voghji River and its tributaries ($r > 0.7$).

WS	Pearson's coefficients of correlations between metals
1	Cu-V (0.70)
2	Cd-Se (0.88), Mo-Cd (0.84), Mo-Se (0.81), Pb-Ti (0.79), Mo-As (0.78), Fe-Mn (0.78), V-Ti (0.75) Se-As (0.74), V-As (0.72), Cd-As (0.70), V-Co (0.70), Pb-Fe (0.70)
3	Mo-As (0.88), Mo-Cd (0.76), Ti-Fe (0.74), Cu-Fe (0.72), Cd-As (0.70)
4	Mo-As (0.95), Cu-Zn (0.89), Sb-As (0.88), Mo-V (0.86), Mo-Sb (0.86), As-V (0.85), Cu-Co (0.82), Co-Zn (0.81), Cd-Zn (0.79), Co-Mn (0.77), Cd-Sb (0.73), Cd-Co (0.72), Sb-V (0.71)
5	Mn-Fe (0.74), Mn-Ti (0.71)
6	As-V (0.76), Pb-Co (0.73), Zn-Cu (0.73), Cu-V (0.70), Cu-Co (0.70), Fe-Cr (0.70), Fe-Ti (0.70), Ti-Cr (0.70)
7	Fe-Ti (0.87), Fe-Co (0.85), Fe-V (0.84), Sb-Co (0.82), V-Ti (0.80), Pb-Ti (0.77), Co-V (0.75), Fe-Pb (0.72), Fe-Sb (0.72), Fe-Cu (0.72), Co-Ti (0.71), Mo-Cr (0.70)
8	Cd-Mo (0.93), As-Mo (0.86), Fe-Pb (0.85), Cu-V (0.84), Fe-Ti (0.83), Cd-As (0.79), Cu-Ti (0.79), Pb-Ti (0.75), Cu-Co (0.75), Cu-Cr (0.73), Fe-Cu (0.72), Cr-Mn (0.72), Ti-V (0.71), Cr-V (0.70), Co-V (0.70), Co-Ti (0.70), Fe-V (0.70), Mn-Ti (0.70), Pb-Ti (0.70)

Table 5: Heavy metals in sediments (mean value in mg/kg) in the Voghji River basin in 2014–2016.

SS	Fe	Ti	V	Cr	Mn	Co	Ni	Cu	Zn	As	Mo	Cd	Sb	Pb
1	8962	840	25.4	8.89	450	5.34	11.3	119	41.4	6.93	24.0	0.32	0.23	11.5
2	4674	2037	45.9	9.42	239	8.12	14.8	620	99.6	9.41	109	0.44	1.54	30.1
3	20018	4203	121	11.1	245	13.8	17.0	494	54.4	29.7	80.0	0.33	2.96	40.5
4	4471	1499	35.3	1.95	75.4	4.36	3.22	137	67.2	11.8	25.4	0.97	1.62	18.4
5	2053	2094	39.3	11.8	172	6.73	18.8	15.4	26.9	2.50	0.27	0.09	0.12	3.52
6	13674	3176	84.6	7.16	176	7.76	5.78	126	92.3	13.1	33.1	0.84	1.46	13.8
8	6537	1382	36.5	7.17	200	5.51	8.14	192	36.8	8.21	12.3	0.14	0.79	15.5
ISQG	-	-	-	37.3	-	-	-	35.7	123	5.9	-	0.6	-	35.0

Pb > Ni > Cr > As > Co > Sb > Cd. In spite of the increase in metal contents at the SS-2, the order of average concentration values of metals remains almost the same.

At the SS-3, Fe, Ti, V, As, and Sb were accumulated in the sediment leading to the highest concentration of these metals in the whole river basin.

The sediments of Norashenik River are polluted with heavy metals because of inflowing wastewater of the Artsvanik tailings dam. This can be seen from the comparison of heavy metal content in sediments of SS-5 (source of Norashenik River) and SS-6 (mouth of Norashenik River). The only difference was observed at the SS-3 where the metals content is inexplicably high. The spatial distribution of metals in sediments, in general, is similar to the distribution of water. As the results demonstrated, the concentration values of Mo, Sb, Cd, Cu, and Fe in the sediments at the mouth of Norashenik River (SS-6) increased sharply. The slight increase in concentrations was observed in the case of Ti, V, Co, Zn, As, and Pb. In the case of Cr and Ni, conversely, the concentrations decreased.

The specific distribution pattern of Mn showed that the concentration in sediments is higher only at SS-1 and lower at SS-4. In the other sites, the concentration range of Mn was not changed indicating that Mn distribution in sediments is not directly related to the mining activities.

The concentrations of Cu and As in sediments exceeded ISQG in all sites besides SS-5. The concentrations of Cd exceeded ISQG in sediments of SS-4 and SS-6. It is noteworthy that cadmium concentration exceeded corresponding ISQG only in the sediments of SS-3.

3.3. Relationship of Heavy Metals Content in Water and Sediment. Waters and sediments surrounding the mining area bear the brunt of industrial discharges and destruct environmental natural balance. To identify changes in the natural chemical composition of heavy metals in water and sediments as a result of mining operations, the ratio of heavy metals in water and sediment and correlation between the ratio of heavy metals in water and sediment were estimated.

In the upper part of the Voghji River (WS-1), the median Cu/Zn ratio in the water samples of background sites varied between 0.8 and 1.6. Then, after ZCMC the ratio of Cu/Zn was 3.5, and after the city of Kapan the ratio was again 1 despite the sharp growth of Cu and Zn. In the sediment samples of upper part of the Voghji River, the ratio of Cu/Zn was 3. After ZCMC, the ratio increased to the same extent and was 6–9.

The ratio of Mo/Zn in the water of sampling sites 1 and 5 was 1.5 and 1.9, respectively. Then, after the influence of ZCMC (below Kajaran city) the ratio of Mo/Zn was 21.5. Due to the inefficient processing, the large amount of Mo remains in the processed rocks and enters into the waters.

The ratio of Ti/V, Ti/Cr, V/Cr, and Ti/Ni changed slightly after the influence of ZCMC in waters of both Voghji and Norashenik Rivers.

Table 6: Water quality of the Voghji River basin based on only heavy metals.

Sampling sites	Main indicator metals	Water quality parameter class	Overall water quality class
1	-	-	Good
2	Fe, Mn, Co	Moderate	Poor
	Mo	Poor	
3	Mo	Moderate	Moderate
4	Mo, Fe	Moderate	Bad
	Cu	Poor	
	Mn, Co	Bad	
5	Fe, Co	Moderate	Moderate
6	Fe, Cd	Moderate	Bad
	Co	Poor	
	Mn, Mo, Sb	Bad	
7	Fe	Moderate	Moderate
8	Mn	Moderate	Moderate

The ratio of Fe/Al in the water of sampling sites 1, 5, and 7 was 2.5, 2.9, and 2.7, respectively. After the influence of mining, the natural composition was changed in the range 1.2–1.9.

The Mo/Ti ratio increased to 6.8 in the upper part (site 1) which increased to 13 after the city of Kajaran, and a sharp growth was observed after the city of Kapan, about 28 in water of river. The Pb/Cd ratio increased from 1.3 to 1.7 after the city of Kajaran, and then a slow decrease was observed before the city of Kapan, reaching the minimum values after ZCMC, which is an evidence that enterprise wastes contain large amounts of toxic metals. Due to diffusion, heavy metal abundant waste and tailings penetrate into the river, becoming pollution sources. In the process of mining, the spatial distribution of metals concentrations is disturbed.

3.4. Assessment of Heavy Metal Pollution in the Voghji River Basin. The assessment of the contents of heavy metals was done based on mean concentrations value for the period of 2014–2016 (see Table 3). The mean values of heavy metals are compared to the national water quality standards (see Section 2.3) and derived quality class. The results of the assessment are presented in Table 6. According to the results (Table 6), in the upper reaches of the Voghji River (WS-1), the water quality corresponds to the "good" quality. Then, in the river receiving drainage wastewater from ZCMC, the water quality was worsened gradually to "poor" class at downstream of Kajaran. The "poor" water quality in the section downstream of Kajaran (site 2) was associated with the high concentration of Mo. Then, after mixing with Geghi River, the water quality of Voghji River was getting better and water quality was classified as "moderate" (WS-3) connected with elevated concentration of Mo. After the influence of KPM and mixing of the Norashenik River, the water quality of the Voghji River worsened to the "bad" quality due to elevated Mn and Co levels. The water quality of the Geghi tributary was classified as "moderate" due to iron. The water quality of the Norashenik tributary was classified as "bad" connected to Mn, Mo, and Sb.

4. Conclusions

Our results indicated a high degree of mining-derived pollution in the Voghji River. Both ZCMC and KPM mining districts with their ore processing center leachate, operated tailings dams, the abandoned mine, and other enterprises located in the Voghji River basin are the major sources of heavy metals pollution. The water quality is worsening after the influence of mining waters from the "good" to the "bad" state.

The research revealed the pollution sources of each metal. ZCMC with its wastewater and diffuse water pollutes the Voghji River mostly with Mo and Sb. The content of other metals increases slightly (less than 10 times) after the influence of ZCMC. The wastewater of Artsvanik tailings dam polluted the Norashenik River and then Voghji River mostly with Mn, Zn, Se, Mo, Cd, As, and Sb. KPM and the abounded mining area Kavart were mainly responsible for the elevated concentrations of Cu, Zn, and Co in the Voghji River (below Kapan city). Both ZCMC and KPM were responsible for the increase in concentrations of Fe, Mn, Zn, Pb, and Cd in Voghji River (below Kapan city). The concentrations of Ti, V, Cr, Ni, and As in the Voghji River changed slightly. The high concentration of V in the waters of the source of Norashenik River was mostly due to natural sources indicating the peculiarities of geohydrochemistry of Norashenik River.

The spatial distribution of metals in sediments, in general, is similar to the distribution of water. The only difference was observed at the SS-3 where the metals content is inexplicably high. The concentration values of Mo, Sb, Cd, Cu, and Fe in the sediments at the mouth of Norashenik River increased sharply. The slight increase in concentrations was observed in the case of Ti, V, Co, Zn, As, and Pb. In the case of Cr and Ni, conversely, the concentrations decreased.

Conflicts of Interest

The authors declare that they have no conflicts of interest.

Acknowledgments

The authors thank the Environmental Monitoring and Information Center, state nongovernmental organization at the Ministry of Nature Protection of the Republic of Armenia, for helping them carry out this study and for providing access to water quality monitoring database and Civil Voice NGO (Armenia) for technical assistance in sediment sampling.

References

[1] P. Kapusta and Ł. Sobczyk, "Effects of heavy metal pollution from mining and smelting on enchytraeid communities under different land management and soil conditions," *Science of the Total Environment*, vol. 536, pp. 517–526, 2015.

[2] A. Liang, Y. Wang, H. Guo, L. Bo, S. Zhang, and Y. Bai, "Assessment of pollution and identification of sources of heavy metals in the sediments of Changshou Lake in a branch of the Three Gorges Reservoir," *Environmental Science and Pollution Research*, vol. 22, no. 20, pp. 16067–16076, 2015.

[3] O. Sracek, B. Kříbek, M. Mihaljevič et al., "Mining-related contamination of surface water and sediments of the Kafue River drainage system in the Copperbelt district, Zambia: An example of a high neutralization capacity system," *Journal of Geochemical Exploration*, vol. 112, pp. 174–188, 2012.

[4] J. J. Marcus, *Mining Environmental Handbook: Effects of Mining on the Environment and American Environmental Controls on Mining*, Imperial College Press, London, UK, 1997.

[5] M. M. Ali, M. L. Alia, M. S. Islamc, and M. Z. Rahmanda, "Preliminary assessment of heavy metals in water and sediment of Karnaphuli River," *Banglades, Environmental Nanotechnology, Monitoring Management*, vol. 5, pp. 27–35, 2016.

[6] M. R. Abraham and T. B. Susan, "Water contamination with heavy metals and trace elements from Kilembe copper mine and tailing sites in Western Uganda; implications for domestic water quality," *Chemosphere*, vol. 169, pp. 281–287, 2017.

[7] M. Olías, J. M. Nieto, A. M. Sarmiento, J. C. Cerón, and C. R. Cánovas, "Seasonal water quality variations in a river affected by acid mine drainage: the Odiel River (South West Spain)," *Science of the Total Environment*, vol. 333, no. 1–3, pp. 267–281, 2004.

[8] E. Dinelli, F. Lucchini, M. Fabbri, and G. Cortecci, "Metal distribution and environmental problems related to sulfide oxidation in the Libiola copper mine area (Ligurian Apennines, Italy)," *Journal of Geochemical Exploration*, vol. 74, no. 1-3, pp. 141–152, 2001.

[9] W. Tang, S. Duan, B. Shan et al., "Concentrations, diffusive fluxes and toxicity of heavy metals in pore water of the Fuyang River, Haihe Basin," *Ecotoxicology and Environmental Safety*, vol. 127, pp. 80–86, 2016.

[10] C. Sierra, O. Ruíz-Barzola, M. Menéndez, J. R. Demey, and J. L. Vicente-Villardón, "Geochemical interactions study in surface river sediments at an artisanal mining area by means of Canonical (MANOVA)-Biplot," *Journal of Geochemical Exploration*, vol. 175, pp. 72–81, 2017.

[11] A. Kabata-Pendias and B. Szteke, *A Trace Elements in Abiotic and Biotic Environment*, Taylor & Francis Group, 2015.

[12] Z. Zhang, L. Juying, and Z. Mamat, "Sources identification and pollution evaluation of heavy metals in the surface sediments of Bortala River, Northwest China," *Ecotoxicology and Environmental Safety*, vol. 126, pp. 94–101, 2016.

[13] A. Gómez-Alvarez, D. Meza-Figueroa, A. I. Villalba-Atondo, J. L. Valenzuela-García, J. Ramírez-Hernández, and J. Almendariz-Tapia, "Estimation of potential pollution from mine tailings in the San Pedro River (1993-2005), Mexico-US border," *Environmental Geology*, vol. 57, no. 7, pp. 1469–1479, 2009.

[14] C. Gao, Q. Lin, K. Bao et al., "Historical variation and recent ecological risk of heavy metals in wetland sediments along Wusuli River, Northeast China," *Environmental Earth Sciences*, vol. 72, no. 11, pp. 4345–4355, 2014.

[15] S. K. Sundaray, B. B. Nayak, S. Lin, and D. Bhatta, "Geochemical speciation and risk assessment of heavy metals in the river estuarine sediments—a case study: Mahanadi basin, India," *Journal of Hazardous Materials*, vol. 186, no. 2-3, pp. 1837–1846, 2011.

[16] J. Wang, R. Liu, P. Zhang, W. Yu, Z. Shen, and C. Feng, "Spatial variation, environmental assessment and source identification of heavy metals in sediments of the Yangtze River Estuary," *Marine Pollution Bulletin*, vol. 87, no. 1, pp. 364–373, 2014.

[17] P. B. Tchounwou, C. G. Yedjou, A. K. Patlolla, and D. J. Sutton, "Heavy metal toxicity and the environment," in *Molecular, Clinical and Environmental Toxicology*, vol. 101, pp. 133–164, Springer, Basel, Switzerland, 2012.

[18] L. Vardumyan, E. Vardumyan, G. Pirumyan, and S. Minasyan, "Water quality assessment of southern River basin in the Republic of Armenia by using principal component analysis method," *Proceedings of Engineering Academy of Armenia*, vol. 8, no. 1, pp. 196–202, 2011.

[19] G. A. Gevorgyan, A. A. Danielyan, K. V. Grigoryan, and S. H. Minasyan, "The level of the pollution of the meghriget, voghchi and artsvanik rivers with heavy metals and aluminium," *Proceedings of the YSU, Chemistry and Biology*, vol. 3, no. 226, pp. 50–53, 2011.

[20] R. Kurkjian, "Metal contamination in the Republic of Armenia," *Journal of Environmental Management*, vol. 25, no. 5, pp. 477–483, 2000.

[21] O. Belyaeva, "Impact of mining enterprises of the city of Kapan on adjacent agroecosystems," *Electronic Journal of Natural Sciences*, vol. 2, no. 19, pp. 26–30, 2012 (Chinese).

[22] "American Un center for responsible mining," 2017, http://crm.aua.am/files/2016/12/Schools-and-Kindergartens-in-Kapan_Final-Report-Eng-Dec-2-2016.pdf.

[23] "AUA Center for Responsible Mining," 2017, http://crm.aua.am/files/2016/12/Schools-and-Kindergartens-in-Kajaran_Artsvanik_Final-Report-Eng-Dec-2-2016.pdf.

[24] Southern River Basin Management Plan (SRBMP) Resource document. USAID, Clean Energy and Water program, 2015.

[25] "RA Government decree," On Definition of Water Quality Norms for Each Water Basin Management Area, taking into Consideration the Peculiarities of the Territory 75-N, 2011.

[26] CCME, "Canadian sediment quality guidelines for the protection of aquatic life: summary tables. Updated Canadian environmental quality guidelines. Resource document," Tech. Rep., Canadian Council of Ministers of the Environment, 1999, http://www.ccme.ca/en/resources/canadian_environmental_quality_guidelines.

Hindawi
Journal of Chemistry
Volume 2018, Article ID 7274020, 9 pages
https://doi.org/10.1155/2018/7274020

Research Article

The Response of Duckweed (*Lemna minor* L.) Roots to Cd and Its Chemical Forms

Yan Xue,[1,2] **Jin-qin Wang**,[3] **Jin Huang**,[3,4] **Feng-ying Li**,[2] **and Ming Wang**[1,2]

[1]*School of Environmental Science and Engineering, Nanjing University of Information Science & Technology, Nanjing 210044, China*
[2]*Collaborative Innovation Center of Atmospheric Environment and Equipment Technology, Nanjing 210044, China*
[3]*School of Applied Meteorology, Nanjing University of Information Science & Technology, Nanjing 210044, China*
[4]*Jiangsu Key Laboratory of Atmospheric Environment Monitoring and Pollution Control, Nanjing 210044, China*

Correspondence should be addressed to Yan Xue; xueyan@nuist.edu.cn

Received 28 November 2017; Revised 8 January 2018; Accepted 21 January 2018; Published 15 February 2018

Academic Editor: Peng Wang

The response of duckweed (*Lemna minor* L.) roots to Cd and its chemical forms was investigated. The relative root growth rate and concentrations of Cd and its different chemical forms in the root, that is, ethanol-extractable (F_E-Cd), HCl-extractable (F_{HCl}-Cd), and residual fractions (F_r-Cd), were quantified. Weibull model was used to unravel the regression between the relative root elongation (RRL) with chemical forms of Cd. Parameters assessed catalase (CAT), peroxidases (POD), and superoxide dismutase (SOD), as well as malondialdehyde (MDA) and total antioxidant capacity (A-TOC). Our results show that both the relative root growth rate and relative frond number were affected by Cd concentrations. The chemical forms of Cd were influenced by Cd content in the medium. Relative root elongation (RRL) showed a significant correlation with chemical forms of Cd. Additionally, POD and SOD increased at lower Cd concentrations followed by a decrease at higher Cd concentrations (at more than 5 μM Cd). Moreover, MDA and A-TOC increased and CAT decreased with increasing Cd exposure. Furthermore, CAT showed a significant correlation with F_{HCl}-Cd. Taken together, it can be concluded that the chemical forms of Cd are statistically significant predictors of Cd toxicity to duckweed and to the other similar aquatic plants.

1. Introduction

Cadmium (Cd) is a major contributor to heavy metal pollution. It is found in both natural and waste waters and is produced by agriculture through pesticides and fertilizers use and wastewater irrigation and by industry through smelting, metalworking, and pigmentation [1, 2]. The metal has a relatively high solubility and mobility in water and then is easily absorbed for aquatic plants [3]. It destroys photosynthetic apparatus and carbohydrate metabolisms of plants [3–5] and can be transferred in the food chain to threat human health [6]. Some evidences also indicated that the presence of Cd affected cell wall construction and vesicular trafficking [7]. Plants have developed several detoxification mechanisms to alleviate Cd toxicity, including the existence of different forms of metals and sequestration into the cell wall [8, 9].

The chemical form of Cd determines the characteristics of Cd migration, potential phytotoxicity, and accumulation in plants and then influences the detoxification and tolerance to Cd of plants [10–13]. Yin et al. [12] found that the different capacity to binding Cd different forms (such as F_{HCl}-Cd and F_r-Cd) played an important role in the genotype difference in Cd accumulation of spinach. Mwamba et al. [14] demonstrated that metals which are both in the form of insoluble phosphate and firmly adsorbed in the cell walls and vacuoles are not free to migrate and have low toxicity, whereas Xu et al. [15] reported that high Cd mobility is often in the forms of the water soluble Cd, inorganic Cd, and Cd complexes with organic acids. Wang et al. [9], in a comparison of watercress genotypes with low- and high Cd-accumulation, found that low-Cd genotypes may convert Cd into pectate/protein-bound forms and insoluble phosphate precipitates to a greater degree than high Cd types, and that this could be the primary method by which Cd toxicity and mobility are reduced in watercress.

Cd has previously been shown to induce reactive oxygen species (ROS) and cause oxidative stress (OS), which damages cell structure and function [16, 17]. Plants have evolved effective scavenging mechanisms to survive the Cd stress [6]. The key components of the ROS-scavenging system are mainly antioxidative enzymes, such as peroxidases (POD), superoxide dismutase (SOD), and catalase (CAT) and also other metabolites, including reduced glutathione, malondialdehyde (MDA), and ascorbic acid [18]. Several studies have found that enzyme activity can be modified by Cd stress before symptoms of toxicity become visible [19]. Considering this, it is inferred that enzymatic activity may signal this biological process and be an indicator of metal toxicity.

Duckweed (*Lemna minor* L.) is a small floating aquatic plant consisting of submerged greenish roots and floating plant bodies (referred to as fronds). In terms of its reproduction, this primarily takes place in a vegetative way through the creation of colonies [20]. To be specific, this involves the formation of daughter fronds at the proximal ends of mother fronds in two meristematic regions (ibid). It is well known that duckweed accumulates heavy metals [21], including Cd [2, 22]. Its physiological response to heavy metal stress [23] has been extensively studied in recent years, and researchers have started to examine its defence mechanisms against heavy metal toxicity [24]. However, relatively few studies have examined the correlation between the heavy metal toxicity (which results from the chemical forms) and antioxidant enzymatic activity in duckweed. This knowledge gap greatly restricts our capability to understand the potential mechanisms of defence against heavy metal toxicity of aquatic plants.

In the present study, an experimental design was developed to achieve the following objectives: firstly, to investigate root growth and the antioxidative enzymatic activity (specifically with respect to CAT, SOD, POD, and MDA) of duckweed roots exposed to different Cd concentration; secondly, to detect the change of different chemical forms of Cd; and thirdly, to quantify the relationship between the antioxidant system and different chemical forms of Cd, which directly reflect different toxicity of different chemical forms. The achievement of these objectives was planned to illuminate the role of chemical forms in detoxification of aquatic plants to heavy metal.

2. Materials and Methods

2.1. Plant Materials and Culture. Sample duckweed seedlings were collected from Yileen Garden in Nanjing, China. The samples were placed in a Hoagland culture solution containing 600 μM $Ca(NO_3)_2$, 300 μM $MgSO_4$, 300 μM K_2HPO_4, 13.8 μM H_3BO_3, 217 μM $MnSO_4$, 0.3 μM Na_2MoO_4, 0.5 μM $CuSO_4$, 16.5 μM Fe(III)-EDTA, and 0.3 μM $ZnSO_4$ under natural light conditions in a greenhouse. The pH of the medium was taken to 5.5 with 0.1 M NaOH and HCl. The medium was replaced every other day. Inoculation of a single 2-3 frond colony was used to initiate experimental cultures for growth measurement and of 10–12 colonies for other analyses.

2.2. Toxicity Experiments. Duckweed plants of similar fronds numbers were selected to place in medium containing Cd (0.1, 0.5, 1, 5, 10, or 20 μM $CdCl_2$). A free Cd treatment (only containing Hoagland medium) was used for control. Each treatment was performed in triplicate. The treatment medium was replaced every other day, and the fresh plant samples were collected after 4 days of treatment. Growth over 4 days was monitored by counting the number of fronds, which were recorded as relative frond numbers after Ensley et al. [25].

To calculate relative root elongation (RRL), the formula $RRL\,(\%) = 100(RL_T - RL_S)/(RL_C - RL_S)$ was applied, where RL_T is the mean root length (RL), where toxicants (i.e., Cd^{2+}) are present, RL_C is RL in a toxicant-free control, and RL_S is RL when the seedling was transferred into the test media. The growth thus quantified can be plotted against toxicant intensity (T) measures such as the overall Cd concentration and its different chemical forms. The results often plot as negatively sigmoidal curves, which have been characterised with a Weibull equation [26, 27]. If T limits growth, $RRL = 100/\exp[(aT)^b]$, where b is a shape coefficient and the strength coefficient a increases with the degree of metal toxicity.

2.3. Extraction of Chemical Forms of Cd. The chemical forms of Cd were determined using a modified version of the following method described by Wu et al. [28]. Cd in its different chemical forms was sequentially extracted as shown below:

(i) 80% (v/v) ethanol, extracting soluble Cd, including chloride, nitrate, and aminophenol cadmium (F_E-Cd),

(ii) 0.6 M HCl, extracting insoluble $CdHPO_4$ and $Cd_3(PO_4)_2$, other Cd-phosphate complexes and Cd integrated with pectates and protein, and so on (F_{HCl}-Cd),

(iii) Cd in residues (F_r-Cd).

Fresh duckweed root samples were rinsed in tap water and deionized water and then dried with paper tissue. Roots were cut into 1-2 mm^2 pieces, which were used separately in the sequential extraction for various forms of Cd. A plant sample of 4 g was placed in a 50 ml centrifugal tube with 25 ml extractant (80% ethanol). The tube was kept in a 30°C water bath for 18 hrs. After the tube was centrifuged for 10 min at 10000 rpm, the supernatant was collected. Another 20 ml of the same extractant was added to the extract for 2 h, and the supernatant was collected and mixed with the previous supernatant collection. The entire extraction solution was collected, evaporated to a constant weight, and then digested using HNO_3–$HClO_4$ (3 : 1, v/v). After one extraction solution had been collected, the next was added to the plant materials still in the beaker using identical procedures. To determine the Cd content in residues, HNO_3–$HClO_4$ (3 : 1, v/v) was used to digest the plant material after the sequential extraction. Atomic absorption spectrophotometry (TAS-986, Beijing, China) was used to determine the concentrations of the different chemical forms of Cd.

2.4. Determination of Antioxidative Enzyme Activities. 5.0 ml of extraction buffer solution (0.05 M NaH_2PO_4 + Na_2HPO_4, pH 7.4) was used to homogenize 0.5 g samples of fresh root material. The resulting homogenate was spun in a centrifuge at 10000g for 10 min. The procedures were all performed at 4°C. The supernatant was utilized for the enzyme activity assays. The increase in 470 nm absorbency as a result of guaiacol oxidation was used to measure POD [29, 30]. To measure the guaiacol-dependent activity of peroxidase, a reaction mixture containing 50 mmol/l phosphate buffer (pH 7.0), 10 mmol/l H_2O_2, 50 mM guaiacol, and enzyme was used. Assay of SOD was based on its inhibition of photochemical reduction in nitro blue tetrazolium [31]. The reaction mixture was made up of 50 mM phosphate buffer (pH 7.4), 75 mM nitro blue tetrazolium, 13 mM methionine, 100 nM EDTA, 0–200 μL of enzyme extract, and 2 mM riboflavin, with the riboflavin being the last to be added. The absorbance of this mixture was read at 560 nm to measure SOD. One unit of SOD activity (U) was defined as the amount of enzyme that caused 50% inhibition of the initial reaction rate in the absence of enzyme. The total activity of SOD was given as U/mg protein. The method of Aebi [32] was used to measure CAT. This method uses decreasing absorbency at 240 nm as an indicator of H_2O_2 hydrolysis. One unit of enzyme activity (U) was equated for the reduction of 0.1 units at A_{240} in 1 min, and the activity of CAT was expressed in terms of U/mg protein.

2.5. Lipid Peroxidation. The formation of MDA was used as an indirect method to estimate lipid peroxidation in vitro, as this is a by-product of the peroxidation of lipids and reacts with thiobarbituric acid [33]. This was performed through homogenization of 100 mg of fresh plant material in 1 ml of 15% (w/v) trichloroacetic acid, 0.25 M HCl, 0.37% (w/v) 2-thiobarbituric acid, and 0.01% (w/v) butylated hydroxytoluene in a ceramic mortar, followed by incubation of the samples for 30 min at 90°C, chilling with ice, and, finally, centrifuging for 10 min at 10000 rpm at 4°C. The 535 nm and 600 nm absorbances of the resulting chromophore were then measured. As a nonspecific turbidity correction, the latter absorbance was subtracted from the former. An extinction coefficient of 156 mM^{-1} cm^{-1} was then used to calculate the concentration of MDA.

2.6. Determination of Total Antioxidant Potential. Both enzymatic and nonenzymatic reactions (e.g., SOD, GSH, GSH-PX, CAT, VC, and VE) are included in the T-AOC of the protective system. Commercial assay kits from the Nanjing JianCheng Institute, China, were used to measure T-AOC [34] in accordance with the manufacturer's instructions. To summarise, the analysis was a colorimetric assay based on the reduction of Fe^{3+} to Fe^{2+} by the antioxidant and the formation of complexes through the reaction of the Fe^{2+} with the phenanthroline. An absorbance measurement was made at 520 nm, and one unit of antioxidant capacity (U) was characterised as an increase of 0.01 units at A_{520} in 1 min/mg protein. T-AOC was expressed in terms of U/mg protein.

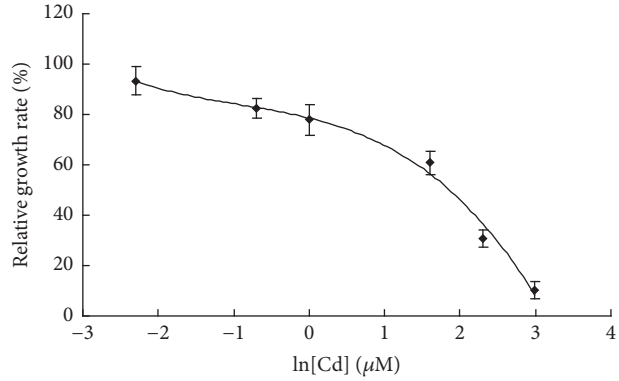

Figure 1: Relative root growth rate (%) as a function of the solution's Cd concentration (μM).

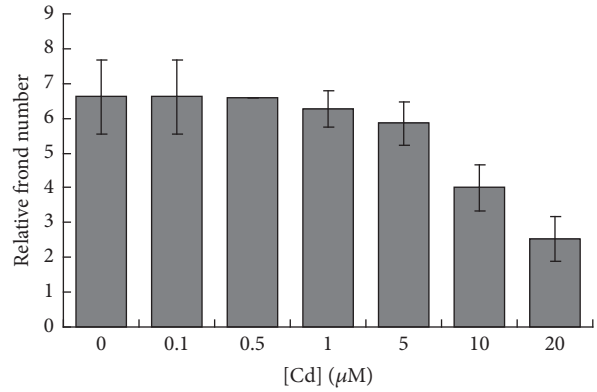

Figure 2: Growth of duckweed during cultivation in medium containing various concentrations of Cd (μM).

2.7. Statistical Analysis. EXCEL 2007 was used for determining the correlation between chemical forms of Cd and toxic response in the data. A one-way ANOVA with a least significant difference (LSD) test was used to identify significant differences, using a confidence level of 95% ($P < 0.05$). Spss was used for the ANOVA analysis.

3. Results

3.1. Effect of Cd on Duckweed Root Elongation and Frond Numbers. Figure 1 shows that the relative root growth rate was significantly related to Cd concentration. The relative root growth rate showed a continuous decrease with an increase of exposed Cd concentrations from 0.1 μM to 20 μM. Critical values corresponding to a 50% reduction of the relative root growth rate were about 10 μM.

It is important to recognize the fact that the relative frond number was also affected by the Cd concentration. Figure 2 indicates that the relative frond number, expressing the growth of Cd-exposed duckweed plants, significantly decreased ($P < 0.05$). As the solution's Cd concentration rose, the frond numbers dropped progressively. The relative frond number was 60.7% lower than that of the control in the solution with a 10-μM Cd concentration. The relative frond

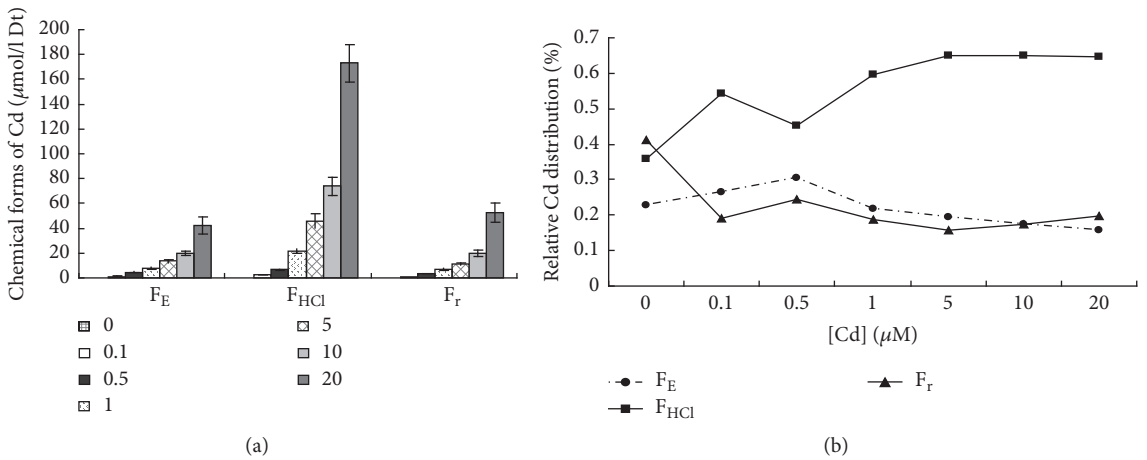

Figure 3: Chemical forms of Cd in duckweed roots (a) and percentage (b) after a 4-day period of exposure to Cd stress.

number dropped to 38.2% when plants were cultivated using a 20 μM Cd concentration medium.

3.2. Chemical Forms of Cadmium in Duckweed Root. The results of chemical forms of Cd and their relative distribution in duckweed were shown in Figure 3. It was found that Cd concentrations bound to different chemical forms in duckweed root increased with an increase of Cd exposure concentrations. For example, when the solution's Cd concentration was 0.1 μM, the F_E-Cd and F_{HCl}-Cd contents were 1.22 and 2.51 mg/kg root, respectively, and these levels increased significantly for duckweed cultivated in 20 μM Cd solution, reaching 42.13 and 172.9 mg/kg root, respectively. When the solution's Cd concentrations were in the range of 0.1–10 μM, F_{HCl}-Cd was the major chemical form, followed by F_E-Cd, and finally F_r-Cd. After exposure to the 20 μM Cd concentration solution, the least prevalent form was F_E-Cd. The relative distribution varied in a concentration-dependent manner with Cd treatment. When the Cd concentration of the solution was 0.5 μM, the relative distribution of both F_E and F_r showed a peak, whereas F_{HCl}-Cd was relatively low. However, when Cd concentration in the solution increased from 0.1 μM to 20 μM, the relative distribution of F_E-Cd and F_r-Cd decreased, while the relative distribution of F_{HCl}-Cd increased. For instance, the percentage decrease for F_E-Cd was from 26.5% to 16.7% (except 30.3% at 0.5 μM), whereas the percentage increase for F_{HCl}-Cd was from 54.4% to 64.5% (except 45.3% at 0.5 μM) (Figure 3(b)).

Figure 4 illustrated the regression results between RRL and F_E-Cd, F_{HCl}-Cd, and F_r-Cd. The data indicated that the relationships conformed to the Weibull model, in which the values of R^2 were above 0.96.

3.3. Effect of Cd on Antioxidant Enzyme Activity. The responses of the antioxidant enzymes to Cd stress were shown in Figure 5. The relative specific activities of SOD and POD increased at lower Cd concentrations until they reached a peak, before decreasing at higher concentrations. Both SOD and POD peaked at 5 μM. The most pronounced 2.67-fold increase of relative specific enzyme activity was measured for SOD, and this occurred when the plants were exposed to the solution with 5 μM Cd concentration. The peak value of POD was 162.0 ± 30.7% (compared to control, $P < 0.01$) at the concentration of 5 μM. At higher Cd concentrations, enzymatic activity decreased significantly and was below the control level reaching 85.2 ± 8.1% of the control value, where the concentration of 20 μM Cd was used. However, the activity of SOD was always above the control level across both low and high Cd concentrations, and it reached 150.8 ± 18.6% of the control value ($P < 0.01$) at 20 μM. At all applied Cd concentrations, T-AOC relative specific activity was greater than in the control samples, showing a gradual, significant increase to 171.6 ± 22.2% of the control value at 0.5 μM Cd ($P < 0.01$). After a 4-day period of exposure to various Cd concentrations, this increased significantly to 410.8 ± 66.7% of the control value at 20 μM Cd. In contrast, the relative specific activity of CAT was lower than that of the control samples at all Cd concentrations, with a gradual decrease at lower Cd concentrations (≤0.5 μM) and with a sharply significant decrease at higher Cd concentrations (>0.5 μM). When the plant was exposed to 20 μM Cd, CAT activity only amounted to 18.9 ± 3.7% of the control value ($P < 0.01$). In addition, a correlation between the chemical form of Cd and Cd was observed (Figure 6). It indicated that the relationships were consistent with the logarithmic curve, in which the values of R^2 were above 0.86. F_{HCl}-Cd exhibited the strongest correlation of the three chemical forms.

3.4. Lipid Peroxidation. The MDA content of the root showed an increase when the medium Cd concentration was increased from 0.1 μM to 10 μM and then dropped slightly at the Cd concentration of 20 μM (Figure 7). That is, the MDA content had a plateau (18.87 U/mg) at 10 μM Cd. The levels of MDA at and above 1 μM Cd significantly exceeded those in the control. For example, the MDA concentration in duckweed roots exposed to 5 μM Cd was 15.8 ± 1.13 U/mg, whereas it was 6.17 ± 0.93 U/mg in the control.

4. Discussion

4.1. Toxicity of Cd on Duckweed. Superfluous heavy metals may inhibit plant root growth and shoot growth [4, 35]. The

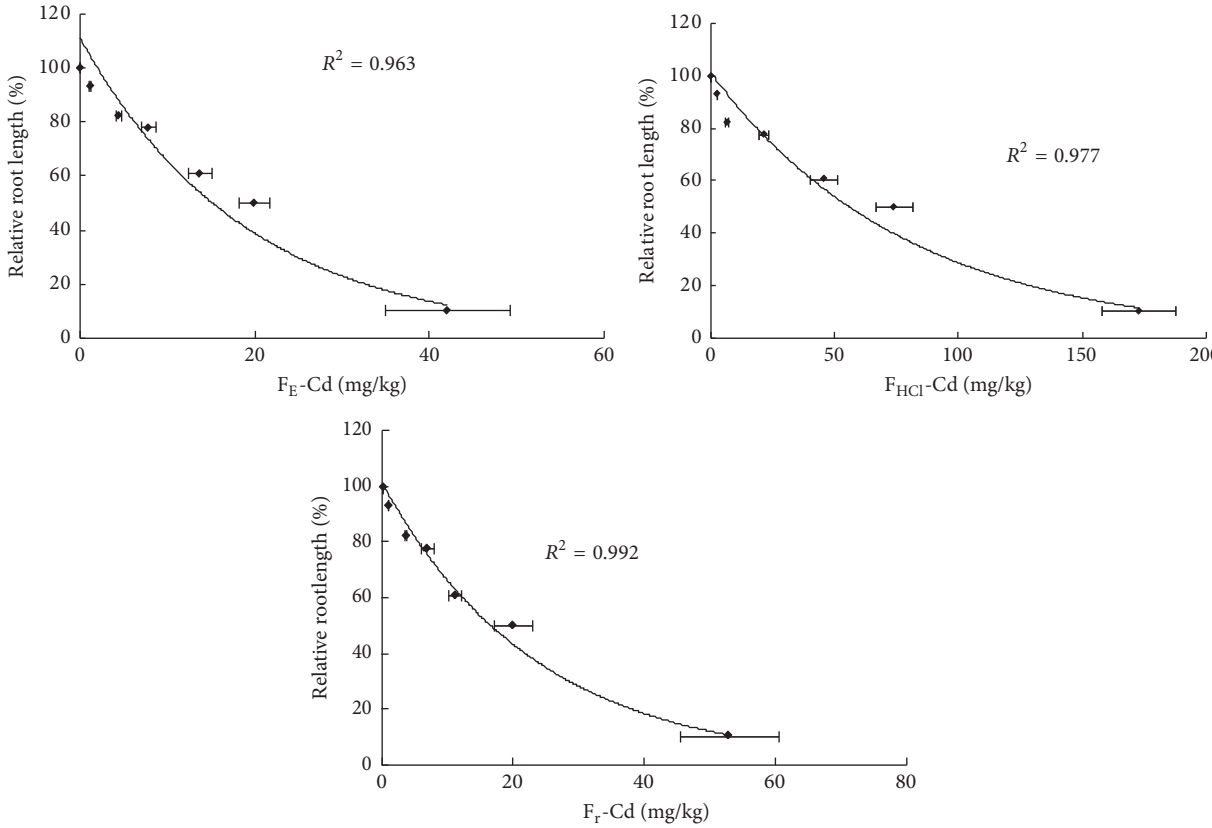

Figure 4: Regression between RRL (%) and the chemical forms of Cd.

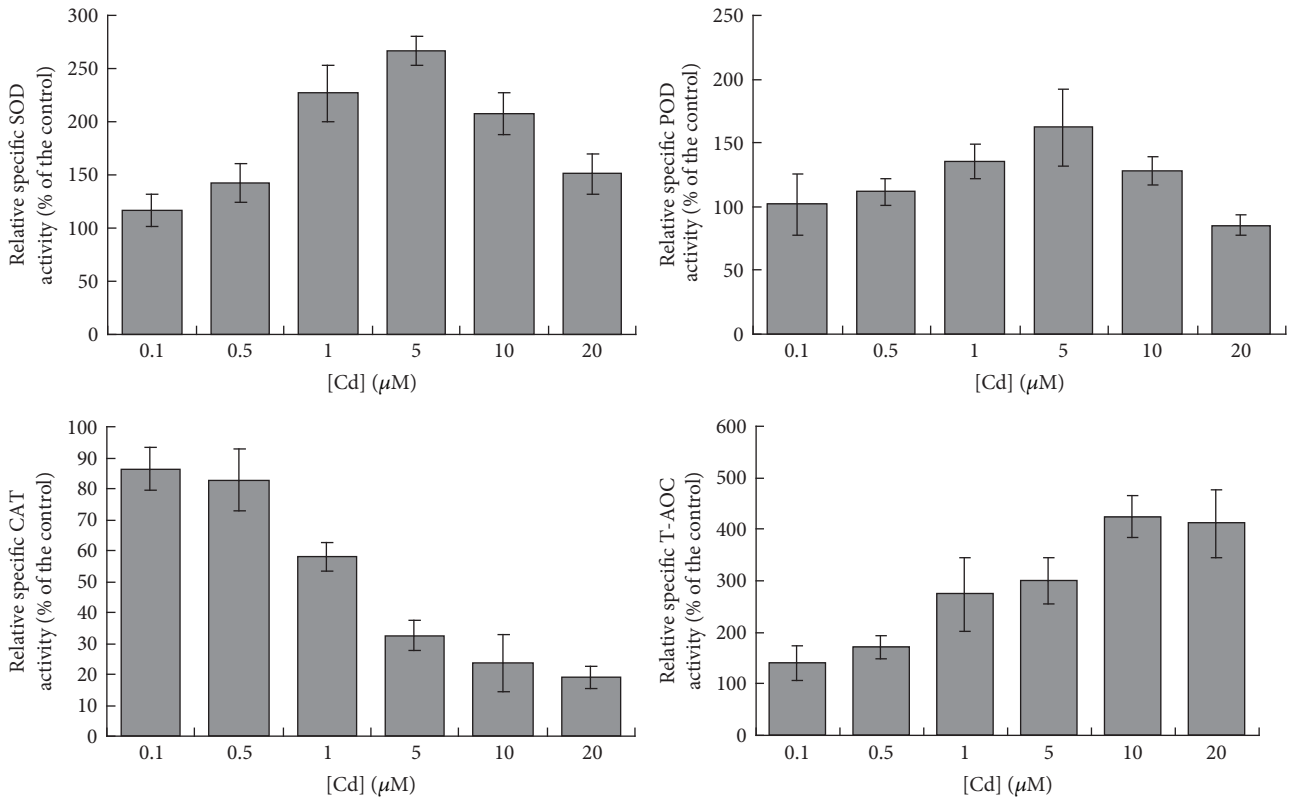

Figure 5: Dependence of relative specific enzyme activities of SOD, POD, CAT, and T-AOC on various Cd concentrations for 4 days.

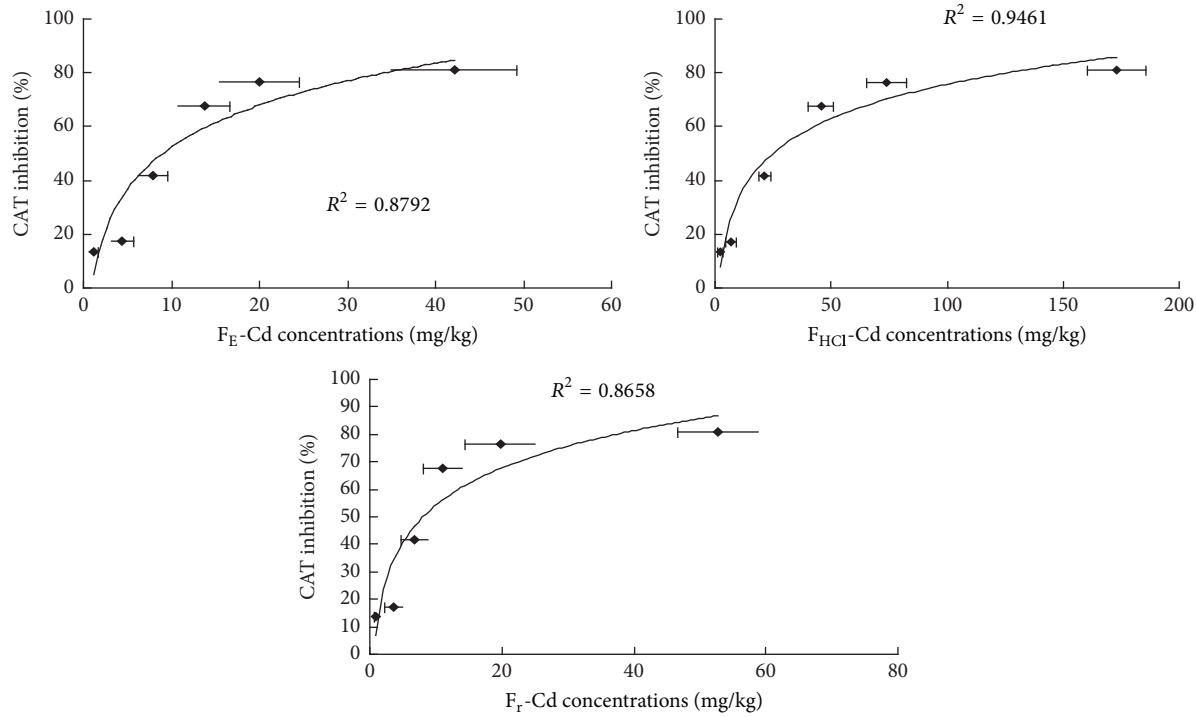

Figure 6: Inhibition of CAT of duckweed root as a function of Cd associated with different chemical forms.

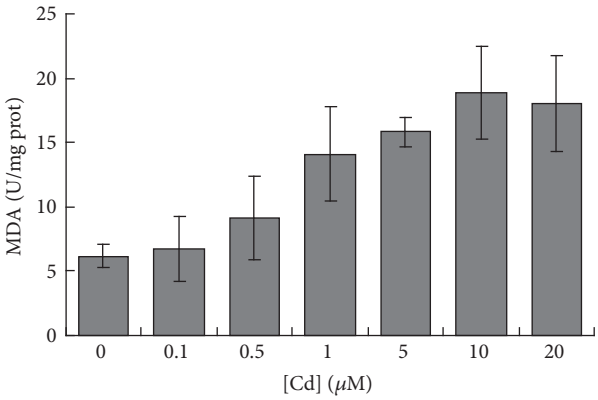

Figure 7: Relation of lipid peroxidation (expressed as amount of MDA) to solutions of various Cd concentrations.

present study found that both root elongation and frond numbers decreased with an increase in the growth medium's Cd concentration. Li et al. [36] found root elongation to be among the most sensitive of the growth parameters to Cd concentration, with an elevated Cd concentration injuring the root [37]. These observations are consistent with the present results (Figure 1). The current results suggested that the elongation of roots was significantly correlated with root Cd concentration, following the Weibull equation. Smith and Kwan [38] demonstrated high Cd toxicity in duckweed and found a Cd level of 1.7 μM as EC_{50} (concentration for 50% of maximal effect) for the reduction in frond number after a 10-day treatment. In the present results, the frond numbers were significantly decreased at the 10 μM Cd concentration after 4 days of treatment. Additionally, the results of the current study indicated the appearance of a hormesis phenomenon at lower Cd concentrations, which accords with results reported in the literature [39, 40].

4.2. Chemical Forms. Different chemical forms correspond to variable transport efficiencies, mobilities, and thus modes of accumulation and distribution [41, 42]. For example, high metal mobility is often associated with ethanol forms (F_E), whereas metals in the form of insoluble phosphates (or those which are firmly adsorbed on the cell wall) cannot migrate freely and effectively [14]. Wu et al. [13] found higher concentrations of protein and pectates when bound by Cd in barley's Cd-resistant genotype compared with that in the Cd-sensitive genotype, implicating the chemical form of Cd as a factor in plant Cd tolerance. The current study recorded higher concentrations of F_{HCl}-Cd than F_E-Cd when Cd concentration in the solution ranged from 0.1 to 20 μM (Figure 3). The implication of this is that F_{HCl}-Cd made contributions to Cd detoxification and, moreover, this was Cd's major chemical form in duckweed. In addition, with increasing Cd, the relative contributions of F_E-Cd and F_r-Cd to total Cd content decreased, except for a peak at 0.5 μM. As the Cd concentration in the solution increased further (up to 10 μM), the F_E-Cd form was less prevalent than the form of F_r-Cd. Moreover, it became the least prevalent chemical form of Cd in duckweed.

These results suggest that duckweed's tolerance to high Cd levels can be attributed to an increase in the relative contribution of forms that are Cd-inactive, along with a decrease in the relative contribution of Cd-active forms. Moreover, F_{HCl}-Cd was depressed relative to the control, suggesting the

action of a protection mechanism. This may also account for the higher root elongation and frond numbers at lower Cd concentrations in the solution. In view of this, we may conclude that it is reasonable to consider the chemical forms in which heavy metals occur to be a useful parameter for the study of metal toxicity in plants.

Ikka et al. [43] found that chemical forms can be used to assess heavy metal toxicity. The results of the present study indicated (Figure 4) a significant correlation between relative root elongation and the F_E-Cd and F_{HCl}-Cd chemical forms of Cd, which not only suggested an association between the chemical forms and Cd toxicity but also suggested that the Cd-sensitive fraction could be a metric for predicting Cd toxicity. A previous study found that the chemical form of F_{HCl}-Cd is more effective for explaining potential toxicity than is the acute toxicity [44]. Assessing the relationship between the chemical forms of heavy metals and their toxicity is therefore crucial. This study provides important evidence that Cd toxicity in duckweed root can be predicted by F_{HCl}-Cd.

4.3. Toxicity of Cd on Antioxidative Enzymatic Activity. Metal phytotoxicity is considered to induce OS [45, 46]. Scandalios [47] found that metals disturbed the normal balance between ROS and antioxidants in all aerobic cells, and a recently conducted study reported that increased antioxidant enzymatic activity has the capability of reducing OS for plants [45]. Under heavy metals conditions, SOD, POD, CAT, and T-AOC play an important protective role against ROS-induced damage [48, 49]. In the present study, the four analysed enzymes responded differently to Cd toxicity (Figure 5). Both SOD and POD were significantly induced at 5 μM Cd, whereas CAT was inhibited at all tested Cd concentrations. In addition, T-AOC was induced with a gradual, significant increase after 4-day exposure to various Cd concentrations. These results are indicative of the plasticity and specificity of duckweed's antioxidative system, which is helping in reducing OS. Similar results were obtained after exposing *Phragmites australis* [50] and *Arabidopsis thaliana* [51] to Cd, with the exception that, for *P. australis*, CAT activity increased. In addition, the inhibition of CAT was significantly and negatively correlated to the chemical form of F_{HCl}-Cd (Figure 6). This indicates that the lower CAT activities may, to some degree, result from the increased fraction of F_{HCl}-Cd.

4.4. Toxicity of Cd on Lipid Peroxidation. The relationship between the toxicity of Cd and OS was also revealed by severe lipid peroxidation, as expressed with reference to MDA [52]. MDA is an indicator of OS and consequent tissue damage [53]. In the present study, MDA increased during Cd exposure in contrast with the reduction in growth of duckweed (Figure 7), which provided support for the potentially disruptive action of peroxidation lipid with respect to Cd. Zhao et al. [23] investigated that MDA content significantly increased when duckweed sp. was exposed to high concentrations of mixed metal contaminants. Singh et al. [54] found similar results when examining an aquatic plant, *Bacopa monnieri*. In the present study, MDA decreased slightly when exposed to high Cd (μM). In the case of *Spirodela polyrhiza*, higher MDA levels were observed with medium exposure concentrations but reduced MDA levels were found at the highest mixed metal exposure concentrations [23], which totally agreed with our results. The researchers stated that these could act either directly or indirectly via toxic derivatives. Zhang et al. [55] found that MDA in leaves of *Kandelia candel* was a concentration-dependent free radical generation. In the leaves of *K. candel*, the collaboration of antioxidative enzyme activities (POD, SOD, and CAT) resulted in the MDA varieties, which are in agreement with the present results.

5. Conclusions

The response of duckweed roots to Cd stress is accompanied by changes in intracellular biological processes, including antioxidant enzymatic activity and the production of different chemical forms of Cd. Taken together, our results attest to the viability of using chemical forms as a means of investigating Cd toxicity in duckweed. This study has confirmed that F_E-Cd is the soluble form of Cd and has high toxicity and that both F_{HCl}-Cd and F_r-Cd are insoluble and have low toxicity. Among the three chemical forms, the potentially toxic Cd fraction (F_{HCl}-Cd) showed the highest level of accumulation. The relative Cd distribution showed more of the Cd-sensitive fraction (F_E-Cd) than the inert fraction (F_r-Cd), but less F_E-Cd than F_r-Cd with increasing Cd concentration. Additionally, relative root elongation was most strongly correlated with chemical forms of Cd. The decrease in CAT activity with increasing Cd concentration and in the activities of POD and SOD at high Cd concentrations indicates that Cd concentration influences the antioxidant enzyme system. As a result of a high sensitivity to Cd, CAT could be a biological indicator of Cd toxicity in duckweed roots. In conclusion, the current study has provided important evidence that illuminates the mechanism of Cd toxicity in duckweed.

Conflicts of Interest

The authors declare that they have no conflicts of interest.

Acknowledgments

This study was supported by the National Natural Science Foundation of China (Grants nos. 51109109 and 41505113) and the Priority Academic Program Development of Jiangsu Higher Education Institutions. The authors extend their thanks to the Jiangsu Engineering Technology Research Center of Environmental Cleaning Materials.

References

[1] G. Fellet, M. Marmiroli, and L. Marchiol, "Elements uptake by metal accumulator species grown on mine tailings amended with three types of biochar," *Science of the Total Environment*, vol. 468-469, pp. 598–608, 2014.

[2] A. Wagner and M. Kaupenjohann, "Suitability of biochars (pyro- and hydrochars) for metal immobilization on former sewage-field soils," *European Journal of Soil Science*, vol. 65, no. 1, pp. 139–148, 2014.

[3] P. Modlitbová, K. Novotný, P. Pořízka et al., "Comparative investigation of toxicity and bioaccumulation of Cd-based quantum dots and Cd salt in freshwater plant Lemna minor L.," *Ecotoxicology and Environmental Safety*, vol. 147, pp. 334–341, 2018.

[4] J. Gao, L. Sun, X. Yang, and J.-X. Liu, "Transcriptomic Analysis of Cadmium Stress Response in the Heavy Metal Hyperaccumulator Sedum alfredii Hance," *PLoS ONE*, vol. 8, no. 6, Article ID e64643, 2013.

[5] J. Xin, B. Huang, Z. Yang, J. Yuan, and Y. Zhang, "Comparison of cadmium subcellular distribution in different organs of two water spinach (Ipomoea aquatica Forsk.) cultivars," *Plant and Soil*, vol. 372, no. 1-2, pp. 431–444, 2013.

[6] Y. Li, H.-D. Pang, L.-Y. He, Q. Wang, and X.-F. Sheng, "Cd immobilization and reduced tissue Cd accumulation of rice (Oryza sativa wuyun-23) in the presence of heavy metal-resistant bacteria," *Ecotoxicology and Environmental Safety*, vol. 138, pp. 56–63, 2017.

[7] L. Wan and H. Zhang, "Cadmium toxicity: effects on cytoskeleton, vesicular trafficking and cell wall construction," *Plant Signaling and Behavior*, vol. 7, no. 3, pp. 345–348, 2012.

[8] N. Luo, X. Li, A. Y. Chen et al., "Does arbuscular mycorrhizal fungus affect cadmium uptake and chemical forms in rice at different growth stages?" *Science of the Total Environment*, vol. 599-600, pp. 1564–1572, 2017.

[9] J. Wang, L. Su, J. Yang et al., "Comparisons of cadmium subcellular distribution and chemical forms between low-Cd and high-Cd accumulation genotypes of watercress (Nasturtium officinale L. R. Br.)," *Plant and Soil*, vol. 396, no. 1-2, pp. 325–337, 2015.

[10] H.-Y. Lai, "Subcellular distribution and chemical forms of cadmium in Impatiens walleriana in relation to its phytoextraction potential," *Chemosphere*, vol. 138, pp. 370–376, 2015.

[11] J. L. W. Lwalaba, G. Zvobgo, M. Mwamba, I. M. Ahmed, R. P. M. Mukobo, and G. Zhang, "Subcellular distribution and chemical forms of Co2+ in three barley genotypes under different Co2+ levels," *Acta Physiologiae Plantarum*, vol. 39, no. 4, article no. 102, 2017.

[12] A. Yin, Z. Yang, S. Ebbs, J. Yuan, J. Wang, and J. Yang, "Effects of phosphorus on chemical forms of Cd in plants of four spinach (Spinacia oleracea L.) cultivars differing in Cd accumulation," *Environmental Science and Pollution Research*, vol. 23, no. 6, pp. 5753–5762, 2016.

[13] F.-B. Wu, J. Dong, Q. Q. Qiong, and G.-P. Zhang, "Subcellular distribution and chemical form of Cd and Cd-Zn interaction in different barley genotypes," *Chemosphere*, vol. 60, no. 10, pp. 1437–1446, 2005.

[14] T. M. Mwamba, L. Li, R. A. Gill et al., "Differential subcellular distribution and chemical forms of cadmium and copper in Brassica napus," *Ecotoxicology and Environmental Safety*, vol. 134, pp. 239–249, 2016.

[15] X. Xu, S. Zhang, J. Xian et al., "Subcellular distribution, chemical forms and thiol synthesis involved in cadmium tolerance and detoxification in," *International Journal of Phytoremediation*, 2017.

[16] M. V. Pérez-Chaca, M. Rodríguez-Serrano, A. S. Molina et al., "Cadmium induces two waves of reactive oxygen species in Glycine max (L.) roots," *Plant, Cell & Environment*, vol. 37, no. 7, pp. 1672–1687, 2014.

[17] J. Razinger, M. Dermastia, J. D. Koce, and A. Zrimec, "Oxidative stress in duckweed (Lemna minor L.) caused by short-term cadmium exposure," *Environmental Pollution*, vol. 153, no. 3, pp. 687–694, 2008.

[18] H. Rui, C. Chen, X. Zhang, Z. Shen, and F. Zhang, "Cd-induced oxidative stress and lignification in the roots of two Vicia sativa L. varieties with different Cd tolerances," *Journal of Hazardous Materials*, vol. 301, pp. 304–313, 2016.

[19] A. X. Da Rosa Corrêa, L. R. Rörig, M. A. Verdinelli, S. Cotelle, J.-F. Férard, and C. M. Radetski, "Cadmium phytotoxicity: Quantitative sensitivity relationships between classical endpoints and antioxidative enzyme biomarkers," *Science of the Total Environment*, vol. 357, no. 1-3, pp. 120–127, 2006.

[20] E. Landolt, "The family of *Lemnaceae*-a monographic study," in *Biosystematic investigations in the family of duckweeds (*Lemnaceae*)*, vol. 2, Veröffentlichungen des Geobotanischen Institutes, Stiftung Rübel, ETH. 71, Zürich, 1986.

[21] Z. Ali, H. Waheed, A. G. Kazi, A. Hayat, and M. Ahmad, "Duckweed: An Efficient Hyperaccumulator of Heavy Metals in Water Bodies," *Plant Metal Interaction: Emerging Remediation Techniques*, pp. 411–429, 2015.

[22] M. S. Al-Khafaji, F. H. Al-Ani, and A. F. Ibrahim, "Removal of some heavy metals from industrial wastewater by Lemmna minor," *KSCE Journal of Civil Engineering*, pp. 1–6, 2017.

[23] Z. Zhao, H. Shi, X. Kang et al., "Inter- and intra-specific competition of duckweed under multiple heavy metal contaminated water," *Aquatic Toxicology*, vol. 192, pp. 216–223, 2017.

[24] S. Y. Tatar, E. Obek, and N. Cikcikoglu Yildirim, "Antioxidant Response in Duckweed After Exposure to Secondary Effluent from Municipal Wastewater Treatment Plant, Elazığ, Turkey," *Bulletin of Environmental Contamination and Toxicology*, vol. 99, no. 3, pp. 399–404, 2017.

[25] H. E. Ensley, J. T. Barber, M. A. Polito, and A. I. Oliver, "Toxicity and metabolism of 2,4-dichlorophenol by the aquatic angiosperm Lemna gibba," *Environmental Toxicology and Chemistry*, vol. 13, no. 2, pp. 325–331, 1994.

[26] P. Wang, D. Zhou, T. B. Kinraide et al., "Cell membrane surface potential *(ψ0)* plays a dominant role in the phytotoxicity of copper and arsenate," *Plant Physiology*, vol. 148, no. 4, pp. 2134–2143, 2008.

[27] G. J. Taylor, K. J. Stadt, and M. R. T. Dale, "Modelling the phytotoxicity of aluminum, cadmium, copper, manganese, nickel, and zinc using the Weibull frequency distribution," *Botany*, vol. 69, no. 2, pp. 359–367, 1991.

[28] H. M. Wu, F. L. Li, H. Q. Mou, and H. Zhang, "Analysis of heavy metal fractions in plants by two steps sequential extraction procedure," *Environmental Science Technology (in Chinese)*, vol. 35, no. 7, pp. 133–137, 2012.

[29] Y. Nakano and K. Asada, "Hydrogen peroxide is scavenged by ascorbate-specific peroxidase in spinach chloroplasts," *Plant & Cell Physiology (PCP)*, vol. 22, no. 5, pp. 867–880, 1981.

[30] F. Tao, M. Zhang, and H.-Q. Yu, "Effect of vacuum cooling on physiological changes in the antioxidant system of mushroom under different storage conditions," *Journal of Food Engineering*, vol. 79, no. 4, pp. 1302–1309, 2007.

[31] C. Beauchamp and I. Fridovich, "Superoxide dismutase: Improved assays and an assay applicable to acrylamide gels," *Analytical Biochemistry*, vol. 44, no. 1, pp. 276–287, 1971.

[32] H. Aebi, "Catalase *in vitro*," *Methods in Enzymology*, vol. 105, pp. 121–126, 1984.

[33] C. Ortega-Villasante, R. Rellán-Álvarez, F. F. Del Campo, R. O. Carpena-Ruiz, and L. E. Hernández, "Cellular damage induced by cadmium and mercury in Medicago sativa," *Journal of Experimental Botany*, vol. 56, no. 418, pp. 2239–2251, 2005.

[34] D.-Q. Sun, A.-W. Li, J. Li et al., "Changes of lipid peroxidation in carbon disulfide-treated rat nerve tissues and serum," *Chemico-Biological Interactions*, vol. 179, no. 2-3, pp. 110–117, 2009.

[35] M. Kopyra and E. A. Gwóźdź, "Nitric oxide stimulates seed germination and counteracts the inhibitory effect of heavy metals and salinity on root growth of Lupinus luteus," *Plant Physiology and Biochemistry*, vol. 41, no. 11-12, pp. 1011–1017, 2003.

[36] H. S. Li, Q. Sun, and S. J. Zhao, *The Physiological and Physiochemical Experiment Theory and Technique*, Higher Education Publishing Company, Beijing, China, 2000.

[37] T. Lambrechts, G. Lequeue, G. Lobet, B. Godin, C. L. Bielders, and S. Lutts, "Comparative analysis of Cd and Zn impacts on root distribution and morphology of Lolium Perenne and Trifolium repens: Implications for phytostabilization," *Plant and Soil*, vol. 376, no. 1, pp. 229–244, 2014.

[38] S. Smith and M. K. H. Kwan, "Use of aquatic macrophytes as a bioassay method to assess relative toxicity, uptake kinetics and accumulated forms of trace metals," *Hydrobiologia*, vol. 188-189, no. 1, pp. 345–351, 1989.

[39] E. J. Calabrese, "Hormesis: Principles and Applications for Pharmacology and Toxicology," *American Journal of Pharmacology and Toxicology*, vol. 3, no. 1, pp. 59–71, 2008.

[40] B. Huang, J. Xin, H. Dai, W. Zhou, and L. Peng, "Identification of low-Cd cultivars of sweet potato (Ipomoea batatas (L.) Lam.) after growing on Cd-contaminated soil: uptake and partitioning to the edible roots," *Environmental Science and Pollution Research*, vol. 22, no. 15, pp. 11813–11821, 2015.

[41] Y. Zhao, J. Wu, D. Shang et al., "Subcellular distribution and chemical forms of cadmium in the edible seaweed, Porphyra yezoensis," *Food Chemistry*, vol. 168, pp. 48–54, 2015.

[42] A. G. Caporale and A. Violante, "Chemical Processes Affecting the Mobility of Heavy Metals and Metalloids in Soil Environments," *Current Pollution Reports*, vol. 2, no. 1, pp. 15–27, 2016.

[43] T. Ikka, T. Ogawa, D. Li, S. Hiradate, and A. Morita, "Effect of aluminum on metabolism of organic acids and chemical forms of aluminum in root tips of Eucalyptus camaldulensis Dehnh.," *Phytochemistry*, vol. 94, pp. 142–147, 2013.

[44] Q. Qiu, Y. Wang, Z. Yang, and J. Yuan, "Effects of phosphorus supplied in soil on subcellular distribution and chemical forms of cadmium in two Chinese flowering cabbage (Brassica parachinensis L.) cultivars differing in cadmium accumulation," *Food and Chemical Toxicology*, vol. 49, no. 9, pp. 2260–2267, 2011.

[45] M. Shahid, B. Pourrut, C. Dumat, M. Nadeem, M. Aslam, and E. Pinelli, "Heavy-metal-induced reactive oxygen species: Phytotoxicity and physicochemical changes in plants," *Reviews of Environmental Contamination and Toxicology*, vol. 232, pp. 1–44, 2014.

[46] T. M. Mwamba, S. Ali, B. Ali et al., "Interactive effects of cadmium and copper on metal accumulation, oxidative stress, and mineral composition in Brassica napus," *International Journal of Environmental Science and Technology*, vol. 13, no. 9, pp. 2163–2174, 2016.

[47] J. G. Scandalios, "The rise of ROS," *Trends in Biochemical Sciences*, vol. 27, no. 9, pp. 483–486, 2002.

[48] Y. Liang, Q. Chen, Q. Liu, W. Zhang, and R. Ding, "Exogenous silicon (Si) increases antioxidant enzyme activity and reduces lipid peroxidation in roots of salt-stressed barley (*Hordeum vulgare* L.)," *Journal of Plant Physiology*, vol. 160, no. 10, pp. 1157–1164, 2003.

[49] C. M. André, Y. Larondelleb, and D. Evers, "Dietary antioxidants and oxidative stress from a human and plant perspective: A review," *Current Nutrition and Food Science*, vol. 6, no. 1, pp. 2–12, 2010.

[50] M. A. Iannelli, F. Pietrini, L. Fiore, L. Petrilli, and A. Massacci, "Antioxidant response to cadmium in Phragmites australis plants," *Plant Physiology and Biochemistry*, vol. 40, no. 11, pp. 977–982, 2002.

[51] W. Maksymiec and Z. Krupa, "The effects of short-term exposition to Cd, excess Cu ions and jasmonate on oxidative stress appearing in Arabidopsis thaliana," *Environmental and Experimental Botany*, vol. 57, no. 1-2, pp. 187–194, 2006.

[52] U.-H. Cho and N.-H. Seo, "Oxidative stress in Arabidopsis thaliana exposed to cadmium is due to hydrogen peroxide accumulation," *Journal of Plant Sciences*, vol. 168, no. 1, pp. 113–120, 2005.

[53] V. Arbona, V. Flors, J. Jacas, P. García-Agustín, and A. Gómez-Cadenas, "Enzymatic and non-enzymatic antioxidant responses of Carrizo citrange, a salt-sensitive citrus rootstock, to different levels of salinity," *Plant & Cell Physiology (PCP)*, vol. 44, no. 4, pp. 388–394, 2003.

[54] S. Singh, S. Eapen, and S. F. D'Souza, "Cadmium accumulation and its influence on lipid peroxidation and antioxidative system in an aquatic plant, *Bacopa monnieri* L.," *Chemosphere*, vol. 62, no. 2, pp. 233–246, 2006.

[55] F.-Q. Zhang, Y.-S. Wang, Z.-P. Lou, and J.-D. Dong, "Effect of heavy metal stress on antioxidative enzymes and lipid peroxidation in leaves and roots of two mangrove plant seedlings (Kandelia candel and Bruguiera gymnorrhiza)," *Chemosphere*, vol. 67, no. 1, pp. 44–50, 2007.

Hindawi
Journal of Chemistry
Volume 2018, Article ID 2340542, 8 pages
https://doi.org/10.1155/2018/2340542

Research Article

Speciation, Fate and Transport, and Ecological Risks of Cu, Pb, and Zn in Tailings from Huogeqi Copper Mine, Inner Mongolia, China

Liwei Chen[1], **Jun Wu**[2], **Jian Lu**[3], **Chulin Xia**[4], **Michael A. Urynowicz**[5], **Zaixing Huang**[5], **Li Gao**[6] and **Mingying Ma**[1]

[1]*School of Chemical Engineering, Qinghai University, Xining, Qinghai 810016, China*
[2]*Key Laboratory of Comprehensive and Highly Efficient Utilization of Salt Lake Resources, Qinghai Institute of Salt Lakes, Chinese Academy of Sciences, Xining, Qinghai 810008, China*
[3]*Key Laboratory of Coastal Environmental Processes and Ecological Remediation, Yantai Institute of Coastal Zone Research, Chinese Academy of Sciences, Yantai, Shandong 264003, China*
[4]*Department of Geological Engineering, Qinghai University, Xining, Qinghai 810016, China*
[5]*Department of Civil and Architectural Engineering, University of Wyoming, Laramie, WY 82071, USA*
[6]*School of Mechanical Engineering, Qinghai University, Xining, Qinghai 810016, China*

Correspondence should be addressed to Jun Wu; junwu@isl.ac.cn

Received 19 December 2017; Revised 8 January 2018; Accepted 18 January 2018; Published 14 February 2018

Academic Editor: Xiao-San Luo

Tailings collected from the tailing reservoir at Huogeqi Copper Mine, located in Inner Mongolia, China, were used in a leachate study to evaluate the acid potential, neutralization potential, and possibility for producing acid mine drainage (AMD) from the site. The speciation of Cu, Pb, and Zn contained in the tailings was also determined during the leachate study to further access the potential migration abilities of these metals. The results showed that the tailings did not produce significant AMD as the pH of the leachate ranged from 7 to 9 and decreased with time. The Cu, Pb, and Zn concentrations were high, ranging from 439.1 to 4527 mg/kg in the tailings and from 0.162 to 7.964 mg/L in the leachate, respectively. Concentrations of metals in the leachate and tailings were positively correlated. Over 60% of the Cu in the tailing samples existed in an oxidizable form. Most of the Pb also existed in its oxidized form, as did the silicate and Zn. Metals usually have higher mobility in their exchangeable and oxidizable forms and as such represent a higher potential risk to the environment. Results of risk assessment code also revealed that metals in tailings exerted medium to high risks to the environment.

1. Introduction

Mining activities are known to significantly alter the geochemical background of the environment. Environmental pollution caused by mining activities includes large amounts of particulate and dust, solid wastes, soil pollution, metal-rich effluents, and acid mine drainage (AMD). AMD is drainage with a pH of 2.0 to 4.5 from mines and mine wastes [1]. Metal-rich effluents and AMD, just like metals in dust and solid wastes, have become a serious environmental problem all over the world [2, 3]. With introduction of AMD, metals are more easily dissolved to migrate into the surrounding water and soil [4, 5]. Due to their toxicity and persistence, metals can exert serious risks to ecosystems and human health [6].

Tailings are the primary solid waste associated with mining activities. Oxidation of tailings can produce large amounts of acids leading to the mobilization and potential release of metals [7] and posing potential health risks [8]. Ore-mining activities over the last century have resulted in an enormous amount of tailings around the world. Almost all of these tailings are piled up in the open pit or in the tailing ponds. Exposure of sulfide minerals in the tailings to atmospheric oxygen and moisture can result in the formation of AMD and the release of high concentrations of metals [9–12].

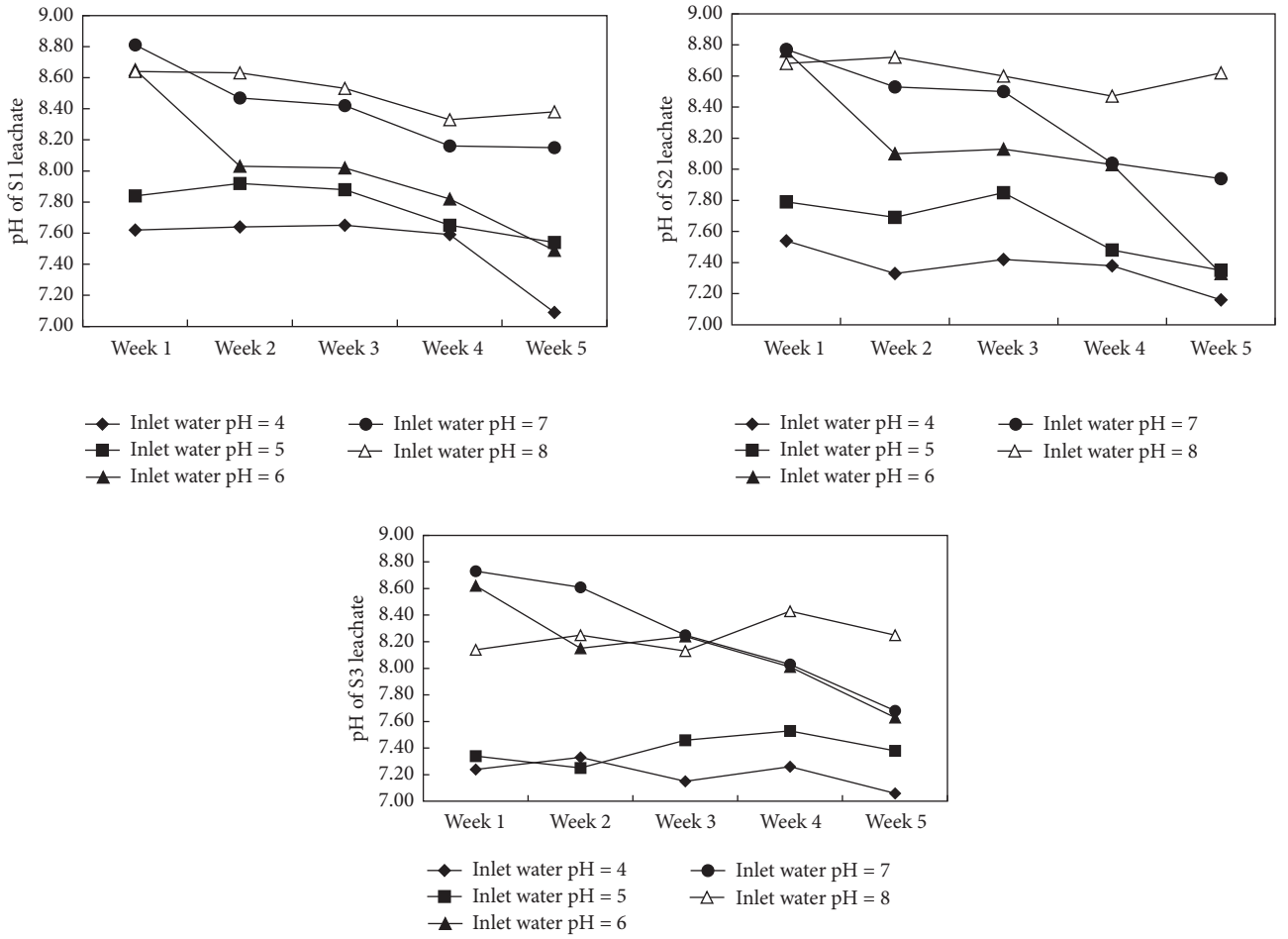

Figure 1: pH variations of tailing leachate.

The release of metals and their environmental fate and transport are a topic of great concern [13–16]. The relationship between metals in tailings and the surrounding environment and properties of tailings/soil/water have also been widely explored [17, 18]. The chemical speciation of metals is also a good indicator for assessing their potential mobility, availability, and toxicity [19, 20].

Mining activities at the Huogeqi Copper Mine, located in Inner Mongolia, China, have been conducted since 1986, resulting in a large quantity of mining wastes including tailings and waste rock. Although most of the CuO, FeS, ZnS, and PbS in the tailings and waste rock are not recycled, the environmental effects have not been well studied. Therefore, the focus of this study is the speciation and potential for migration of Cu, Pb, and Zn in the tailings with the aim of quantitatively describing the distribution and potential for metal migration.

2. Materials and Methods

2.1. Sampling and Sample Preparation. Fresh tailing samples were collected from 3 different sites of the tailing reservoir on March 25, 2015. Sampling sites 1 and 3 were located on the back of the east side and the front edge of the west side of the tailing reservoir while sampling site 2 was located in the middle of the reservoir. Approximately 5 kg of surface tailings was collected at each sampling site using a spade. The tailings were collected in polyethylene containers and transported to the laboratory. The samples were then air dried, crushed, and passed through a 100 micron nylon sieve. The sieved samples were then transferred to polyethylene bottles and stored at room temperature for further use.

2.2. Chemical Analysis. Chemical analysis was carried out at the Analytical Centre of Qinghai University. The concentrations of main elements, including S, were measured by X-ray fluorescence (XRF) spectroscopy (ZSXPrimus II, Rigaku, Japan). The concentrations of Cu, Pb, and Zn were measured by Atomic Absorption Spectrometer (TAS-990, Persee, China) after digestion by H_2SO_4-HNO_3-HF-$HClO_4$. Only guarantee reagents (GR) were used in the study and all test methods followed the National Standardization of China (GB/T14506-1993). The acid potential (AP) values of the tailing samples were obtained according to the counting method (AP = S% × 31.25) [21] and the neutralization potential (NP) was determined by the improved neutralization potential

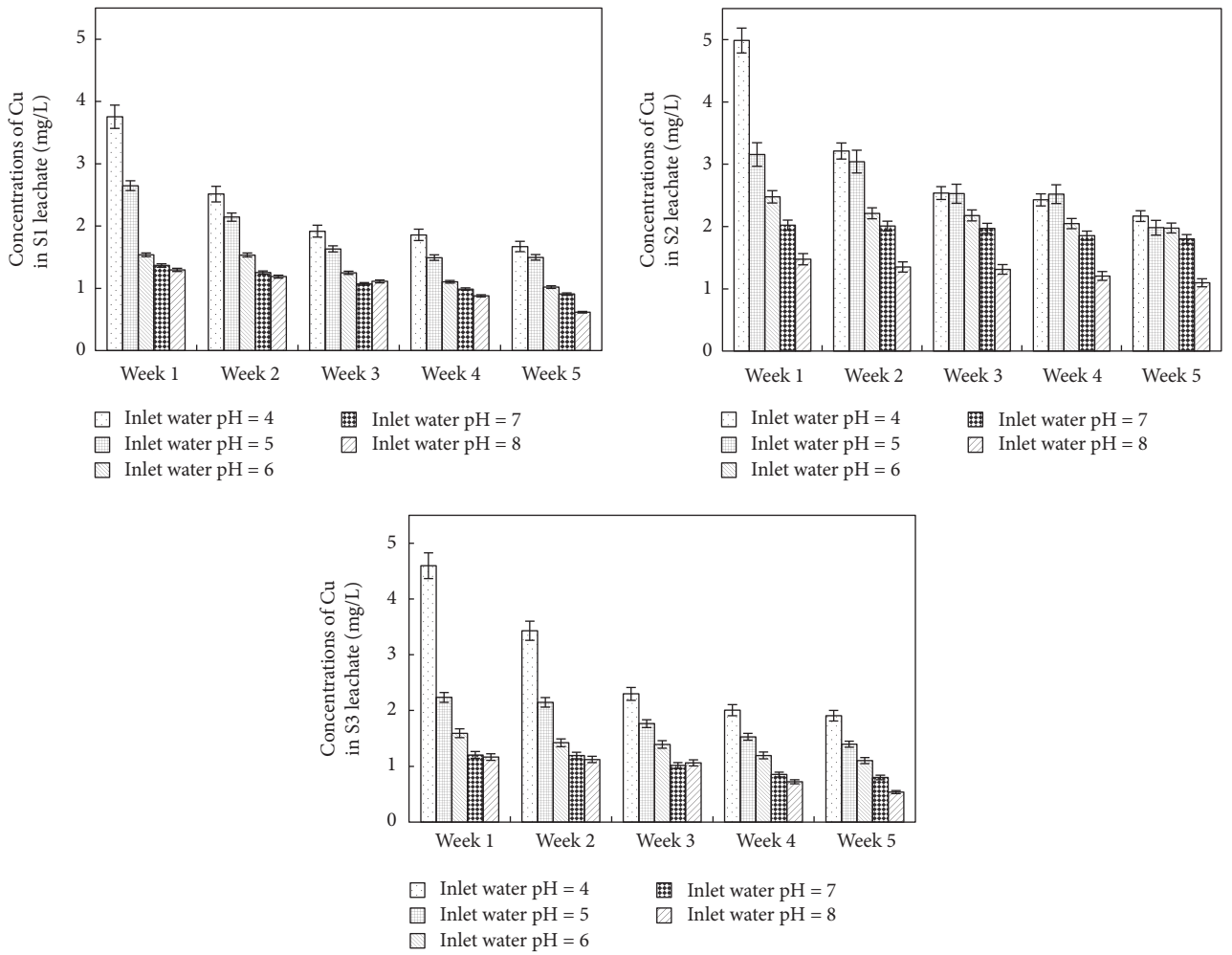

Figure 2: Variation of Cu concentrations in leachate of different tailings.

acid-alkali counting method [22]. In summary, the weight of every tailing sample was 1 g. The concentrations of HCl and NaOH were 12.3 and 0.70 mol/L, respectively. The ratio of volume of HCl and NaOH of blank experiment was 0.057. Thus, NP = {[volume of HCl (mL) × the concentration of HCl (mol/L) − volume of NaOH (mL) × the concentration of NaOH (mol/L)] × 49 × 0.057}/2. NAPP was used to represent AP-NP; and APR was used to represent NP/AP.

2.3. Leaching Study. The leaching study was performed in laboratory to investigate the migration of heavy metals from the tailings. Each column was loaded with 50 g tailings and saturated with deionized water. Then 4 ml of deionized water with different pH values (4, 5, 6, 7, and 8) was added to the top of the columns each week for 5 weeks. Thus, the total quantity of water added in a column during the experiment was 16 mL, corresponding to a local average annual precipitation.

After each addition of water, the percolation rate was monitored and the leachate was collected. Each leachate sample was analyzed in terms of pH (PHSJ-3F, Leici, China) and trace metal element concentrations (Atomic Absorption Spectrometer).

2.4. Sequential Extraction Procedure. The classical sequential extraction technique [23] was employed to study the speciation of heavy metals in the tailings. This method was widely proved to be effective in the studies on speciation of metals in soils, sediments, and tailings [24–26]. The speciation (exchangeable, carbonate, deoxidize, oxidizable, and silicate) of Cu, Pb, and Zn was obtained by Tessier et al. The experiments were performed in duplicate.

2.5. Risk Assessment of Heavy Metals. Based on the method of sequential extraction procedure, risk assessment code (RAC) was proposed as (exchangeable fraction + carbonate fraction) percent concentration [27]. The metals in the samples can be classified by RAC as no risk (less than 1%), low risk (1–10%), medium risk (11–30%), high risk (31–50%), and very high risk (more than 50%) [28].

3. Results and Discussion

3.1. Possibility of Producing AMD of Tailings. All samples based on the classification of NAPP and APR had negative NAPP values (Table 1). They were all larger than −20. APR

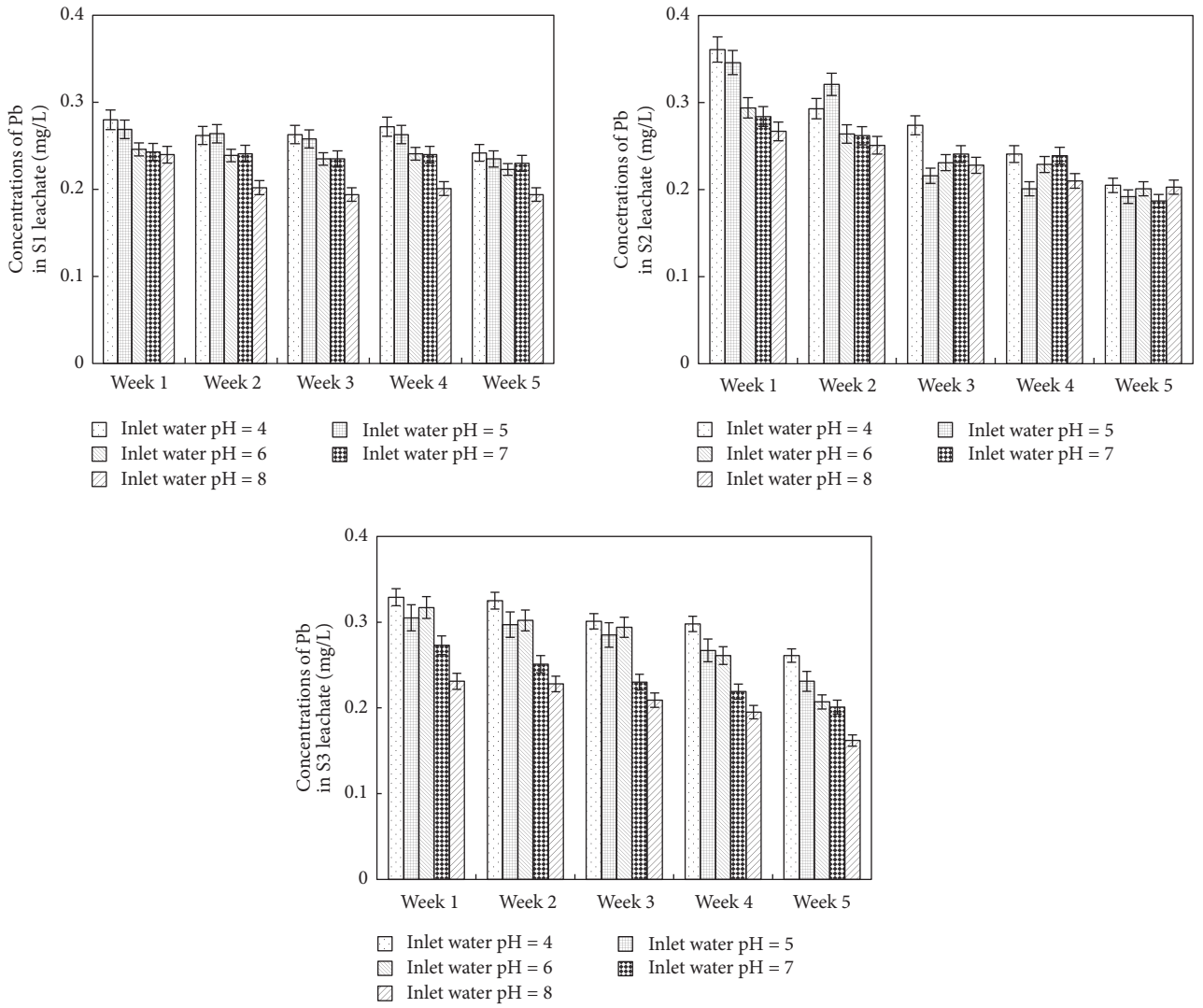

Figure 3: Variation of Pb concentrations in leachate of different tailings.

Table 1: Physicochemical properties and producing-AMD features of tailings.

Sample	Cu (mg/kg)	Pb (mg/kg)	Zn (mg/kg)	S (%)	AP	NP	APR	NAPP
S1	2141	439.1	3939	3.89%	1.22	12.57	10.30	−11.35
S2	3561	528.5	4527	6.21%	1.94	8.07	4.16	−6.13
S3	2945	487.2	4103	5.54%	1.73	9.24	5.34	−7.51

Note. AMD refers to acid mine drainage; AP and NP mean acid potential and neutralization potential, respectively; NAPP represents AP-NP; APR refers to NP/AP.

values were all larger than 3. According to NAPP and APR criteria [29], all tailings did not generate significant AMD.

3.2. pH of Leachate. The pH of the various leachates is shown in Figure 1. All leachate samples collected were alkaline with pH ranging from 7 to 9, which might be caused by the higher NP of the tailings. The H^+ in the acidic inlet water were neutralized by tailings so that the pH of the leachate increased. Although all collected tailing samples did not produce significant AMD, the pH of mine drainage was shown to gradually decrease over time. Therefore, the potential for the production of AMD may still exist.

3.3. Migration Regularity of Cu, Pb, and Zn. The concentrations of Cu, Pb, and Zn in leachate were measured under different leaching conditions (Figures 2–4). As shown, the concentrations of each metal decreased with time. The metals also showed a direct correlation with the concentration of the hydronium ion. In other words, a lower pH resulted in higher metal concentrations. Table 1 summarizes the concentrations

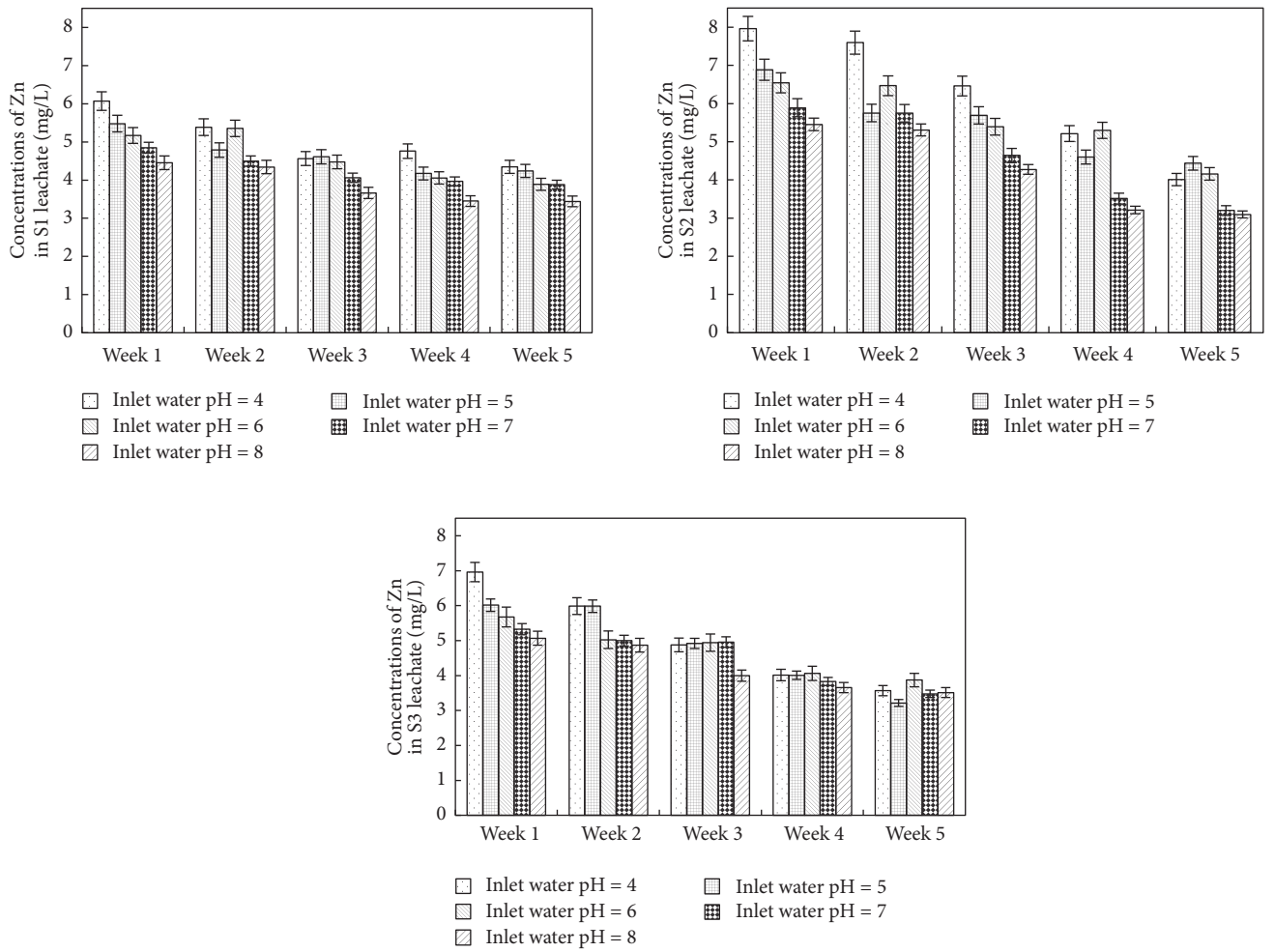

Figure 4: Variation of Zn concentrations in leachate of different tailings.

of heavy metals in the tailings which followed the order of Zn > Cu > Pb. There was also a strong correlation between the concentration of metals in the leachate and tailings, which is similar to the findings of other researchers [30, 31].

The variation of the Pb concentration in the leachate was relatively small while concentrations of Cu varied sharply, especially under acidic leaching conditions. Different tailings exhibited different leaching features, indicating that that tailing properties had a significant effect impact on the metal distribution of the leachate. The concentrations of the three metals in the leachate were higher than the limits of Surface Water Quality Standards (GB 3838-2002, level IV). It showed that the metals in tailings could migrate and pollute the environment.

3.4. Speciation of Cu, Pb, and Zn. The speciation of metals in tailings is shown in Figure 5. Copper existed mainly in oxidizable form (over 60%). Silicate was the second form for Cu in the tailings while deoxidized and exchangeable forms existed little. Contents of carbonate-form Cu and oxidizable form Cu in S2 and S3 were higher than those in S1. Cu in silicate form was very stable so as not to do harm to the environment under normal conditions. The oxidizable form Cu could slightly decline under specific environmental conditions such as acid rains to potentially cause a drastic increase in the dissolved contaminants to subsequently pose pollution threats to the environment [32]. Deoxidized form and oxidizable form heavy metals would easily transform to the exchangeable form. Therefore, heavy metals in these forms would be released from the tailings and migrate into the water and soil to pollute the environment [33]. Therefore Cu in tailings potentially posed risks to the surroundings.

Pb was mainly in the silicate, oxidizable and exchangeable forms, while small portion was observed in the deoxidize-form and carbonate-form. Deoxidized form Pb was produced on the surface of Fe-oxyhydroxides and Mn-oxyhydroxides or lied in the structures of Fe-oxyhydroxides and Mn-oxyhydroxides by isomorphous replacement of Fe and Mn elements [34]. The oxidizable and exchangeable forms of Pb covered more than 56% in three samples, indicating that the migration ability of Pb was stronger to potentially do harm to the environment.

Zn was mainly in the exchangeable and oxidizable forms while forms of deoxidize, silicate, and carbonate were in small

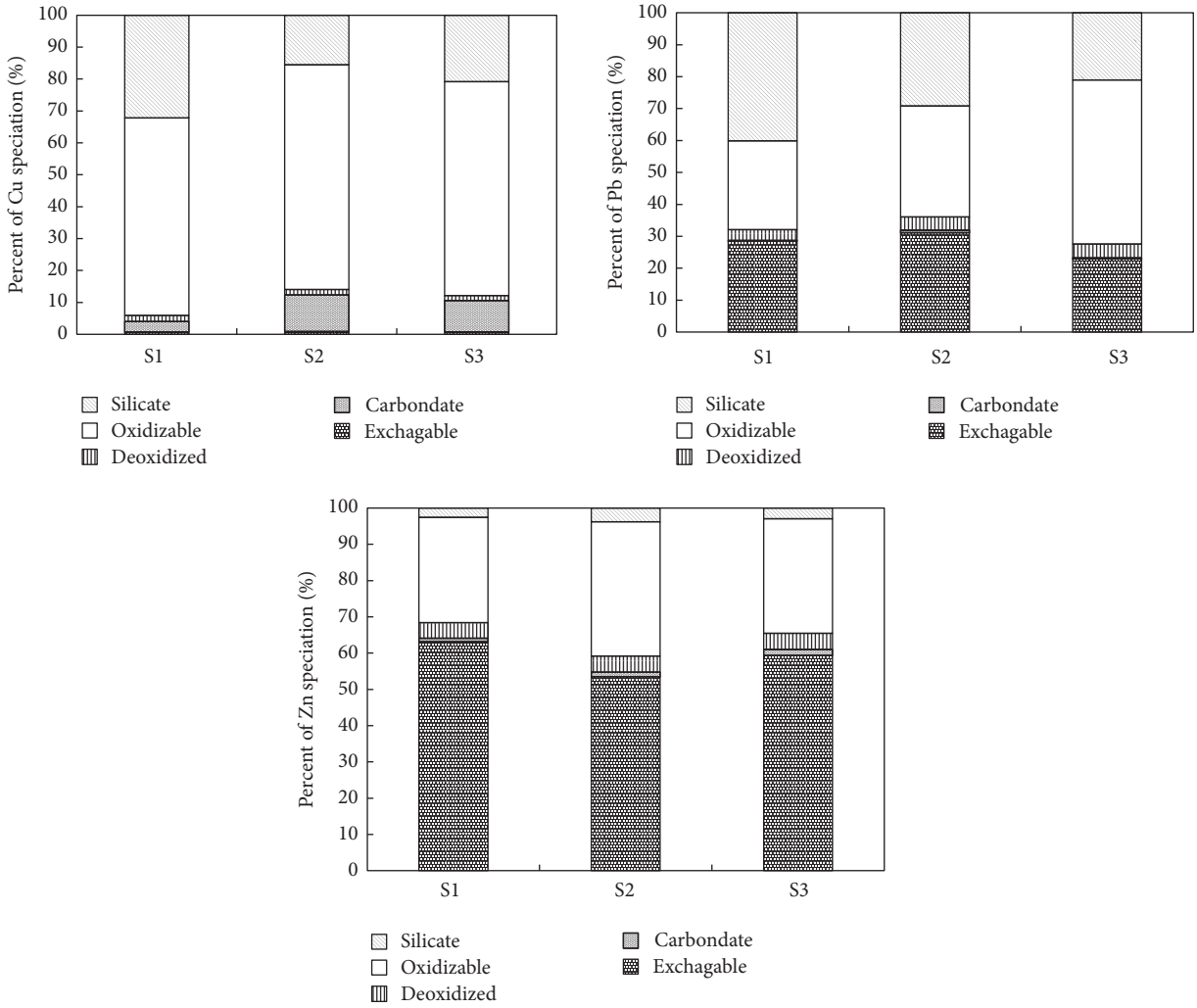

Figure 5: Speciation of heavy metals in different tailings.

portion. The oxidizable and exchangeable forms covered more than 90% in three samples, suggesting that the migration ability of Pb was the strongest in three heavy metals.

3.5. Potential Risk Assessment. Results of RAC were displayed in Figure 6. The RAC values of Cu in S1 showed low risk while Cu in S2 and S3 showed medium risk to the environment. Pd in S1 and S3 exerted medium risk whereas Pd in S2 exerted high risk. RAC values of Zn in all samples were higher than 50%, indicating high risk. The risk levels of heavy metals in tailings by RAC assessment followed the order of Zn > Pb > Cu.

4. Conclusions

Though the neutralization capability of target tailings was high, there was still a potential possibility of producing AMD so as to pose potential risks to the environment. Metal concentrations in the leachate and tailings were positively correlated. The concentrations of metals in leachate followed the order of Zn > Cu > Pb. Moreover, the concentrations of metals in leachate decreased with longer leaching time and increased pH. Therefore, the metals in tailings could potentially migrate and pollute the environment, especially under the condition of rainfall. Cu in tailings was mainly in oxidizable and silicate forms. Pb was mainly in the silicate, oxidizable and exchangeable forms while Zn was mainly in the exchangeable and oxidizable forms. They were potentially hazardous to the environment. The evaluation results of risk assessment code approach exhibited that these metals exerted medium to high risks to the environment, following the order of Zn > Pb > Cu. The influence of specific hydrological geological and climate conditions is important in evaluating the damage degree to the environment caused by metals in tailings. It will be the focus of future research.

Conflicts of Interest

The authors declare that there are no conflicts of interest regarding the publication of this paper.

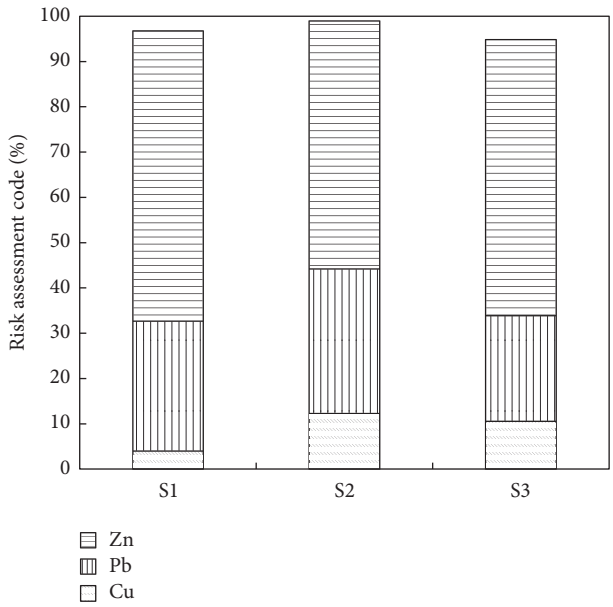

Figure 6: Risk assessment code of heavy metals in different tailings.

Acknowledgments

The authors are grateful for financial support from the Natural Science foundation of Qinghai Province, China (no. 2016-ZJ-952Q), Applied Basic Research Program of Qinghai Science and Technology Department (no. 2016-ZJ-755), One Hundred-Talent Plan of Chinese Academy of Sciences (nos. Y610061033 and Y629041021), and Thousand Talents Plan of Qinghai Province (Y740171071).

References

[1] H. Herrmann and H. Bucksch, *Dictionary Geotechnical Engineering/Wörterbuch GeoTechnik*, Springer, Berlin, Germany, 2014.

[2] A. J. Romero-Baena, I. González, and E. Galán, "Soil pollution by mining activities in Andalusia (South Spain)—the role of Mineralogy and Geochemistry in three case studies," *Journal of Soils and Sediments*, pp. 1–17, 2017.

[3] T. Assawincharoenkij, C. Hauzenberger, K. Ettinger, and C. Sutthirat, "Mineralogical and geochemical characterization of waste rocks from a gold mine in northeastern Thailand: application for environmental impact protection," *Environmental Science and Pollution Research*, pp. 1–13, 2017.

[4] A. Courtin-Nomade, T. Waltzing, C. Evrard et al., "Arsenic and lead mobility: From tailing materials to the aqueous compartment," *Applied Geochemistry*, vol. 64, pp. 10–21, 2016.

[5] O. Pourret, B. Lange, J. Bonhoure et al., "Assessment of soil metal distribution and environmental impact of mining in Katanga (Democratic Republic of Congo)," *Applied Geochemistry*, vol. 64, pp. 43–55, 2016.

[6] V. A. Mesquita, C. F. Silva, and E. V. Soares, "Toxicity Induced by a Metal Mixture (Cd, Pb and Zn) in the Yeast Pichia kudriavzevii: The Role of Oxidative Stress," *Current Microbiology*, vol. 72, no. 5, pp. 545–550, 2016.

[7] D. W. Blowes, E. J. Reardon, J. L. Jambor, and J. A. Cherry, "The formation and potential importance of cemented layers in inactive sulfide mine tailings," *Geochimica et Cosmochimica Acta*, vol. 55, no. 4, pp. 965–978, 1991.

[8] F. M. Tack, O. W. J. J. Callewaert, and M. G. Verloo, "Metal solubility as a function of pH in a contaminated, dredged sediment affected by oxidation," *Environmental Pollution*, vol. 91, no. 2, pp. 199–208, 1996.

[9] U. Förstner and G. T. W. Wittmann, *Metal Pollution in the Aquatic Environment*, Springer-Verlag, Berlin, Germany, 1979.

[10] C. A. J. Appelo and D. Postma, *Geochemistry Groundwater and Pollution*, Balkema, Rotterdam, Netherlands, 1996.

[11] K. G. Stollenwerk, "Geochemical interactions between constituents in acidic groundwater and alluvium in an aquifer near Globe, Arizona," *Applied Geochemistry*, vol. 9, no. 4, pp. 353–369, 1994.

[12] R. B. Herbert Jr., "Metal retention by iron oxide precipitation from acidic ground water in Dalarna, Sweden," *Applied Geochemistry*, vol. 11, no. 1-2, pp. 229–235, 1996.

[13] E. S. Sağlam and M. Akçay, "Chemical and mineralogical changes of waste and tailings from the Murgul Cu deposit (Artvin, NE Turkey): implications for occurrence of acid mine drainage," *Environmental Science and Pollution Research*, vol. 23, no. 7, pp. 6584–6607, 2016.

[14] J.-Y. Kim, K.-W. Kim, J. S. Ahn, I. Ko, and C.-H. Lee, "Investigation and risk assessment modeling of As and other heavy metals contamination around five abandoned metal mines in Korea," *Environmental Geochemistry and Health*, vol. 27, no. 2, pp. 193–203, 2005.

[15] M. A. Ashraf, M. J. Maah, and I. Yusoff, "Heavy metals accumulation in plants growing in ex tin mining catchment," *International Journal of Environmental Science & Technology*, vol. 8, no. 2, pp. 401–416, 2011.

[16] F. Páez-Osuna, H. Bojórquez-Leyva, M. Bergés-Tiznado et al., "Heavy Metals in Waters and Suspended Sediments Affected by a Mine Tailing Spill in the Upper San Lorenzo River, Northwestern México," *Bulletin of Environmental Contamination and Toxicology*, vol. 94, no. 5, article no. 1473, pp. 583–588, 2015.

[17] L. Wang, Y. Liu, A. Lu et al., "The modes of occurrence of Ni and Cu in tailings of Jinchuan nickel mine," *Acta Petrologica et Mineralogica*, vol. 32, no. 6, pp. 873–881, 2013 (Chinese).

[18] C. Candeias, P. F. Ávila, E. F. da Silva, A. Ferreira, N. Durães, and J. P. Teixeira, "Water–Rock Interaction and Geochemical Processes in Surface Waters Influenced by Tailings Impoundments: Impact and Threats to the Ecosystems and Human Health in Rural Communities (Panasqueira Mine, Central Portugal)," *Water, Air, & Soil Pollution*, vol. 226, no. 2, p. 23, 2015.

[19] A. A. Bogush and E. V. Lazareva, "Behavior of heavy metals in sulfide mine tailings and bottom sediment (Salair, Kemerovo region, Russia)," *Environmental Earth Sciences*, vol. 64, no. 5, pp. 1293–1302, 2011.

[20] G. Guo, T. Yuan, W. Wang et al., "Bioavailability, mobility, and toxicity of Cu in soils around the Dexing Cu mine in China," *Environmental Geochemistry and Health*, vol. 33, no. 2, pp. 217–224, 2011.

[21] A. A. Sobek, W. A. Schuller, and J. R. Freeman, *Field and Laboratory Methods Applicable to Overburdens and Mine Soil*, EPA/600/2-78/054 (NTIS PB280495), U.S. Environmental Protection Agency, Washington, DC, USA, 1978.

[22] R. W. Lawrence and M. Scheske, "A method to calculate the neutralization potential of mining wastes," *Environmental Geology*, vol. 32, no. 2, pp. 100–106, 1997.

[23] A. Tessier, P. G. C. Campbell, and M. Blsson, "Sequential extraction procedure for the speciation of particulate trace metals," *Analytical Chemistry*, vol. 51, no. 7, pp. 844–851, 1979.

[24] L. Fanfani, P. Zuddas, and A. Chessa, "Heavy metals speciation analysis as a tool for studying mine tailings weathering," *Journal of Geochemical Exploration*, vol. 58, no. 2-3, pp. 241–248, 1997.

[25] P.-K. Lee, M.-J. Kang, H. Y. Jo, and S.-H. Choi, "Sequential extraction and leaching characteristics of heavy metals in abandoned tungsten mine tailings sediments," *Environmental Earth Sciences*, vol. 66, no. 7, pp. 1909–1923, 2012.

[26] M. Wang, K. Hu, D. Zhang, and J. Lai, "Speciation and Spatial Distribution of Heavy Metals (cu and Zn) in Wetland Soils of Poyang Lake (China) in Wet Seasons," *Wetlands*, vol. 11, special issue on lake poyang, pp. 1–10, 2017.

[27] Z. Xiao, X. Yuan, L. Leng et al., "Risk assessment of heavy metals from combustion of pelletized municipal sewage sludge," *Environmental Science and Pollution Research*, vol. 23, no. 4, pp. 3934–3942, 2016.

[28] M. Z. Hossen, M. M. Islam, and M. S. Hossain, "Heavy Metal Contents in Sediments of an Urban Industrialized Area-A Case Study of Tongi Canal, Bangladesh," *Asian Journal of Water, Environment and Pollution*, vol. 14, no. 1, pp. 59–68, 2017.

[29] I. P. G. Hutchison and R. D. Ellison, *Mine Waste Management*, Lewis Publisher, London, UK, 1992.

[30] C. Nikolaidis, I. Zafiriadis, V. Mathioudakis, and T. Constantinidis, "Heavy metal pollution associated with an abandoned lead-zinc mine in the Kirki Region, NE Greece," *Bulletin of Environmental Contamination and Toxicology*, vol. 85, no. 3, pp. 307–312, 2010.

[31] V. Misra, A. Tiwari, B. Shukla, and C. S. Seth, "Effects of soil amendments on the bioavailability of heavy metals from zinc mine tailings," *Environmental Monitoring and Assessment*, vol. 155, no. 1-4, pp. 467–475, 2009.

[32] L. Lei, B. Mo, W. Fu, J. Mo, Z. Shi, and S. Chen, "Occurrence state of heavy metals in the carbonate-rich sulfide tailings in Bali inactive impoundment, Dachang Tin-polymetallic Mine (Gaungxi, China)," *Earth and Environment*, vol. 42, no. 5, pp. 604–610, 2014 (Chinese).

[33] A. M. Gbadebo and Y. A. Ekwue, "Heavy metal contamination in tailings and rocksamples from an abandoned goldminein southwestern Nigeria," *Environmental Modeling & Assessment*, vol. 186, no. 1, pp. 165–174, 2014.

[34] Z. Feketeová, V. Hulejová Sládkovičová, B. Mangová, and I. Šimkovic, "Biological activity of the metal-rich post-flotation tailings at an abandoned mine tailings pond (four decades after experimental afforestation)," *Environmental Science and Pollution Research*, vol. 22, no. 16, pp. 12174–12181, 2015.